ACTIVE COUNTERBALANCING
OF ROBOT ARMS

BY

MARC PAUL FERNANDEZ

A THESIS PRESENTED TO
THE SCHOOL OF GRADUATE STUDIES
UNIVERSITY OF OTTAWA
IN PARTIAL FULFILLMENT OF
THE REQUIREMENTS FOR THE DEGREE OF
MASTER OF APPLIED SCIENCE
IN
THE MECHANICAL ENGINEERING DEPARTMENT

OTTAWA, ONTARIO, CANADA.

JANUARY, 1987

ISBN 0-315-36493-9

ABSTRACT

Robot arms in most automation applications go through a fixed cycle where different loads are carried during each part of the cycle. Different links on the robot arms are generally equipped with a fixed counterweight so as to increase their load carrying capacity for a given link actuator motor. The counterweight is either designed to balance the link alone, or is designed to balance the link plus a portion of the maximum load intended. This fixed counterweight approach fails to provide perfect balancing throughout the entire operation cycle, particularly so during high operation speed when the dynamic effects become dominant.

This thesis deals with an active counterweight system that has been developed, and provides optimum balancing of the robot arm links. A simplified dynamic analysis of a robot arm equipped with the active counterweight system is conducted. A dynamic simulation of this analysis shows that the active counterweight system enhances the load carrying capacity of a robot arm. A prototype has been built and the analysis for the operation control of the active counterweight system is presented. Experiments carried out with the prototype, confirmed the theoretical behaviour predicted of a robot equipped with an active counterweight system.

ACKNOWLEDGEMENTS

The author acknowledges the patient guidance and help of his supervisor Dr. Atef E. Fahim throughout this work.

Special thanks to the professors and the graduate students of the department, especially Dr. S. Tavoularis, Dr. M. B. Munro, Dr. R. C. Flanagan, Dr. D. Redekop, Dr. S. Mirza, Dr. D. Necsulescu, Miss J. Sevigny, Mr. M. Mahjoub and Mr. Y. Q. Xia for their kind support, suggestions and cooperation.

The assistance of Mr. G. Tóth and Mr. A. Laewen in the realization of the prototype is appreciated.

TABLE OF CONTENTS

LIST OF FIGURES

LIST OF TABLES

NOMENCLATURE

a : Determined variable

$\vec{a}$: Absolute acceleration of the counterweight in the parallel configuration

$\vec{a}_{G_i}$: Acceleration of the center of mass of link i

$\vec{a}_{E_i}$: Acceleration of the center of mass of the counterweight of link i

$\vec{a}_{E'_3}$: Acceleration of the center of mass of the counterweight of link 3 in the parallelogram configuration

$\vec{a}_{G_4}$: Acceleration of the payload

$a^X_{E'_3}$, $a^Y_{E'_3}$, $a^Z_{E'_3}$: x, y and z components of $\vec{a}_{E'_3}$ in the $(\vec{i}_1, \vec{j}_1, \vec{k}_1)$ frame

$a^X_{G_3}$, $a^Y_{G_3}$, $a^Z_{G_3}$: x, y and z components of $\vec{a}_{G_3}$ in the $(\vec{i}_1, \vec{j}_1, \vec{k}_1)$ frame

b : Determined variable

b_i : Length of link i

c : Determined variable

$D(s)$: Laplace transform of the controller transfer function

$D(z)$: Z-transform of the controller transfer function

e_i : Location of the center of mass of link i

$e_{ss}(\infty)$: Steady state error

$e(k)$: Discrete time error signal

E_i : Center of mass of the counterweight of link i

E'_3 : Center of mass of the counterweight of link 3 in the parallelogram configuration

$E(s)$: Laplace transform of the error signal

f : Friction coefficient of the counterweight motors

$\vec{g}$: Acceleration of gravity

$G'(s)$: Laplace transform for the motor and load system

$H(s)$: Laplace transform of the overall transfer function of the counterweight control loop

I, i_2 : Currents

I_i' : Matrix of inertia of link i

I_i : Matrix of inertia for the counterweight of link i

I_X, I_Y, I_Z : Mass moments of inertia of the upper link in the 3 principal directions

I_X', I_Y', I_Z' : Mass moments of inertia for the counterweight of the upper link in the 3 principal directions

$\vec{F}$: Force necessary to move the counterweight

$(\vec{i}_i, \vec{j}_i, \vec{k}_i)$: Frame attached to link i

J : Mass moment of inertia of the rotors of the counterweights motors

k_0 : Gain of the position feedback

k_1 : Gain of the velocity feedback

k_b : Back EMF coefficient of the counterweights motors

k_I : Integral gain

k_M : Torque constant of the counterweights motors

k_P : Proportional gain

k_a : Gain of the power amplifier

K : Equivalent gain proportional to k_P

L : Armature inductance of the counterweights motors

$F(s)$: Laplace transform of the feedback transfer function

m : Mass of the payload

m_i : Mass of link i

m_i' : Mass of the counterweight of link i

n : Gear ratio for the counterweights motors

O_i	: Point defining the robot arm: a link i is defined by the 2 points O_i and O_{i+1} .
p_1, p_2, p_3	: poles
$p(k)$	: Discrete time command signal of the counterweights controllers
$\vec{P}_{i,j}$	: Force applied on link j due to link i
$\vec{P}_i$	: Force due to the counterweight i acting on link i
$P(s)$	: Laplace transform of the disturbance
$P'(s)$	: Laplace transform of the equivalent disturbance
$\vec{Q}_{i,j}$	: Torque applied on link j due to link i
$\vec{Q}_i$	: Torque due to the counterweight i acting on link i
R	: Armature resistance of the counterweights motors
r_3	: Location of the center of mass of the counterweight of the upper link
R_3	: Reference position
T	: Sampling periods
T_i	: Driving torque of link i
x	: Location of the dynamic counterweight
x_d	: Desired position of the dynamic counterweight
$X(s)$	: Laplace transform of x
z_1	: A zero
α	: Angular position of the counterweights pinions
$\alpha_0\ \alpha_1\ \alpha_2$	: Adjustable feedback gains
β	: Current gain of the power transistors
δ_3	: Relative position of the counterweight
Δ_3	: Range of motion of the active counterweight
γ_2	: Angular inclination of the counterweight of the lower arm

$\vec{\Omega}_i$: Absolute angular velocity of link i

θ : Angular position of the counterweights motors

θ_i : Angular position of link i with respect to link i-1

Throughout this thesis, $\dot{var}$ represents the first derivative of the variable var with respect to time, and $\ddot{var}$ represents its second derivative with respect to time.

1. INTRODUCTION

1.1 Robotics

Current trends in manufacturing are towards low inventory both of the raw materials and the manufactured goods so as to increase profit. In the manufacturing sense, this trend translates into small but varied batch runs to satisfy the immediate customer demands. This type of manufacturing environment requires a manufacturing system that can be easily reconfigured, the "flexible manufacturing systems" (FMS), to handle the different requirements of the batch runs [1]. A good example of flexible manufacturing systems are those employed in modern plants for manufacturing cars. Production lines in such plants would handle different models of cars. The production machinery on such lines have to be able to perform different tasks depending on the type of model of the vehicle being worked on, as well as rapidly change between tasks so as to respond to changes on the line [4].

Components of a FMS line are numerically controlled (NC) machine tools, programmable conveyer systems and robot manipulators. Robot manipulators are the component of the FMS that carry out the manual work of a human operator in the manufacturing environment. Consequently, such industrial robots have to be very flexible and programmable.

This thesis deals with the subject of robotics. According to the Robot Institute of America (RIA), the definition of a robot is as follows:

"A robot is a reprogrammable multifunctional manipulator designed to move material, parts, tools or specialized devices, through variable programmed motions for the performance of a variety of tasks."

Four basic types of robots architectures are available. The distinction between these architectures depends upon the type of joints used and their sequence. Two types of joints are commonly employed, the revolute joint "R", and the prismatic joint "P". Table 1.1 presents the four basic robot architectures and the salient features of each type. The spherical and the revolute robot configurations are the most commonly used in industry nowadays. The spherical configuration was launched by Unimate over 20 years ago, and is used mainly in applications requiring a high load carrying capacity. The revolute configuration is mainly used in applications requiring a high level of flexibility like painting, welding or assembly applications.

The major operational characteristics distinguishing robots of the same configuration are the resolution, the accuracy, the load carrying capacity and the maximum operating speed. These characteristics are interl~~ined~~ and depend upon the strength of the links, the joints, and the joint drives of the robot. The

CONFIGURATION	TYPE OF JOINT AND ITS SEQUENCE	SALIENT FEATURES
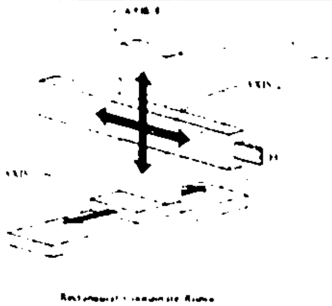	P-P-P	Work volume: Rectangular Strength : Very high Flexibility: Fair Accuracy : Constant
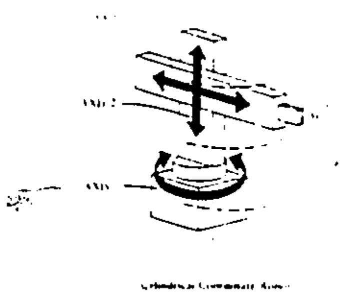	R-P-P	Work volume: Cylindrical Strength : Good Flexibility: Good Accuracy : Varies with the extention of ~~the~~ arms
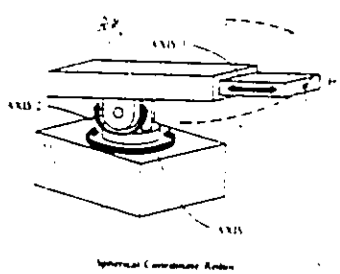	R-R-P	Work volume: Spherical Strength : Good Flexibility: Good Accuracy : Varies with the extention of the arms
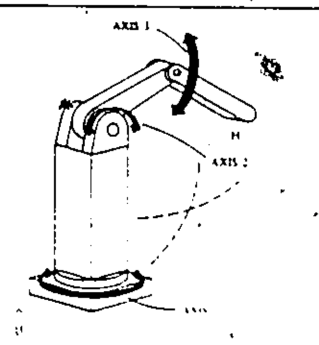	R-R-R	Work volume: Resembles partial spheres Strength : Fair Flexibility: Very good Accuracy : Varies throughout the work space

Table 1.1. Robot architectures and their salient features

method of specifying these characteristics varies from one robot manufacturer to another. The most common approach of defining these characteristics is to specify a resolution and accuracy, and a maximum payload for a given maximum speed. This approach, however, is on the conservative side since a lower than the maximum specified payload can be moved at higher than the maximum speed and vice versa. Another approach used by some manufacturers of robots is to give the specifications in the form of a loading diagram.

An example of one type of this diagram is shown in Figure 1.1 for the ASEA Irb-6 revolute robot. With reference to Figure 1.1, in

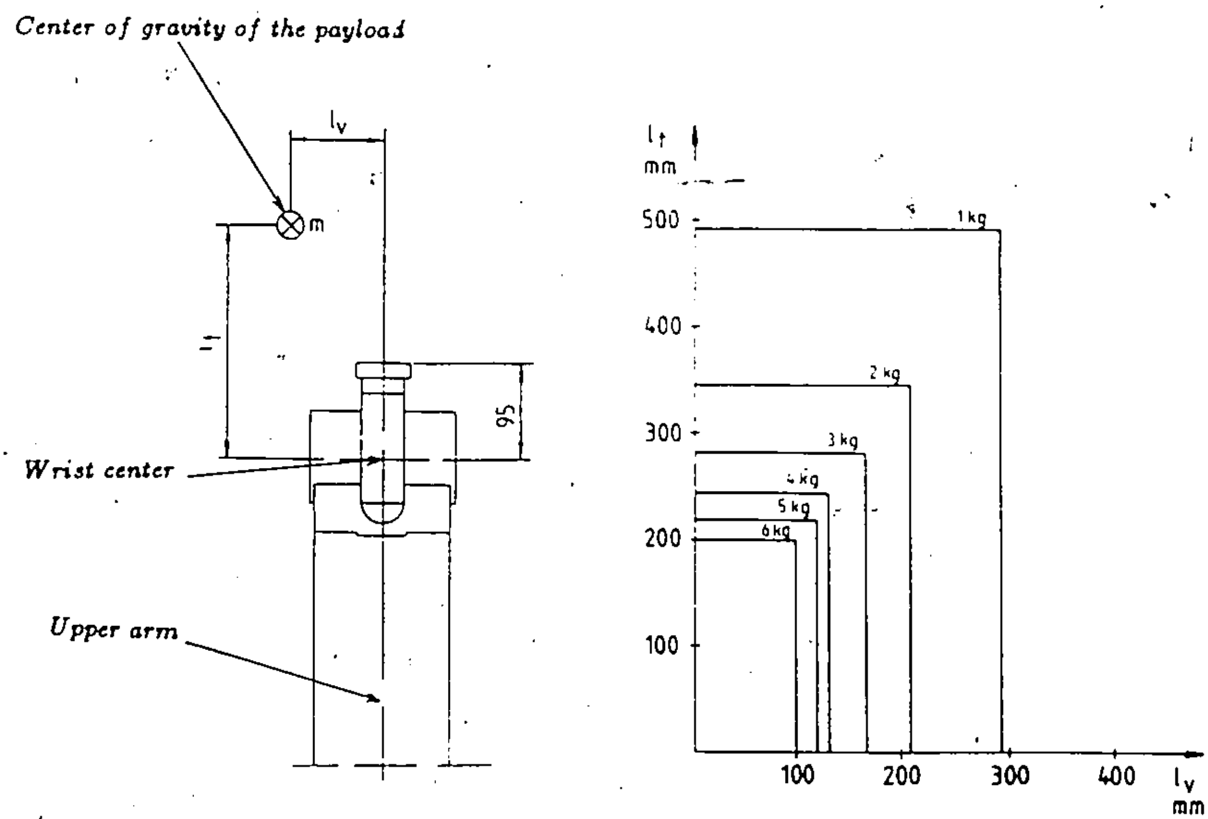

Figure 1.1. ASEA Irb 6 loading diagram

this example, the manufacturer implicitly guaranties the accuracy and maximum operating speed for a combination of payload and distance of the payload from the center of the robot wrist. The larger the distance between the center of mass of the payload and the center of the robot wrist, the less the load that can be handled at the stated accuracy and maximum speed.

The operation of a robot that is purchased for a particular task might not be found satisfactory if it is assigned a new task in which the payload required to be handled exceeds that specified by the loading diagram. This overloading may result in a slower motion or loss of accuracy and hence a lower productivity of the flexible manufacturing system employing that robot. At present, in situations where payloads that are higher than the load carrying capacity of a robot have to be handled, there is no recourse but to substitute the robot with a higher load carrying capacity one. In some cases, the low payload capacity robot may be used at reduced speeds with the consequence of low productivity of the manufacturing system.

It is this overloading situation that prompted the current study of alternate means to enhance the operational characteristics of existing industrial robots at lowest possible cost. This work will show that the operational characteristics of polar or revolute type robots can be dramatically enhanced by dealing with the problems of balancing the revolute joints that are affected by the gravitational pull.

1.2. Robot link balancing

Balancing of the link of a revolute joint is the means of reducing the torque necessary to rotate a link about a horizontal axis within a vertical gravitational field. Balancing is therefore a topic of a particular interest for enhancing the characteristics of revolute-type robots where two cascaded revolute links rotate about a horizontal axis. Balancing is usually achieved through the use of a lumped mass acting as a counterweight as shown in Figure 1.2.

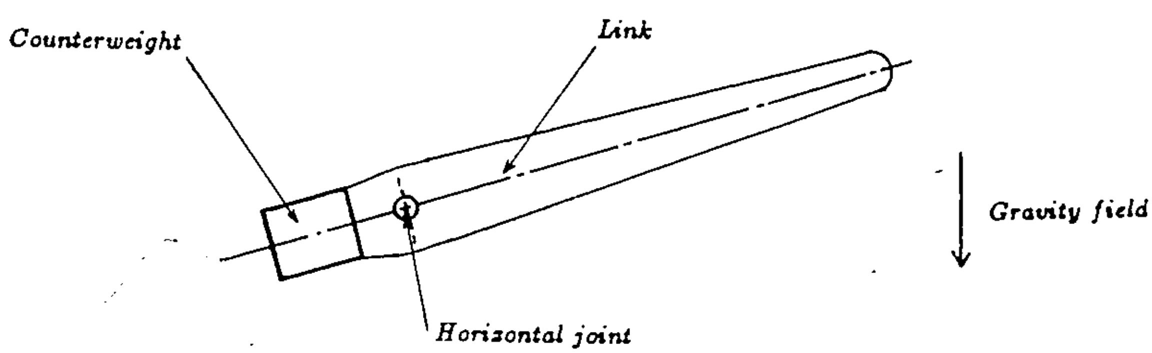

Figure 1.2. Balancing of a revolute joint

For a revolute type robot the second link or "lower arm" and the third link or "upper arm" are the ones that require balancing. The driving moment of the two links is commonly applied through one of the following two methods:

a) A torque directly acting on the link at the joint as in the case of a PUMA robot shown in Figure 1.3, or

b) A force acting on an extention of the link as in the case of an ASEA robot shown in Figure 1.4.

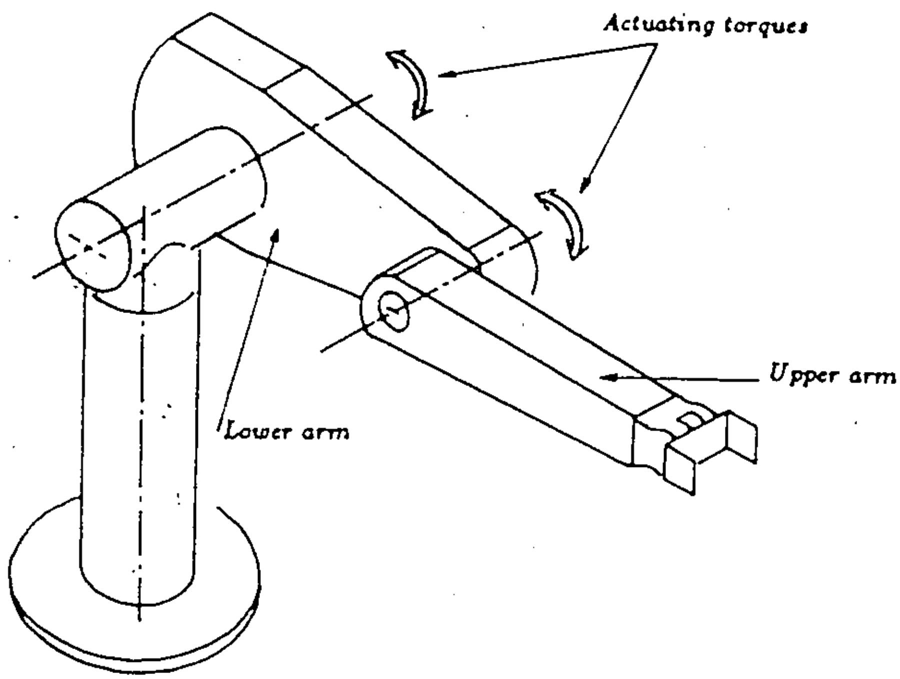

Figure 1.3. PUMA type revolute manipulator

Robot links driven using method (a) above are flexible in the sense that they can be made to rotate through 360 degrees or close to that, but are generally weaker in construction than those driven using method (b). Furthermore, counterbalancing the upper arm in this case is of limited benefit since any increase in the counterweight mass results also in an increase in the inertia of the link as well as of the total mass and inertia driven by the motor drive of the lower arm.

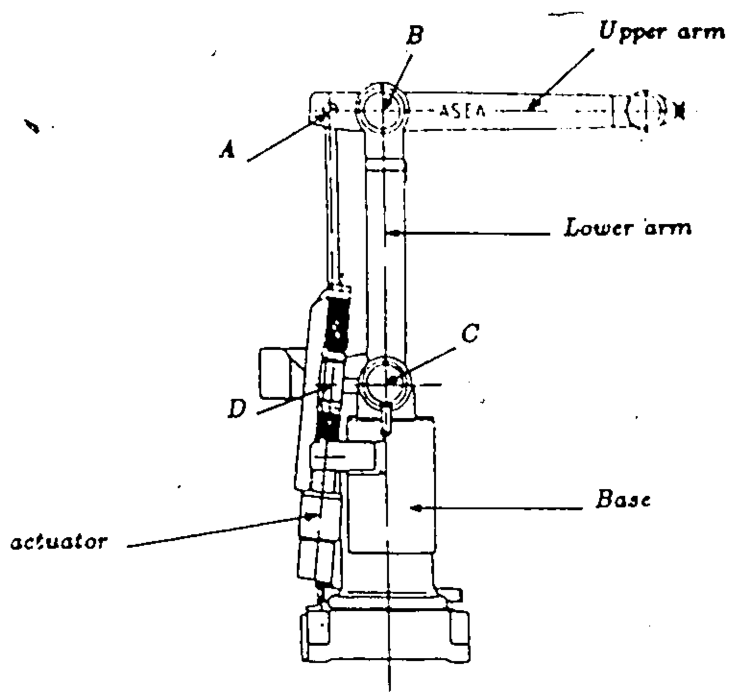

Figure 1.4. ASEA Revolute Manipulator

In the case of robot links driven using method (b) above, the driving force for both the upper and the lower arms is usually generated using linear actuators attached to the first link as shown on figure 1.4. With reference to Figure 1.4, the motive force of the upper arm is applied at point D, and is transmitted through the A-B-C-D parallelogram mechanism. This method of driving the upper arm increases the effectiveness of counterbalancing the upper arm. This is due to the fact that the counterweight can be located in this case along the line C-D and not along the upper arm itself, and thus does not increase the mass and inertia that the lower arm has to drive as will be seen in a later chapter.

When balancing the lower arm, the angular displacements of both the upper arm and lower arm have to be considered since they contribute significantly to the load carried by the motor drive of the lower arm. In this case, however, the added counterweight and its inertial effect is carried by the first link and contributes marginally to the torque required from the first link drive.

1.3. Concept of the Active Counterweight

As the robot arm moves along its trajectory, the torques of the joint drives vary due to the load, the masses and dynamics of the links, as well as the interaction between these links. The links of a revolute type robot are usually balanced using a fixed counterweight. The counterweight is typically designed to statically balance the corresponding link, or the link and part of the payload. At low operational speeds, the dynamic forces are negligible. The approach of utilising a fixed counterweight is appropriate for such cases. However, at high operational speeds, the dynamic forces cannot be neglected. The magnitude and direction of these forces vary considerably for the same payload along a trajectory, and a fixed counterweight can no longer provide adequate balancing at such operational speeds.

A literature survey showed little work done on dynamic balancing of robot arms [12], and improvement of the actuating torques of robot links is currently achieved only through direct drives and high torque brushless motors [13].

1.4. Thesis outline

This thesis deals with a new approach to balancing the links of revolute robot arms. An active counterweight varies its location along the link axis as the robot arm traverses its trajectory. The location of the counterweight is calculated based on the load, the interaction between the links, and the dynamic forces. As a result of better balancing, more torque will be available from the joint drives of the balanced links to carry extra load or enhance the performances.

A simplified model of the dynamics of a revolute type manipulator is derived. The model is sufficiently general to represent the two methods of driving the revolute links that have been presented above. The advantages of driving the revolute links through the parallelogram mechanism are outlined. A simulations of the dynamics of a robot equipped with an active counterweight system is carried out using the specifications of the ASEA Irb 6 industrial robot. The simulation shows the enhancement in operational characteristics of the robot due to the active counterweight system. The simulation results are used to guide the design of a prototype active counterweight system. The prototype as well as the control scheme necessary for the operation of the counterweight are designed and built. Detailed description of the system that have been built is presented in this thesis. Experiments are conducted with the prototype to test the improvement in operational characteristics of the total robot system. Results of these experiments are presented.

2. DYNAMIC MODELLING OF THE ROBOT-ARM

2.1. General model

Figure 2.1 shows a schematic of the robot arm under investigation. With reference to Figure 2.1, the robot is a 3-link revolute manipulator with both upper and lower arms balanced using counterweights. Each counterbalanced link i is defined by the following components:

- its joint location O_i and its center of gravity G_i ;
- its length b_i and the location of the center of mass with respect to the joint axis e_i ;
- its mass m_i ;
- a coordinate frame defined as follows:
  - (1) the x_{i-1} axis lies along the axis of motion of the i^{th} joint
  - (2) the x_i axis is normal to the x_{i-1} axis, pointing away from it
  - (3) the y_i axis completes the right-handed coordinate system as required;
- a counterweight of mass m_i' whose center of mass E_i is located at a distance r_i from the joint of the link.

The dynamic analysis of both the upper and lower arms of the robot provides the relationship between the actuator torque necessary to move the arm, and the effect of its counterweight. From these relations, it is possible to derive an optimum position of the given active counterweight in order to minimize these torques.

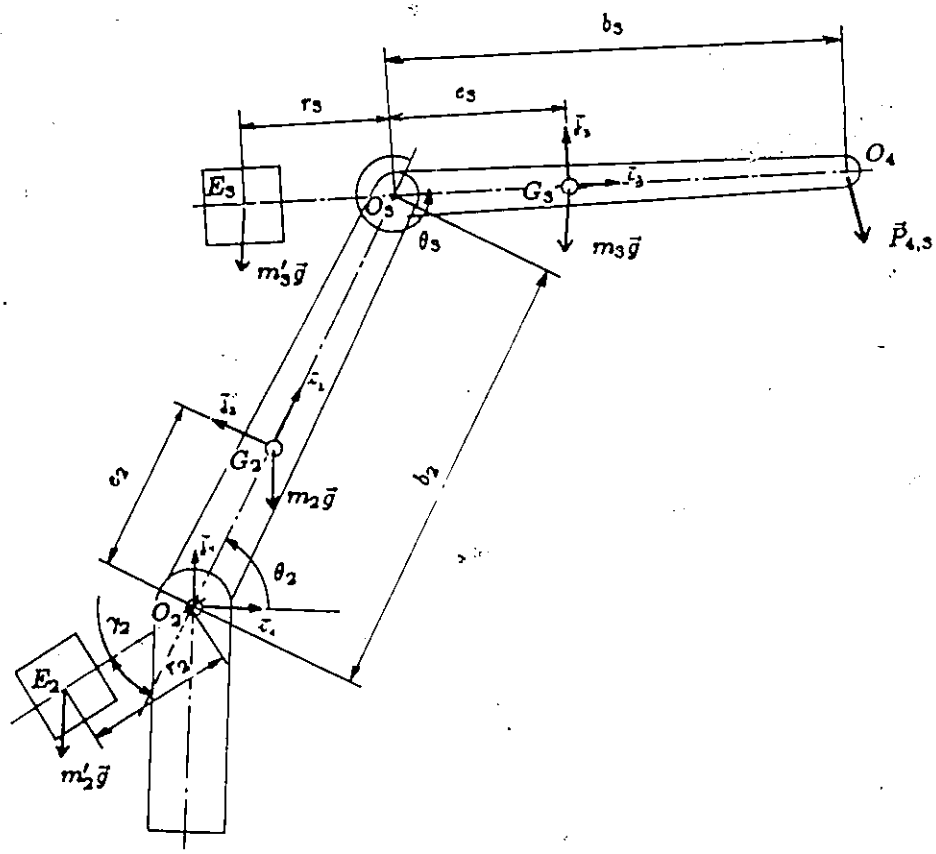

Figure 2.1. Schematic diagram of the robot

The analysis is conducted with the following conditions assumed in order to obtained a simplified model. This is necessary in order for the model to be usable for real time implementation of the active counterweight system.

(i) The dynamic effects due to the translation motion of the counterweight are neglected. That is to say the counterweight motion is assumed to be quasistatic.

(ii) The orientation of the wrist of the manipulator is assumed to have little effect on the dynamics of the system, compared with the motion of the three first links.
Therefore, only the three first degrees of freedom are taken into consideration.

(iii) The robot arms are assumed to be symmetric along their longitudinal axis, thus reducing the inertia matrices to diagonal ones.

(iv) The wrist and payload are combined and assumed to be a point mass, and the dynamics of their motion with respect to their reference frame ignored. This assumption is reasonable due to the relative magnitude between the mass and motion of the wrist and payload with respect to the entire system.

2.2. Kinetic analysis of the 3 link robot manipulator

The acceleration of the key points, like the center of mass of the links Gi and of the counterweight Ei , as well as the acceleration of the wrist base of the manipulator O4 are necessary for the derivation of the robot dynamics. Since the robot arm is statically determinate, the accelerations of all the points are related to each other. In robot applications, the wrist base acceleration can be calculated from the robot trajectory [3-5]. Using this acceleration, all other accelerations can be readily derived.

With reference to Figure 2.1, the link frame of motion $(G_1, \vec{i}_1, \vec{j}_1, \vec{k}_1)$ is defined with respect to the inertial frame $(O_2, \vec{i}_0, \vec{j}_0, \vec{k}_0)$ as shown in Figure 2.2.

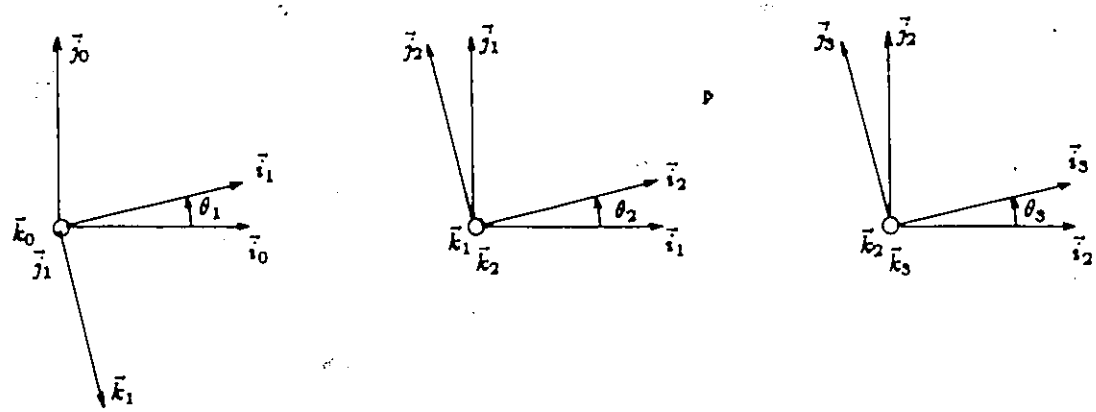

Figure 2.2. Link frame definition

With reference to Figures 2.1 and 2.2, the kinematic relations are derivdd as follows:
using the following notations for brevity:

$$\theta_{ij} = \theta_i + \theta_j \qquad \dot{\theta}_{ij} = \dot{\theta}_i + \dot{\theta}_j \qquad \ddot{\theta}_{ij} = \ddot{\theta}_i + \ddot{\theta}_j$$

$$C_i = \cos(\theta_i) \qquad S_i = \sin(\theta_i)$$

$$C_{ij} = \cos(\theta_i + \theta_j) \qquad S_{ij} = \sin(\theta_i + \theta_j)$$

The position vector of the wrist location O_4 with respect to the base frame origin O_2 is given by:

$$\overline{O_2O_4} = C_1(b_2C_2 + b_3C_{23})\vec{i}_0 + S_1(b_2C_2 + b_3C_{23})\vec{j}_0 + (b_2S_2 + b_3S_{23})\vec{k}_0 \qquad 2.1$$

Differentiating this position vector with respect to time provides the velocity of the wrist base as follows:

$$\begin{aligned}\vec{V}_{O_4} = &-[\dot{\theta}_1 S_1(b_2C_2 + b_3C_{23}) + C_1(b_2S_2\dot{\theta}_2 + b_3S_{23}\dot{\theta}_{23})]\vec{i}_0 \\ &+ [\dot{\theta}_1 C_1(b_2C_2 + b_3C_{23}) - S_1(b_2S_2\dot{\theta}_2 + b_3S_{23}\dot{\theta}_{23})]\vec{j}_0 \\ &+ [\dot{\theta}_2 b_2C_2 + \dot{\theta}_{23}b_3C_{23}]\vec{k}_0 \end{aligned} \qquad 2.2$$

The acceleration of O_4 is obtained by further differentiation and is expressed in the frame $(\vec{i}_1, \vec{j}_1, \vec{k}_1)$ for convenience as follows:

$$\begin{aligned}\vec{a}_{O_4} = &-[\ddot{\theta}_2 b_2S_2 + \ddot{\theta}_{23}b_3S_{23} + \dot{\theta}_1^2(b_2C_2 + b_3C_{23}) + \dot{\theta}_2^2 b_2C_2 + \dot{\theta}_{23}b_3C_{23}]\vec{i}_1 \\ &+ [\ddot{\theta}_2 b_2C_2 + \ddot{\theta}_{23}b_3C_{23} - \dot{\theta}_2^2 b_2S_2 - \dot{\theta}_{23}^2 b_3S_{23}]\vec{j}_1 \\ &+ [-\ddot{\theta}_1(b_2C_2 + b_3C_{23}) + 2\dot{\theta}_1\dot{\theta}_2 b_2S_2 + 2\dot{\theta}_1\dot{\theta}_{23}b_3S_{23}]\vec{k}_1 \end{aligned} \qquad 2.3$$

All other necessary accelerations, derived from equation 2.2, are summarised in Appendix A.

2.3. Dynamic analysis of the link/counterweight system

The free body diagram of a balanced arm shown in Figure 2.3 can be split into two parts, as shown in Figure 2.4, in order to isolate the counterweight from the link itself. Figure 2.3 show an isolated link/counterweight system and the external forces acting on that system. With reference to Figure 2.3, $\vec{Q}_{i-1,i}$ represents the torque due to the previous link, and $\vec{F}_{i-1,i}$ the force due to that link both acting on the balanced link i, whereas $\vec{Q}_{i+1,i}$ and $\vec{P}_{i+1,i}$ are the torque and force due to the next link acting on link i. The free body diagrams of the link and counterweight are shown in Figure 2.4.

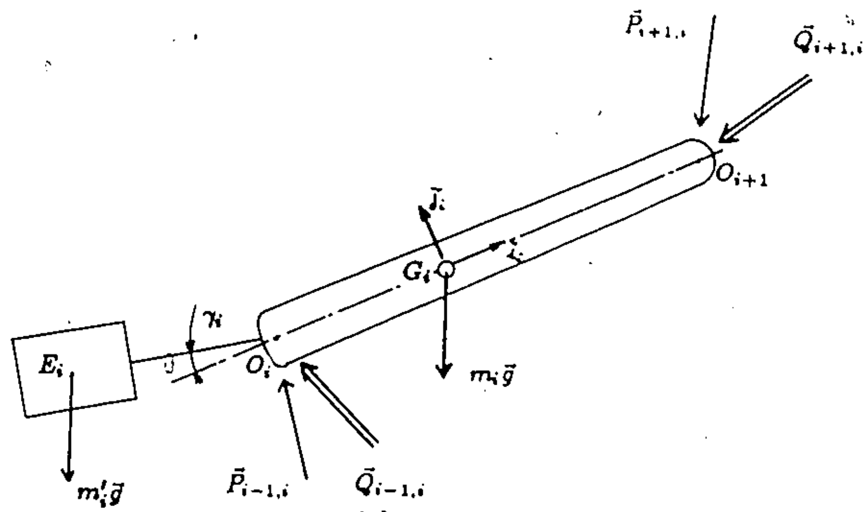

Figure 2.3. Free Body Diagram for link i

With reference to the figure, $\vec{P}_i$ and $\vec{Q}_i$ represent the force and torque due to the counterweight acting on the link itself. The sum of forces and torques acting on the link are given by:

$$m_i\vec{a}_{G_i} = m_i\vec{g} + \vec{P}_{i-1,i} + \vec{P}_i + \vec{P}_{i+1,i} \qquad 2.4$$

$$I_i\dot{\vec{\Omega}}_i + \vec{\Omega}_i \times I_i\vec{\Omega}_i = \vec{Q}_{i-1,i} + \vec{Q}_i + \vec{Q}_{i+1,i} + \overline{G_iO_i} \times (\vec{P}_{i-1,i} + \vec{P}_i) + \overline{G_iO}_{i+1} \times \vec{P}_{i+1,i} \qquad 2.5$$

Similarly, the sum of forces and torques acting on the counterweight are given by:

$$m_i^{\prime}\vec{a}_{E_i} = m_i^{\prime}\vec{g} - \vec{P}_i \tag{2.6}$$

$$I_i^{\prime}\dot{\vec{\Omega}}_i + \vec{\Omega}_i \times I_i^{\prime}\vec{\Omega}_i = -\vec{Q}_i - \overline{E_iO_i} \times \vec{P}_i \tag{2.7}$$

The torque T_i required for the motion of the link i can be expressed in terms of the torque $\vec{Q}_{i-1,i}$ as follows:

$$T_i = \vec{Q}_{i-1,i} \cdot \vec{k}_i \tag{2.8}$$

Solving Equations 2.4 to 2.7 simultaneously and rearranging give :

$$\begin{aligned}\vec{Q}_{i-1,i} =& (I_i + I_i^{\prime})\dot{\vec{\Omega}}_i + \vec{\Omega}_i \times (I_i + I_i^{\prime})\vec{\Omega}_i + m_i\overline{G_iO_i} \times (\vec{g} - \vec{a}_{G_i}) \\ &+ m_i^{\prime}\overline{E_iO_i} \times (\vec{g} - \vec{a}_{E_i}) + \overline{O_{i+1}O_i} \times \vec{P}_{i+1,i} - \vec{Q}_{i+1,i}\end{aligned} \tag{2.9}$$

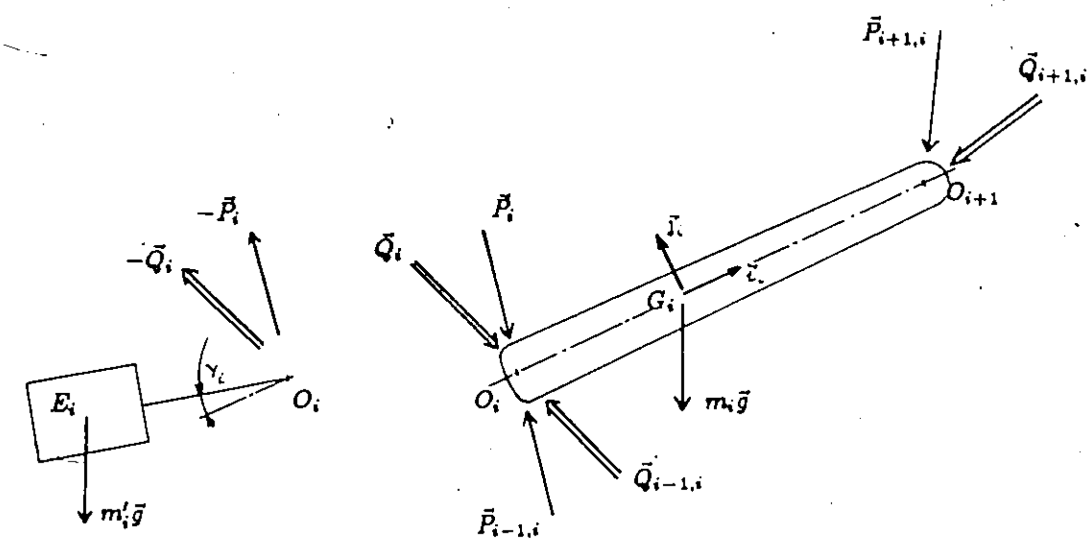

Figure 2.4. Expended Free Body Diagram

Equation 2.9 yields the general torque acting on the joint of link i. From this expression, we can now obtain the general torques for both upper and lower arms (link 3 and 2 respectively) as well as the driving torques that we want to optimize.

For the upper arm (link 3), $\vec{P}_{4,3}$ and $\vec{Q}_{4,3}$ represent the force and torque due to the wrist and payload. As mentioned earlier, the wrist and payload are assumed to be a point mass located at the wrist base O_4 on link 3. Hence,

$$\vec{P}_{4,3} = m(\vec{g} - \vec{a}_{O_4}) \quad 2.10$$

$$\vec{Q}_{4,3} = \vec{O} \quad 2.11$$

where m is the combined mass of the wrist, the end effector and the payload.

The torque due to the lower arm acting on the upper arm , $\vec{Q}_{2,3}$ can now be expressed as follows:

$$\vec{Q}_{23} = (I_3 + I_3')\dot{\vec{\Omega}}_3 + \vec{\Omega}_3 \times (I_3 + I_3')\vec{\Omega}_3 + m_3\overrightarrow{G_3O_3} \times (\vec{g} - \vec{a}_{G_3})$$
$$+ m_3'\overrightarrow{E_3O_3} \times (\vec{g} - \vec{a}_{B_3}) + m\overrightarrow{O_4O_3} \times (\vec{g} - \vec{a}_{O_4}) \quad 2.12$$

The driving torque for the upper arm is obtained by substituting $\vec{Q}_{2,3}$ from Equation 2.12 into Equation 2.08 as follows:

$$T_3 = \vec{Q}_{2,3} \cdot \vec{k}$$

$$T_3 = [(I_3 + I_3')\dot{\vec{\Omega}}_3] \cdot \vec{k} + [\vec{\Omega}_3 \times (I_3 + I_3')\vec{\Omega}_3] \cdot \vec{k} + m_3[\overrightarrow{G_3O_3} \times (\vec{g} - \vec{a}_{G_3})] \cdot \vec{k}$$
$$+ m_3'[\overrightarrow{E_3O_3} \times (\vec{g} - \vec{a}_{B_3})] \cdot \vec{k} + m[\overrightarrow{O_4O_3} \times (\vec{g} - \vec{a}_{O_4})] \cdot \vec{k} \quad 2.13$$

For the lower arm (link 2), $\vec{Q}_{1,2}$ is the torque due to link 1 and acting on link 2. Substituting the indices in Equation 2.5 gives $\vec{Q}_{1,2}$ as follows:

$$\vec{Q}_{1,2} = (I_2 + I_2')\dot{\vec{\Omega}}_2 + \vec{\Omega}_2 \times (I_2 + I_2')\vec{\Omega}_2 + m_2\overrightarrow{G_2O_2} \times (\vec{g} - \vec{a}_{G_2})$$
$$+ m_2'\overrightarrow{E_2O_2} \times (\vec{g} - \vec{a}_{B_2}) + \overrightarrow{O_3O_2} \times \vec{P}_{3,2} - \vec{Q}_{3,2} \quad 2.14$$

where $\vec{P}_{3,2}$ is the force acting on link 2 due to link 3. $\vec{P}_{3,2}$ is given by:

$$\vec{P}_{3,2} = m_3'(\vec{g} - \vec{a}_{B_3}) + m_3(\vec{g} - \vec{a}_{G_3}) + m(\vec{g} - \vec{a}_{O_4}) \quad 2.15$$

2.4. Parallelogram type robot configuration

The leading manufacturers of revolute manipulators such as General Electric, ASEA and ACMA have chosen the parallelogram type power transmission mechanism for their industrial robots. In this configuration, the upper arm motion is transmitted from an actuator attached to the base of the robot through the parallelogram mechanism as shown on Figure 2.5 [6].

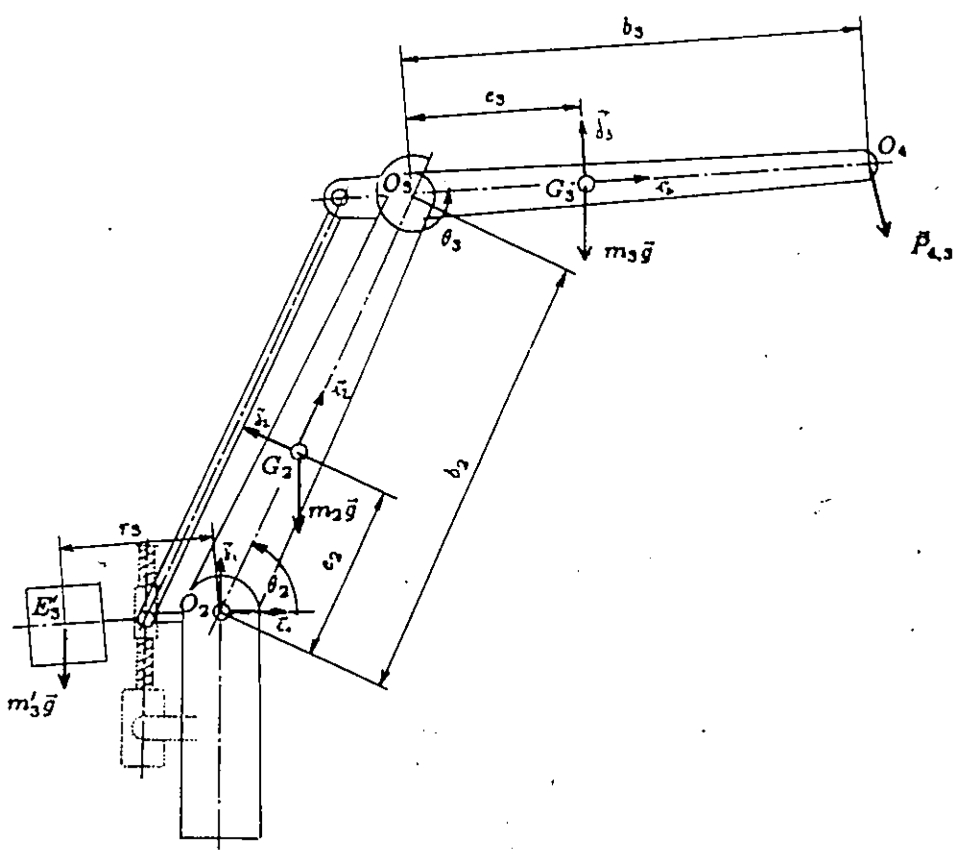

Figure 2.5. Parallelogram type robot arm

Such a configuration results in a lighter and lower inertia upper structure since both the actuator and the counterweight of the upper arm are located on the body (first link) of the manipulator. The accelerations of the masses of the counterweight and actuator are not subjected to large variations in this configuration as compared to the case where the counterweight would be aligned with the link, and the actuator acts directly on the upper arm.

The following derivation proves that the driving torque T_3 of the upper arm for the robot configuration shown on Figure 2.5 is equivalent to that of the general configuration given in Section 2.3. The only outstanding difference between both configurations is that in the parallelogram type robot, the acceleration of the counterweight , $\bar{a}_{B_1}$, does not depend on the motion of the lower arm as in the case of the general configuration shown in Figure 2.1.

The free body diagram of the upper arm and counterweight for the parallelogram type robot is shown in Figure 2.6. Let $\bar{P}_M$ be the actuating force acting at location B through the nut and power screw arraignment. With reference to Figure 2.6, $\bar{P}_M$ can be expressed as follows:

$$\bar{P}_M = P_{M_3}\bar{i}_2 + N_{M_3}\bar{j}_2 = \bar{P}_{M_3} + \bar{N}_{M_3} \qquad 2.16$$

The sum of forces and torques acting on the upper arm are expressed as follows:

$$m_3\vec{a}_{G_3} = m_3\vec{g} + \vec{P}_{2,3} + \vec{P}_{4,3} + \vec{P}_3 + \vec{P}_{M_3} \qquad 2.17$$

$$I_3\dot{\vec{\Omega}}_3 + \vec{\Omega}_3 \times I_3\vec{\Omega}_3 = \vec{Q}_{2,3} + \overrightarrow{G_3O_4} \times \vec{P}_{4,3} + \overrightarrow{G_3O_3} \times \vec{P}_{2,3} + \overrightarrow{G_3A} \times (\vec{P}_3 + \vec{P}_{M3}) \qquad 2.18$$

Similarly, the sum of forces and torques acting on the counter-weight are expressed as follows:

$$m_3'\vec{a}_{E_3'} = m_3'\vec{g} + \vec{P}_{1,3}' - \vec{P}_3 - \vec{P}_{M_3} + \vec{P}_M \qquad 2.19$$

$$I_3'\dot{\vec{\Omega}}_3 + \vec{\Omega}_3 \times I_3'\vec{\Omega}_3 = \vec{Q}_{1,3}' + \overrightarrow{E_3'B} \times (\vec{N}_{M_3} - \vec{P}_3) + \overrightarrow{E_3'O_2} \times \vec{P}_{1,3}' \qquad 2.20$$

Solving Equations 2.16 to 2.20 simultaneously and rearranging give:

$$\begin{aligned}\overrightarrow{O_2B} \times \vec{P}_M + \vec{Q}_{2,3} = &(I_3 + I_3')\dot{\vec{\Omega}}_3 + \vec{\Omega}_3 \times (I_3 + I_3')\vec{\Omega}_3 + \overrightarrow{O_4O_3} \times \vec{P}_{4,3} \\ &+ m_3\overrightarrow{G_3O_3} \times (\vec{g} - \vec{a}_{G_3}) + m_3'\overrightarrow{E_3'O_2} \times (\vec{g} - \vec{a}_{E_3'}) - \vec{Q}_{1,3}'\end{aligned} \qquad 2.21$$

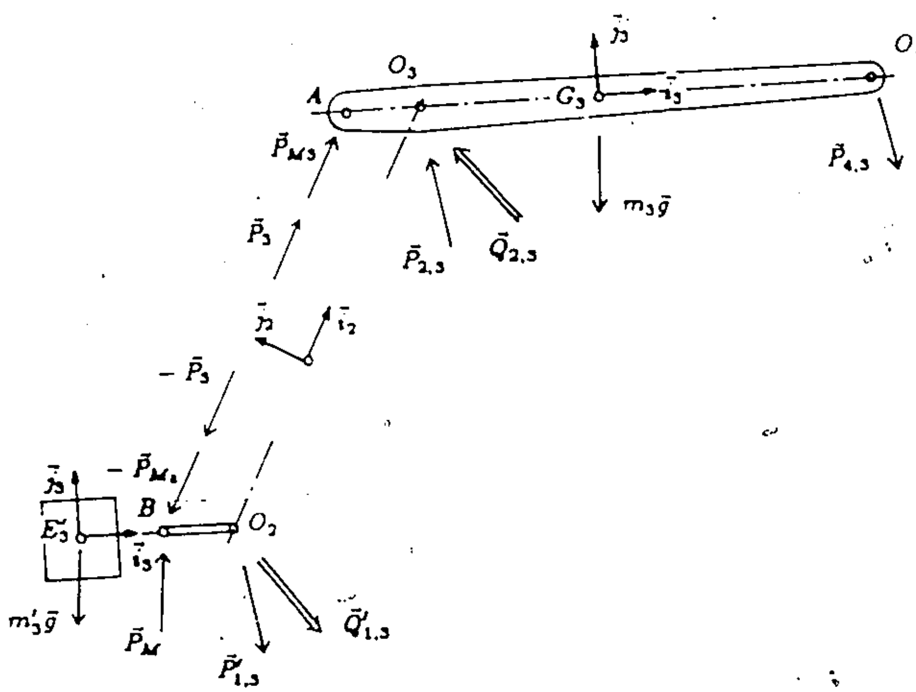

Figure 2.6. Free body Diagram for link 3 and its counterweight for the parallelogram configuration

Rotary and linear joints of industrial robots are generally constructed using rotary and linear ball bearings respectively. Furthermore, the vast majority of industrial robots utilizing a power screw and nut assembly for the conversion of rotary torque to linear force use ball type screws. Consequently, for all practical purposes, the friction forces and torques can be neglected. Neglecting the friction torque at joint O_2, the torque due to link 1 acting on the counterweight of link 3 is given by:

$$\vec{Q}'_{1,3} \cdot \vec{k}_3 = 0 \qquad 2.22$$

In the parallelogram type configuration, there is no driving torque between link 2 and link 3. Therefore,

$$\vec{Q}_{2,3} \cdot \vec{k}_3 = 0 \qquad 2.23$$

The driving torque of the upper arm due to the power screw and nut assembly is given by:

$$T_3 = \overrightarrow{O_2B} \times \vec{P}_M \qquad 2.24$$

Solving Equations 2.16 to 2.24 simultaneously and rearranging yields:

$$\begin{aligned} T_3 =& [(I_3 + I_3')\dot{\vec{\Omega}}_3] \cdot \vec{k} + [\vec{\Omega}_3 \times (I_3 + I_3')\vec{\Omega}_3] \cdot \vec{k} + (\overrightarrow{O_4O_3} \times \vec{P}_{4,3}) \cdot \vec{k} \\ &+ m_3[\overrightarrow{G_3O_3} \times (\vec{g} - \vec{a}_{G_3})] \cdot \vec{k} + m_3'[\overrightarrow{E_3'O_2} \times (\vec{g} - \vec{a}_{E_3'})] \cdot \vec{k} \end{aligned} \qquad 2.25$$

Because of the parallelogram configuration,

$$\overrightarrow{E_3'O_2} = \overrightarrow{E_3O_3}$$

Referring to Equation 2.10, the force acting at point O_4, $\vec{P}_{4,3}$ is given by:

$$\vec{P}_{4,3} = m(\vec{g} - \vec{a}_{O_4})$$

Taking into account these two remarks, one can see that Equations

2.13 and 2.25 are equivalent in their form. The only difference is the expression of the acceleration of the counterweight, $\vec{a}_{E_3'}$. Equation A.4.a in Appendix A gives the expression of the acceleration of the counterweight as follows:

$$\begin{aligned} \vec{a}_{E_3'} = & (\ddot{\theta}_{23} r_3 S_{23} + \dot{\theta}_1^2 r_3 C_{23} + \dot{\theta}_{23}^2 r_3 C_{23}) \cdot \vec{i}_1 \\ & + r_3(-\ddot{\theta}_{23} C_{23} + \dot{\theta}_{23}^2 S_{23}) \cdot \vec{j}_1 \\ & + r_3(\ddot{\theta}_1 C_{23} - 2\dot{\theta}_1 \dot{\theta}_{23} S_{23}) \cdot \vec{k}_1 \end{aligned} \qquad 2.26$$

From the above discussion and keeping in mind the assumptions outlined in Section 2.1, the equations of motion of the general configuration robot derived in Section 2.3 apply equally well to the parallelogram type of robot.

The parallelogram type robot configuration is chosen for the study of the active counterweight system.

Typical industrial robots utilizing the parallelogram type configuration are constructed with the lower arm not counterbalanced. Furthermore, there is no torque transmitted between lower and upper arms in the k-direction at point O_3 . That is to say:

$$m_2' = 0$$

$$I_2' = 0$$

and $\vec{Q}_{2,3} \cdot \vec{k} = 0$

Substituting these results and Equation 2.15 into Equation 2.14

gives:

$$\overrightarrow{O_3O_2} \times \vec{P}_{3,2} = \overrightarrow{O_3O_2} \times [m_3(\vec{g} - \vec{a}_{G_3}) + m(\vec{g} - \vec{a}_{O_4})]$$
$$+ \overrightarrow{O_3O_2} \times (\vec{P}_3 + \vec{P}_{M_3}) \qquad 2.27$$

For the last term in Equation 2.27 and with reference to Figure 2.6, both vectors $\overrightarrow{O_3O_2}$ and $(\vec{P}_3 + \vec{P}_{M_3})$ are in the same direction i_2. Therefore, the cross product

$$\overrightarrow{O_3O_2} \times (\vec{P}_3 + \vec{P}_{M_3})$$

is identically <u>zero</u>.

The driving torque equation is hence given by:

$$T_2 = \vec{Q}_{1,2} \cdot \vec{k}$$

$$T_2 = I_2\dot{\vec{\Omega}}_2 \cdot \vec{k} + [\vec{\Omega}_2 \times I_2\vec{\Omega}_2] \cdot \vec{k} + m_2[\overrightarrow{G_2O_2} \times (\vec{g} - \vec{a}_{G_2})] \cdot \vec{k}$$
$$+ \{\overrightarrow{O_3O_2} \times [m_3(\vec{g} - \vec{a}_{G_3}) + m(\vec{g} - \vec{a}_{O_4})]\} \cdot \vec{k} \qquad 2.28$$

None of the terms in this equation are function of the location of the counterweight r_3. Therefore, the position of the counterweight of the upper arm has no effect on the driving torque of the lower arm. This is a further advantage of the parallelogram type robot configuration.

The purpose of this study is to prove the feasibility of robot balancing through an active counterweight system. It is thus not necessary at this point to attempt to counterbalance both upper and lower arms simultaneously, since this would result in a complicated system from which the exact contribution of each active counterweight system cannot be easily isolated. Only the active balancing of the upper arm is considered in the following.

2.5. Expended form of the dynamic equations for the parallelogram type robot configuration

In this section, the equation of the torque acting on the upper arm is expended in order to express it as a function of the upper arm counterweight location r_3 . This form of the equation is necessary in order to be able to optimize T_3 with respect to the counterweight motion. With reference to Equation 2.13, each of the five terms comprising this equation are fully expended as follows:

1) $(I_3 + I_3')\dot{\vec{\Omega}}_3 \cdot \vec{k}$

As the result of the assumption that the robot links are symmetric along their longitudinal axis, the products of inertia terms are identically zero; the matrices of inertia for link 3 and for its counterweight are as follow:

$$I_3 = \begin{pmatrix} I_{X_3} & 0 & 0 \\ 0 & I_{Y_3} & 0 \\ 0 & 0 & I_{Z_3} \end{pmatrix}$$

and

$$I_3' = \begin{pmatrix} I'_{X_3} & 0 & 0 \\ 0 & I'_{Y_3} & 0 \\ 0 & 0 & I'_{Z_3} \end{pmatrix}$$

The absolute angular velocity of link 3 is given by;

$$\begin{aligned} \vec{\Omega}_3 &= \dot{\theta}_1 \vec{j}_1 + \dot{\theta}_2 \vec{k}_3 + \dot{\theta}_3 \vec{k}_3 \\ &= \dot{\theta}_1 S_{23} \vec{i}_3 + \dot{\theta}_1 C_{23} \vec{j}_3 + \dot{\theta}_{23} \vec{k}_3 \end{aligned} \qquad 2.29$$

The absolute angular acceleration is hence given by:

$$\dot{\vec{\Omega}}_3 = \left(\frac{d\vec{\Omega}_3}{dt}\right)_{F_3}$$

$$= (\ddot{\theta}_1 S_{23} + \dot{\theta}_1\dot{\theta}_{23}C_{23})\vec{i}_3 + (\ddot{\theta}_1 C_{23} - \dot{\theta}_1\dot{\theta}_{23}S_{23})\vec{j}_3 + \ddot{\theta}_{23}\vec{k}_3 \quad 2.30$$

Therefore,

$$(I_3 + I'_3)\dot{\vec{\Omega}}_3 = (I_{X_3} + I'_{X_3})(\ddot{\theta}_1 S_{23} + \dot{\theta}_1\dot{\theta}_{23}C_{23})\vec{i}_3$$
$$+ (I_{Y_3} + I'_{Y_3})(\ddot{\theta}_1 C_{23} - \dot{\theta}_1\dot{\theta}_{23}S_{23})\vec{j}_3$$
$$+ (I_{Z_3} + I'_{Z_3})\ddot{\theta}_{23}\vec{k}_3 \quad 2.31$$

The component of the torque along the z-axis is given by:

$$(I_3 + I'_3)\dot{\vec{\Omega}}_3 \cdot \vec{k} = (I_{Z_3} + I'_{Z_3})\ddot{\theta}_{23} \quad 2.32$$

2) $\underline{[\vec{\Omega}_3 \times (I_3 + I'_3)\vec{\Omega}_3] \cdot \vec{k}}$

The expression $\vec{\Omega}_3 \times (I_3 + I'_3)\vec{\Omega}_3$ can be written as:

$$\vec{\Omega}_3 \times (I_3 + I'_3)\vec{\Omega}_3 = \begin{bmatrix} \dot{\theta}_1 S_{23} \\ \dot{\theta}_1 C_{23} \\ \dot{\theta}_{23} \end{bmatrix} \times \begin{bmatrix} (I_{X_3} + I'_{X_3})\dot{\theta}_1 S_{23} \\ (I_{Y_3} + I'_{Y_3})\dot{\theta}_1 C_{23} \\ (I_{Z_3} + I'_{Z_3})\dot{\theta}_{23} \end{bmatrix}$$

Hence, the component of the torque along the z-axis is given by:

$$[\vec{\Omega}_3 \times (I_3 + I'_3)\vec{\Omega}_3] \cdot \vec{k} = (I_{Y_3} + I'_{Y_3} - I_{X_3} - I'_{X_3})\dot{\theta}_1^2 S_{23}C_{23} \quad 2.33$$

3) $\underline{m_3[\overrightarrow{G_3O_3} \times (\vec{g} - \vec{a}_{G_3})] \cdot \vec{k}_3}$

With reference to Figure 2.5, the vector $\overrightarrow{G_3O_3}$ is given by

$$\overrightarrow{G_3O_3} = -e_3\vec{i}_3$$
$$= -e_3(C_{23}\vec{i}_1 + S_{23}\vec{j}_1) \quad 2.34$$

Utilizing Equation 2.34, the expression $\overrightarrow{G_3O_3} \times (\vec{g} - \vec{a}_{G_3})$ can be written as:

$$\overrightarrow{G_3O_3} \times (\vec{g} - \vec{a}_{G_3}) = \begin{bmatrix} -e_3 C_{23} \\ -e_3 S_{23} \\ 0 \end{bmatrix} \times \begin{bmatrix} -a^X_{G_3} \\ -(g + a^Y_{G_3}) \\ -a^Z_{G_3} \end{bmatrix}$$

Hence, the component of the torque along the z-axis is given by:

$$m_3[\overrightarrow{G_3O_3} \times (\vec{g} - \vec{a}_{G_3})] \cdot \vec{k} = m_3 e_3[C_{23}(g + a^Y_{G_3}) - S_{23}a^X_{G_3}] \quad 2.35$$

Substituting for $a_{G_3}^X$ and $a_{G_3}^Y$ from Equations A.2.b and A.2.c in Appendix A into Equation 2.35 gives:

$$m_3[\overrightarrow{G_3O_3} \times (\vec{g} - \vec{a}_{G_3})] \cdot \vec{k} = m_3 e_3[C_{23}g + \ddot{\theta}_2 b_2 C_3 + \ddot{\theta}_{23} e_3 + S_3\dot{\theta}_2^2 b_2 + S_{23}\dot{\theta}_1^2(b_2C_2 + e_3C_{23})] \qquad 2.36$$

4) $\underline{m_3'[\overrightarrow{E_3'O_2} \times (\vec{g} - \vec{a}_{E_3'})] \cdot \vec{k}}$

With reference to Figure 2.5, the vector $\overrightarrow{E_3'O_2}$ represents the radial displacement of the counterweight and is given by:

$$\begin{aligned}\overrightarrow{E_3'O_2} &= r_3\vec{i}_3 \\ &= r_3(C_{23}\vec{i}_1 + S_{23}\vec{j}_1)\end{aligned} \qquad 2.37$$

Substituting Equation 2.37 into the expression 4) above gives:

$$\overrightarrow{E_3'O_2} \times (\vec{g} - \vec{a}_{E_3'}) = \begin{bmatrix} r_3C_{23} \\ r_3S_{23} \\ 0 \end{bmatrix} \times \begin{bmatrix} -a_{E_3'}^X \\ -(g + a_{E_3'}^Y) \\ -a_{E_3'}^Z \end{bmatrix}$$

The component of the torque along the z-axis is given by:

$$m_3'[\overrightarrow{E_3'O_2} \times (\vec{g} - \vec{a}_{E_3'})] \cdot \vec{k} = -m_3' r_3[C_{23}(g + a_{E_3'}^Y) - S_{23}a_{E_3'}^X] \qquad 2.38$$

Substituting for $a_{E_3'}^X$ and $a_{E_3'}^Y$ from Equations A.4.b and A.4.c in Appendix A into Equation 2.38 gives:

$$m_3'[\overrightarrow{E_3'O_2} \times (\vec{g} - \vec{a}_{E_3'})] \cdot \vec{k} = -m_3' r_3[C_{23}g - \ddot{\theta}_{23} r_3 - \dot{\theta}_1^2 r_3 C_{23} S_{23}] \qquad 2.39$$

5) $\underline{m_3[\overrightarrow{O_4O_3} \times (\vec{g} - \vec{a}_{O_4})] \cdot \vec{k}}$

The expression 5) is similar to that in 3) above. With reference to Figure 2.5, replacing e_3 by b_3, m_3 by m, and the acceleration $\vec{a}_{G_3}$ by $\vec{a}_{O_4}$ in Equation 3.36 gives:

$$m[\overrightarrow{O_4O_3} \times (\vec{g} - \vec{a}_{O_4})] \cdot \vec{k} = mb_3[C_{23}g + \ddot{\theta}_2 b_2 C_3 + \ddot{\theta}_{23} b_3 + S_3\dot{\theta}_2^2 b_2 + S_{23}\dot{\theta}_1^2(b_2C_2 + b_3C_{23})] \qquad 2.40$$

Substituting Equations 2.32 , 2.33 , 2.36 , 2.39 and 2.40 into

Equation 2.13 gives:

$$\begin{aligned} T_3 = & (I_{Z_3} + I'_{Z_3})\ddot{\theta}_{23} + (I_{Y_3} + I'_{Y_3} - I_{X_3} - I'_{X_3})\dot{\theta}_1^2 S_{23} C_{23} - m'_3 r_3 (C_{23} g - \ddot{\theta}_{23} r_3 - \dot{\theta}_1^2 r_3 C_{23} S_{23}) \\ & + m_3 e_3 [C_{23} g + \ddot{\theta}_2 b_2 C_3 + \ddot{\theta}_{23} e_3 + S_3 \dot{\theta}_2^2 b_2 + S_{23} \dot{\theta}_1^2 (b_2 C_2 + e_3 C_{23})] \\ & + m b_3 [C_{23} g + \ddot{\theta}_2 b_2 C_3 + \ddot{\theta}_{23} b_3 + S_3 \dot{\theta}_2^2 b_2 + S_{23} \dot{\theta}_1^2 (b_2 C_2 + b_3 C_{23})] \end{aligned} \tag{2.41}$$

It should be noted here that the components of the torque along i and j are absorbed in the joint structure and do not contribute to the driving torque.

Equation 2.41 can also be rewritten as follows:

$$T_3 = a r_3^2 + b r_3 + c \tag{2.42}$$

where

$$a = m'_3 (\ddot{\theta}_{23} + \dot{\theta}_1^2 C_{23} S_{23}) \tag{2.43}$$

$$b = -m'_3 g C_{23} \tag{2.44}$$

$$\begin{aligned} c = & \ddot{\theta}_{23} (I_{Z_3} + I'_{Z_3} + m_3 e_3^2 + m b_3^2) + g C_{23} (m_3 e_3 + m b_3) \\ & + \dot{\theta}_1^2 S_{23} C_{23} (I_{Y_3} + I'_{Y_3} - I_{X_3} - I'_{X_3} + m_3 e_3^2 + m b_3^2) \\ & + (\ddot{\theta}_2 C_3 + \dot{\theta}_2^2 S_3 + \dot{\theta}_1^2 S_{23} C_2)(m_3 e_3 + m b_3) b_2 \end{aligned} \tag{2.45}$$

The driving torque of the upper arm is thus a quadratic expression of the location of the active counterweight.

2.6. Upper arm torque minimization problem

Minimizing the driving torque of the upper arm can therefore be achieved by solving the following equation:

$$ar_3^2 + br_3 + c = 0 \qquad 2.46$$

It is interesting to notice that whenever the discriminant of Equation 2.46 is positive, two locations for the counterweight exist for which the driving torque of link 3 is equally zero. As far as the real physical problem is concerned, the counterweight will not travel from $-\infty$ to $+\infty$, but its motion will be restricted inside boundary positions. Therefore, whenever a root for Equation 2.46 happens to be located in between these physical limits, the motion of the active counterweight to this particular position reduces the driving torque of the upper arm to a zero value. In the case where there is no root inside the boundaries, the one of the two extreme position for which the torque is minimum is chosen to locate the active counterweight.

In the next section, the optimization process is fully detailed and simulated given the actual shape of the upper arm torque curves for various counterweight locations.

3.SIMULATIONS

In this chapter, a comparison is conducted between the performances of a standard industrial revolute robot, the ASEA Irb-6, equipped with an active counterweight system, and the performances of the same robot when equipped with the conventional fixed counterweight system. To carry out this comparison, a general trajectory is chosen and the performances of the robot when equipped with the fixed counterweight is simulated. A realistic range of displacement for the active counterweight system is chosen. The location of that range along the axis of the upper arm is optimised in order to statically minimize the torque for a given payload. This operation yields the concept of a "quasistatic counterweight".

The dynamic counterweight is allowed to traverse its range of motion in order to minimize the driving torque of the upper arm around zero whenever possible. Power consumptions are compared for both cases. The ASEA Irb-6 robot has a general revolute configuration. Thus the comparison carried out in this chapter may be easily extended to examine the performances of any revolute robot equipped with the conventional counterweight system to that when the robot is equipped with an active counterweight system.

3.1. Robot arm used for analysis and testing

The ASEA Irb 6 shown on Figure 3.1 is a parallelogram type revolute robot manipulator mostly used in industry for assembly and welding purposes. With reference to Figure 3.1, the fixed counterweight (F) that balances the upper arm (U) is to be replaced by the active counterweight. The maximum payload this robot can carry is 6 kg and the maximum velocity of its tip point is 2.5 m/s when both arms are fully extended.

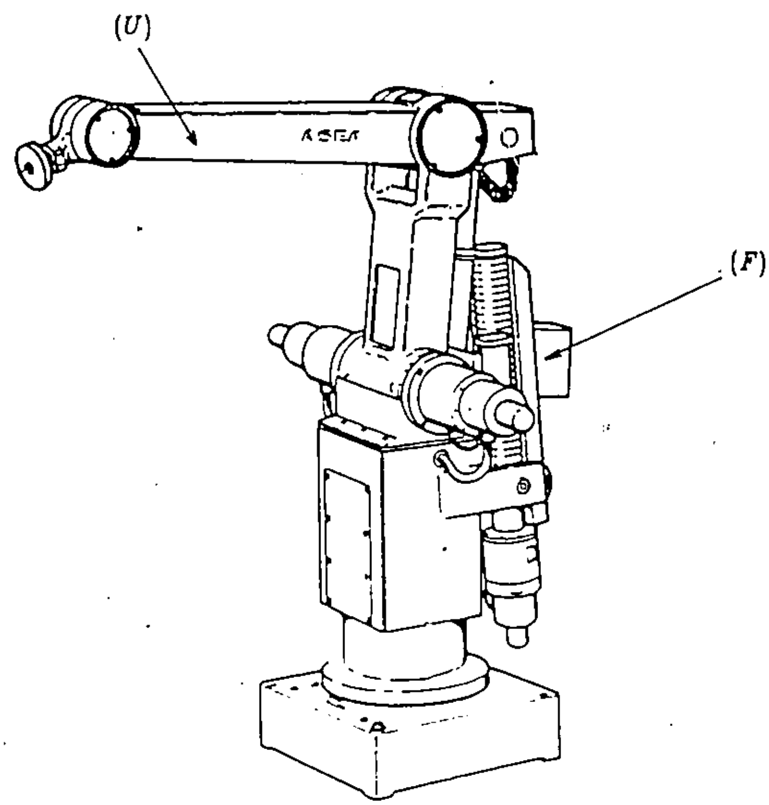

Figure 3.1. ASEA Irb 6 robot arm

3.2. The trajectory used for the simulation

A trajectory is chosen such that it results in the most demanding conditions of maximum angular velocity for the first three links while the tip of the robot is travelling close to, or along its envelope. Figure 3.2 shows a sketch of the robot configuration along this trajectory.

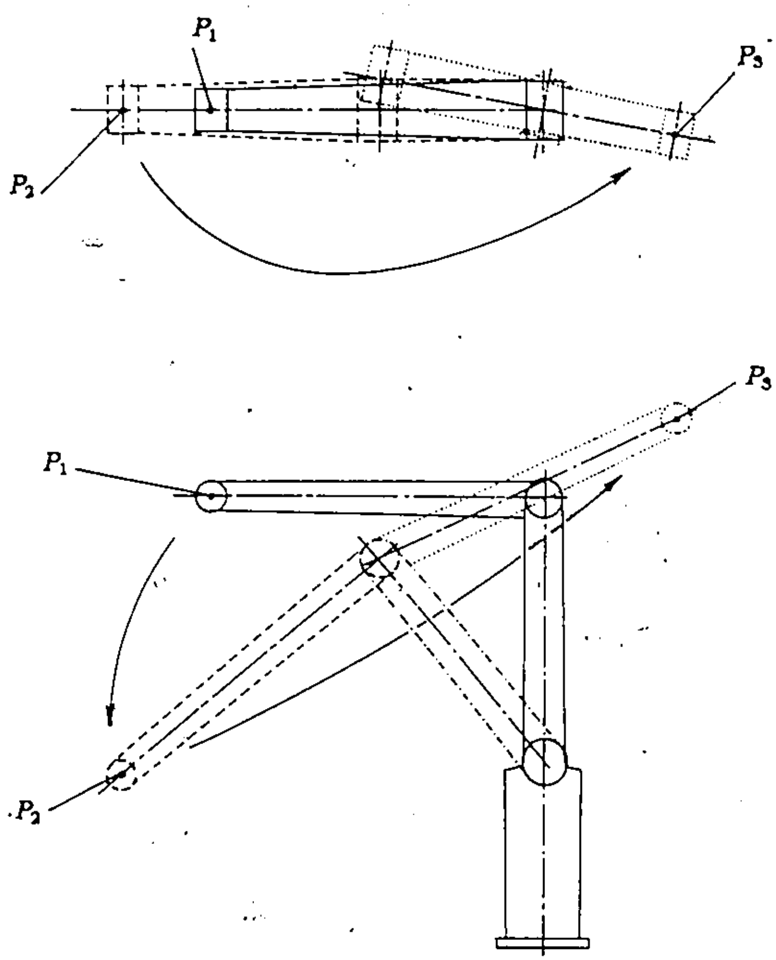

Figure 3.2. Trajectory

With reference to the figure, the payload travels from P_1 to P_3 via P_2, and returns to P_1 through P_2 again. The robot is made to stop at each of the defined points.

Figures 3.3 to 3.5 show the kinematics of the three primary joints of the robot, joint 1 for the base link, joint 2 for the lower arm and joint 3 for the upper arm as they are defined on Figure 2.1. It has to be noted here that θ_3 is the angular position of the upper arm measured with respect to the longitudinal axis of link 2, and θ_2 is the angular position of the lower arm with respect to the horizontal. Therefore the actuator of link 2 (lower arm) inscribes the angle θ_2 whereas because of the parallelogram configuration, the actuator of link 3 (upper arm) inscribes the angle ($\theta_2 + \theta_3$).

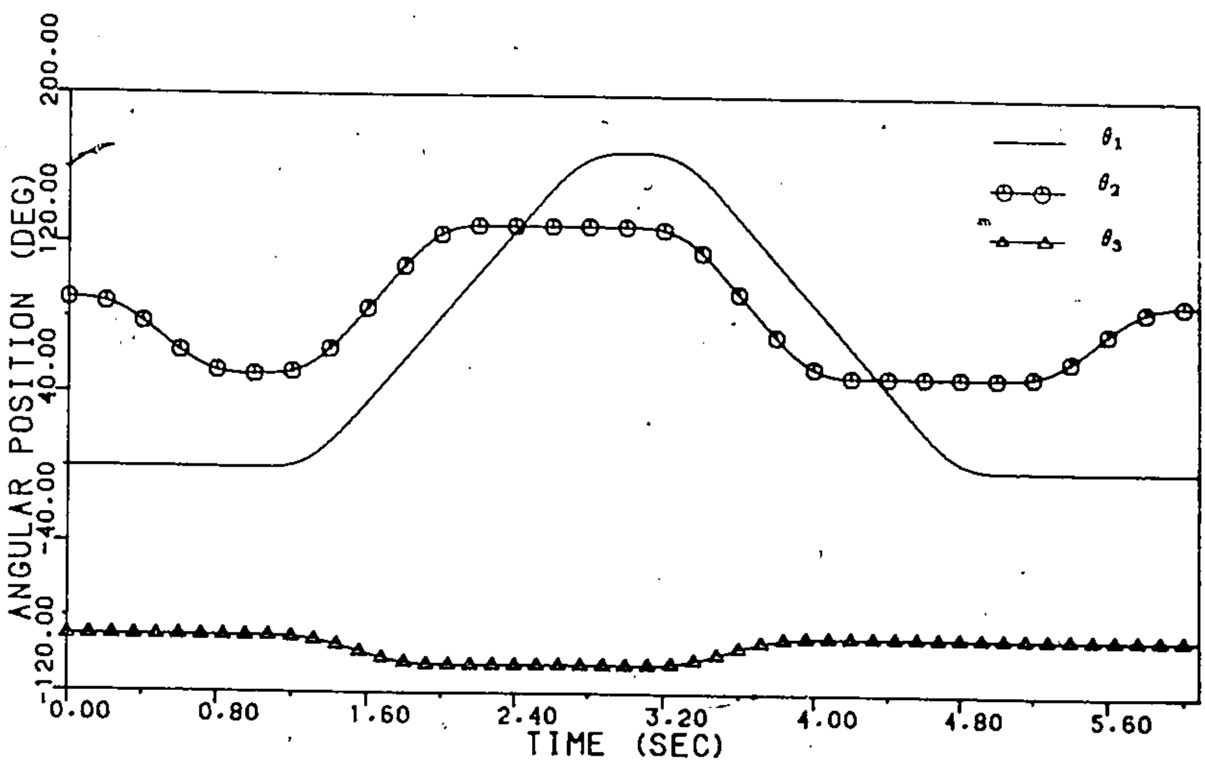

Figure 3.3. Angular positions of the 3 first links

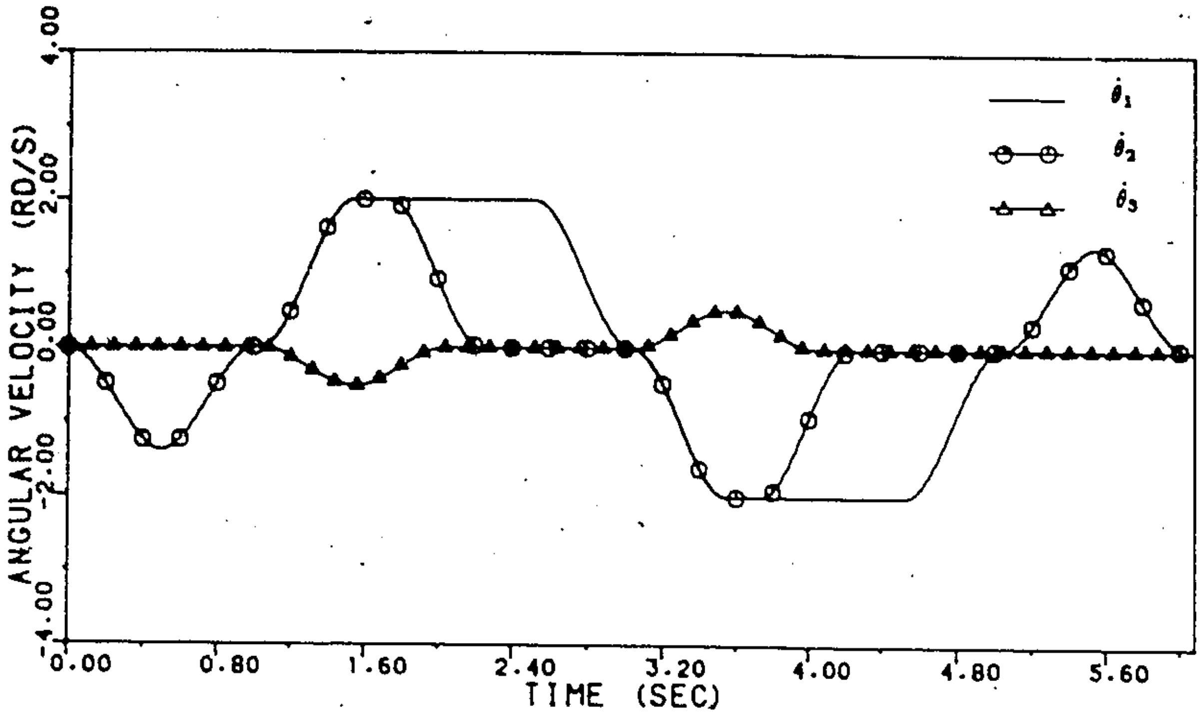

Figure 3.4. Angular velocities of the 3 first links

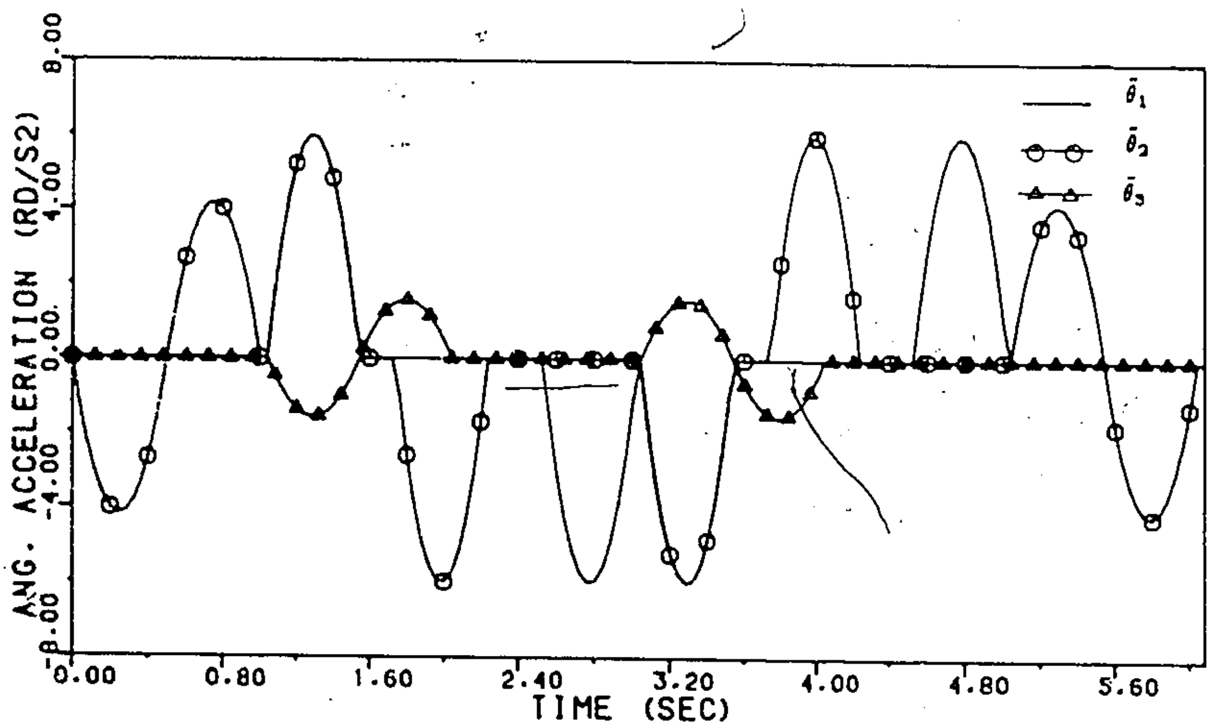

Figure 3.5. Angular accelerations of the 3 first links

3.3. Concept of the active counterweight system

Equation 2.41 is used to calculate the joint torque with respect to time for a given counterweight location r_3. The equation gives the torque of the upper arm as a quadratic function of the location of the active counterweight as follows:

$$T_3 = ar_3^2 + br_3 + c$$

The location r_3 of the active counterweight can be expressed as the sum of a reference position R_3 and a relative position δ_3, as follows:

$$r_3 = R_3 + \delta_3$$

where δ_3 varies between 0 and Δ_3, and Δ_3 is the range of motion of the active counterweight.

The difference in torque required to move the upper arm is hence calculated as follows:

$$\Delta T_3 = a(R_3 + \Delta_3)^2 + b(R_3 + \Delta_3) + c - (aR_3^2 + bR_3 + c)$$

$$= (2a\Delta_3)R_3 + a\Delta_3^2 + b\Delta_3 \qquad 3.1$$

Equation 3.1 as well as the plot of that equation shown in Figure 3.6.a shows that ΔT_3 varies linearly as the range of movement of the active counterweight is translated along link 3. The intercept of the linear relation is given by ($a\Delta_3^2 + b\Delta_3$) and corresponds to the condition where this reference is located at the joint of the link, R_3 = 0. The slope of the relation is given by ($2a\Delta_3$).

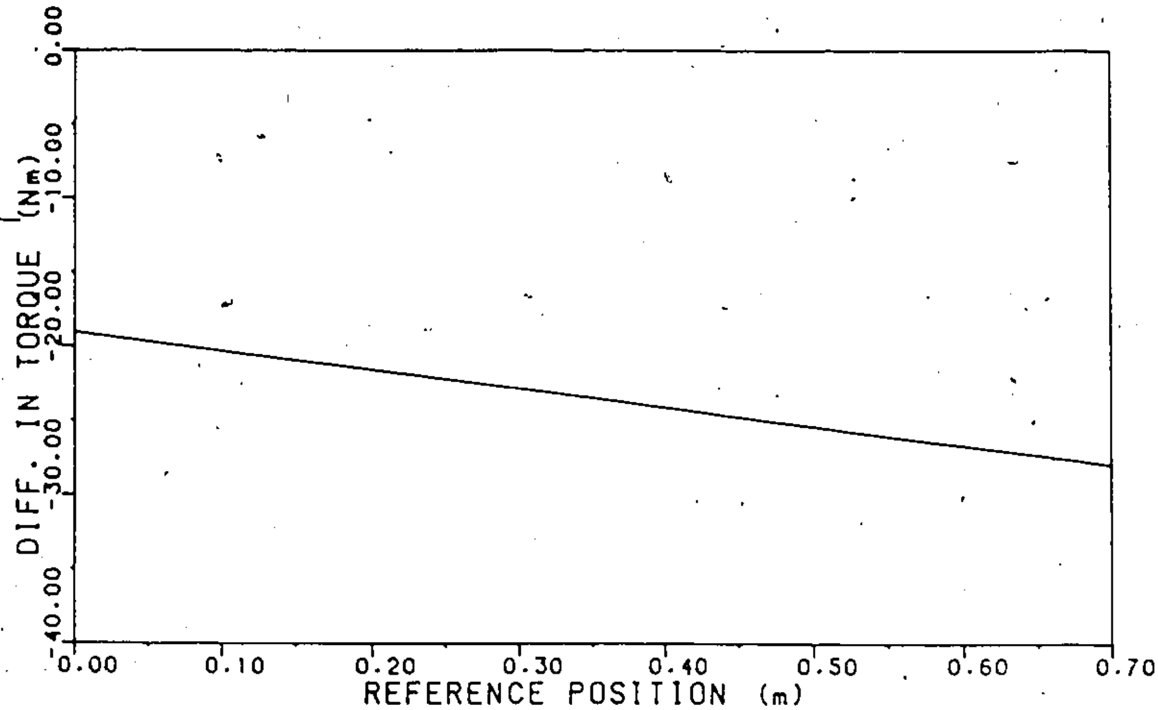

Figure 3.6.a. Difference in torque

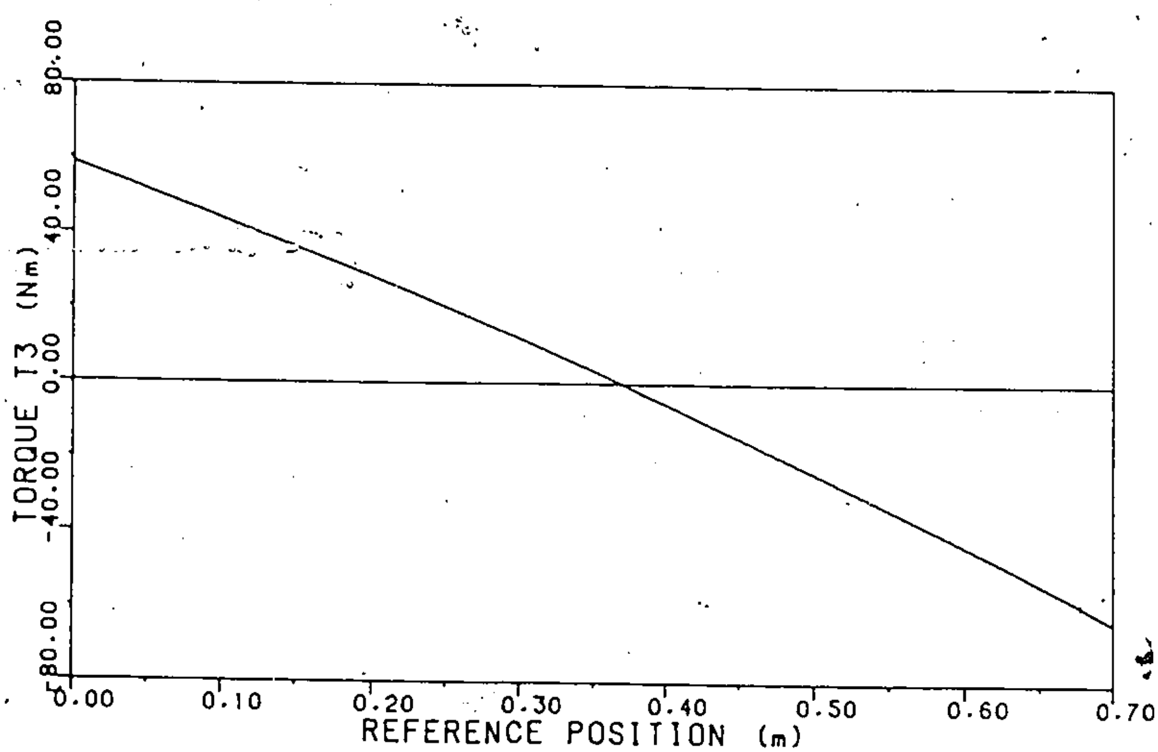

Figure 3.6.b. Torque -vs- reference position

The torque required to move the upper arm when the active counterweight is located at the reference position, R_3, is given by:

$$T_3(R_3) = aR_3^2 + bR_3 + c \qquad 3.2$$

A plot of this equation is shown in Figure 3.6.b. The plot shows that it is possible to bias this range of motion of the active counterweight so as to minimize the torque required to move the upper arm.

When considering the concept of active counterweight, two different approaches may be considered; these are:

a) The total mass of the counterweight is allowed to move as the robot traverses its trajectory.

b) The mass of the counterweight is divided into two parts; the first part is positioned so as to balance the payload and is locked in place during the motion of the robot. This part is termed the "quasistatic counterweight". The second part of the counterweight is allowed to move as the robot traverses its trajectory so as to balance the dynamic forces resulting from the robot motion. This part is termed "dynamic counterweight".

The second approach is used in this work since it requires less counterweight mass to be dynamically moved. Figure 3.7 shows a schematic diagram of the proposed active counterweight system. With reference to the figure, the quasistatic counterweight is designed to be approximately one third of the total counterweight mass. Furthermore, the dynamic counterweight is moved relative to the quasistatic one.

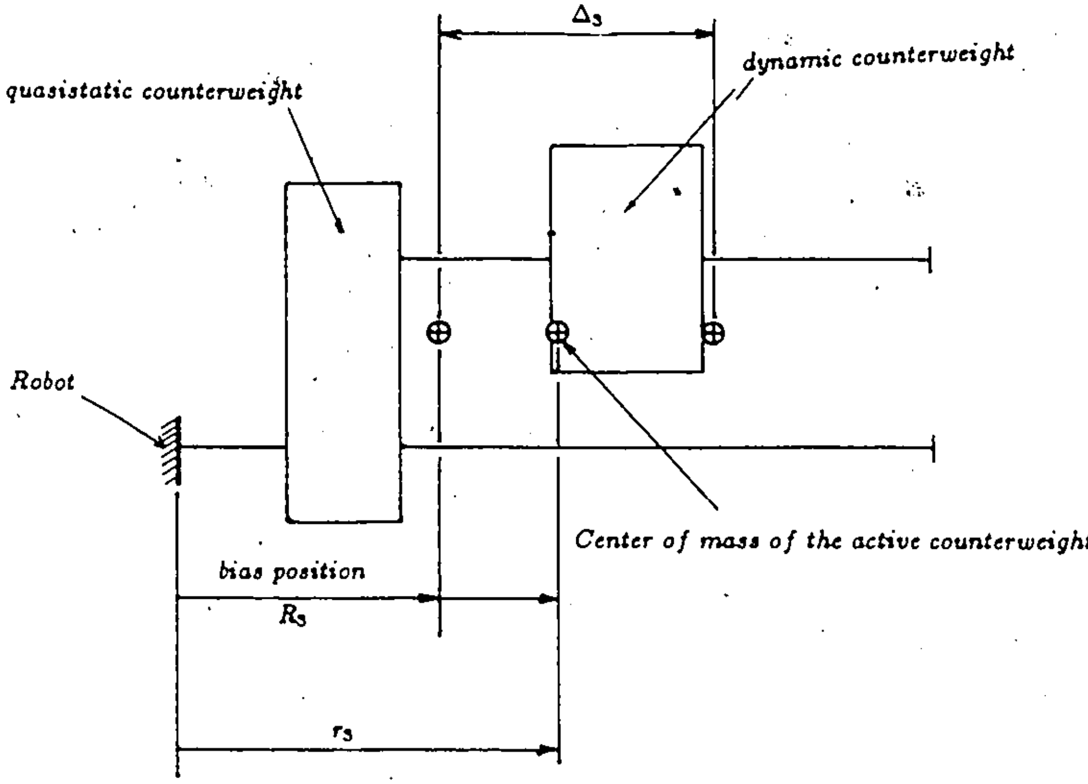

Figure 3.7. Active counterweight system

Figure 3.8 shows the torque curve for three counterweight locations; these are:

a) The standard fixed counterweight location supplied by the manufacturer.

b) A location corresponding to the fully retracted position of the dynamic system, and

c) A location corresponding to the fully extended position of the dynamic counterweight.

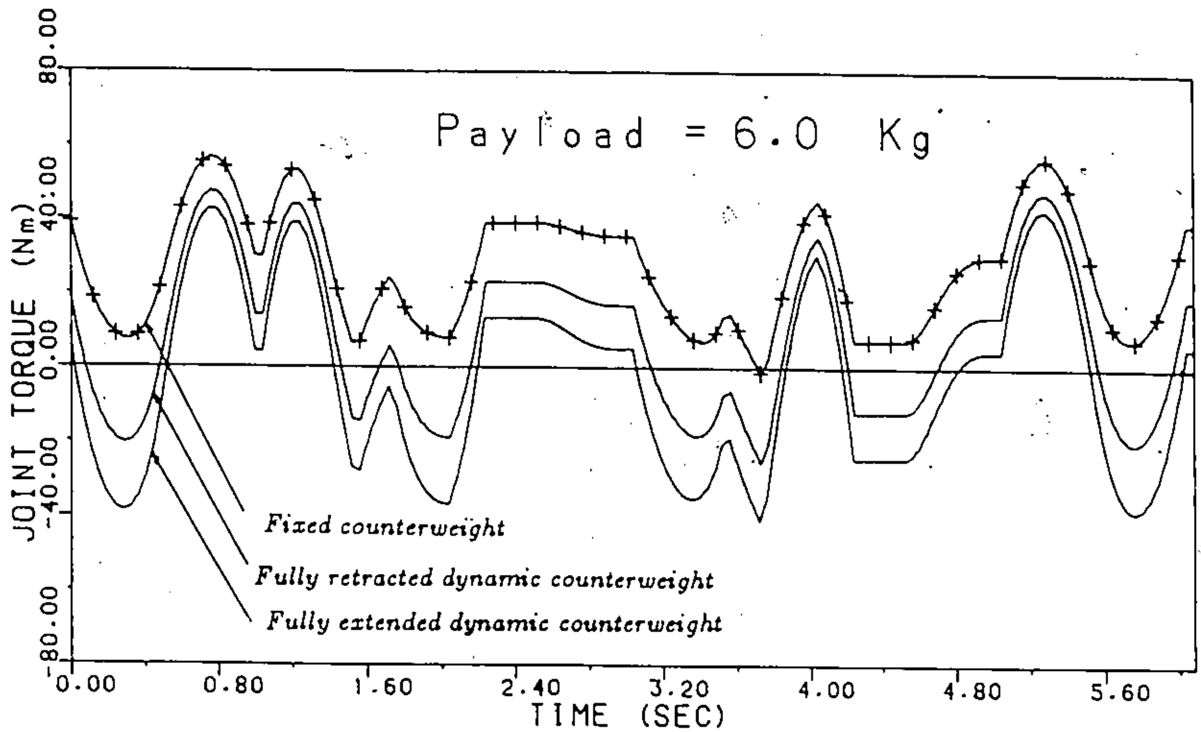

Figure 3.8. Torque curves for the upper arm

With reference to Figure 3.8, the difference between the torque curves for the fully retracted and fully extended dynamic counterweight represents the range of torques that would be required to move the upper arm as the dynamic counterweight traverses its range of motion. The position of the two curves themselves is governed by the bias position, R_3, of the quasistatic counterweight as can be deduced from Equation 3.2 and Figure 3.6.b. This bias also affects the space between the two curves as can be deduced from Equation 3.1 and Figure 3.6.a.

Assuming that the drive motor of the upper arm is capable of delivering the same amount of torque in the forward and reverse rotation, the bias R_3 can be calculated as follows:

Let the middle of the range of motion of the dynamic counterweight correspond to a torque T_3, where T_3 is the average torque required from the drive motor as the upper arm traverses its trajectory. This condition results in expending the range between the maximum of the required torque and the torque available from the axis drive. Substituting the condition in Equation 2.42 gives:

$$T_3 = a\left(R_3 + \frac{\Delta_3}{2}\right)^2 + b\left(R_3 + \frac{\Delta_3}{2}\right) + c$$

or:

$$R_3 = \frac{-(a\Delta_3 + b) \pm \sqrt{b^2 - 4ac + 4aT_3}}{2a}$$

3.4. Dynamic counterweight motion

Once the upper arm has been balanced through the quasistatic counterweight for a given payload, the dynamic counterweight location that provides a minimum absolute value for the driving torque of the upper arm can be defined by solving Equation 2.46. When one or both roots of this equation fall within the range of motion of the dynamic counterbalance, the root indicates the location where the torque required to move the upper arm is identically zero.

In the case where none of the roots fall within the range of motion of the dynamic counterbalance, one of the two extrema of the range would yield the minimum of the driving torque.

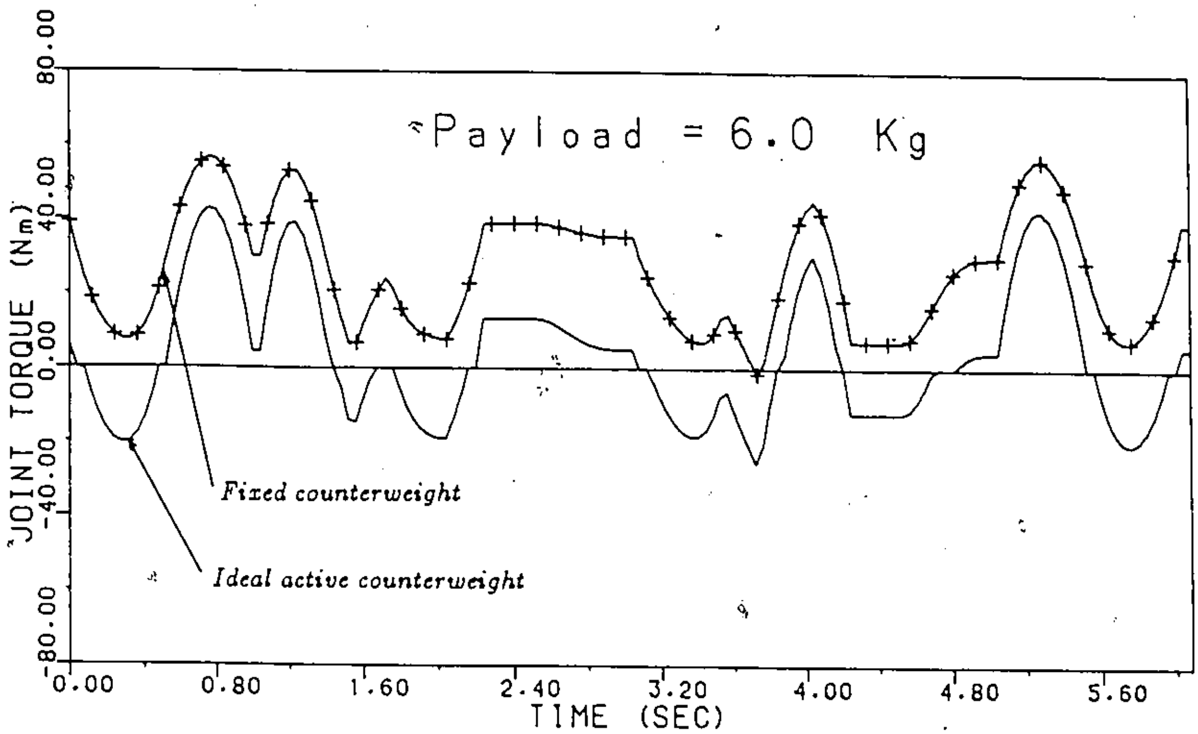

Figure 3.9. Ideal torque curve

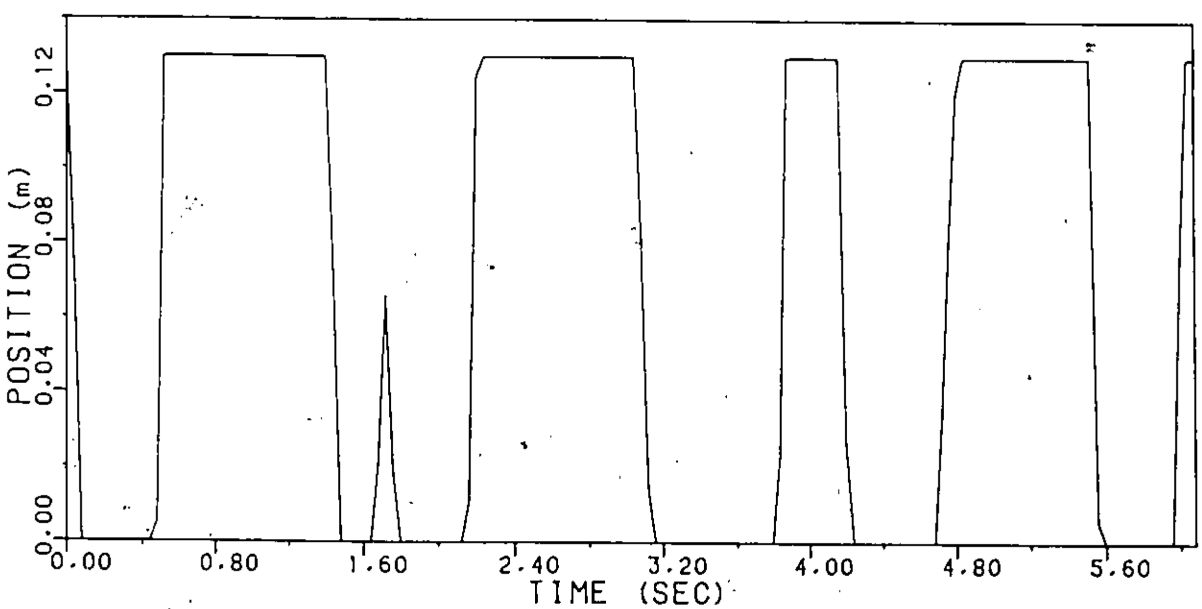

Figure 3.10. Ideal dynamic counterweight displacement

Figure 3.9 shows the torque curve under the assumption that the dynamic counterweight can reach its desired location instantaneously; the corresponding displacement of the active counterweight is shown in Figure 3.10.

The large displacements of the dynamic counterweight that have to be carried out rapidly yield non realistic maximum counterweight velocities and accelerations in the order of 3.1 m/s and 78 m/s^2 respectively.

The dynamic counterweight drive of the prototype is capable of a maximum acceleration of 7 m/s^2 and a maximum velocity of 0.2 m/s. Figure 3.11 shows the torque plots when these practical limits are imposed on the velocity and the acceleration of the dynamic counterweight drive. The torque plot for the case where the fixed counterweight balances the upper arm is shown in Figure 3.11 for comparison purposes.

Figure 3.12 shows the displacement of the dynamic counterweight corresponding to the plots of Figure 3.11.

With reference to Figure 3.12, a finite amount of time is now necessary for the active counterweight to move from one extreme location to the other. As a result of this limitation, the drive torque of the joint is no longer instantaneously minimum when a change in the dynamic counterweight location is required.

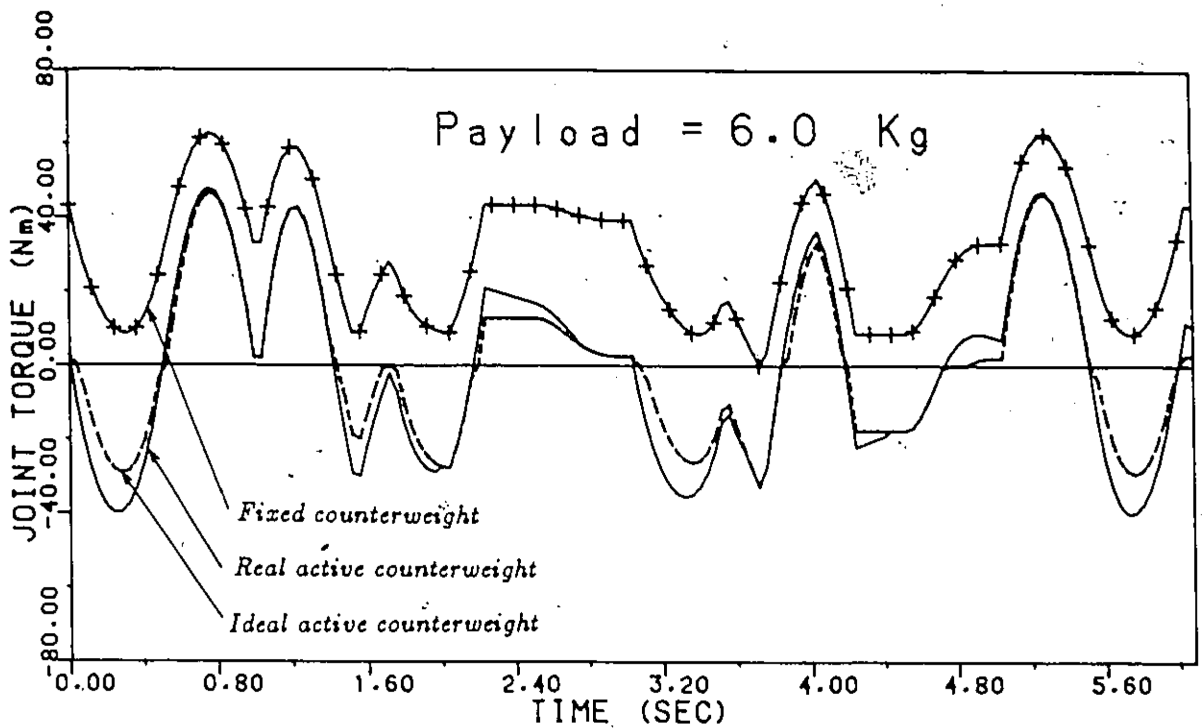

Figure 3.11. Real torque curve

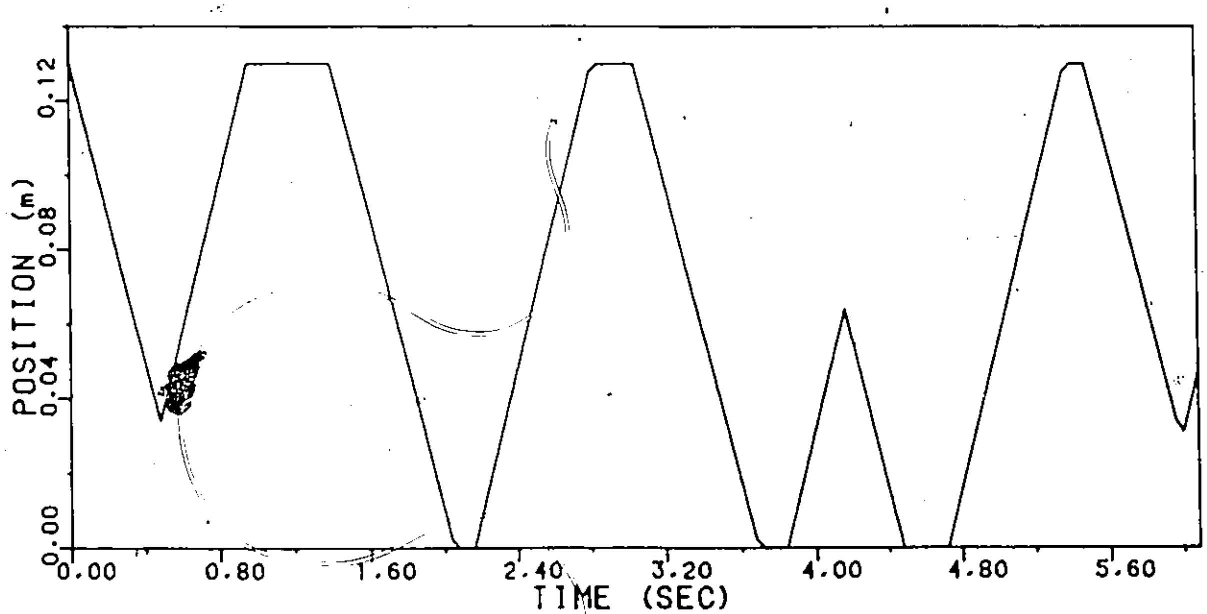

Figure 3.12. Dynamic counterweight displacement

3.5. Performance enhancement due to the active counterweight

Figure 3.13 shows the torque plots for the upper arm drive when the robot arm is overloaded by 17%. This corresponds to a 7 kg payload. The Figure shows the limit of the torque available from the upper arm drive to be approximately 60 Nm. The torque required to carry the payload of 7 kg, when the robot is equipped with the standard fixed counterweight, exceeds that limit at a few points, thus indicating the inability of the robot to carry such a payload. The torque plots when the robot is equipped with the active counterweight for the case of an ideal dynamic counterweight motion as well as for the practical one are also shown on this figure.

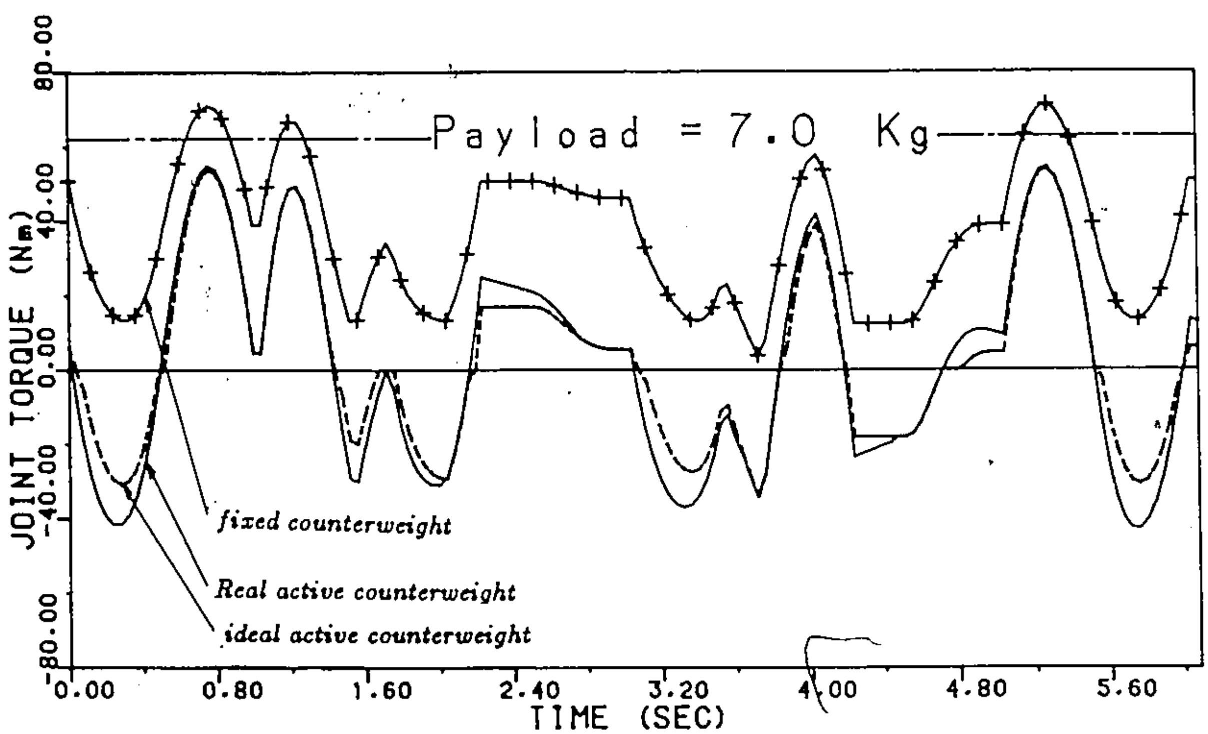

Figure 3.13. Torque curves for a 7 kg payload

The quasistatic counterweight has been adjusted in this case so as to equalize the peaks of the torque curve on either sides of the 0 Nm axis. These plots show that when the active counterweight system is utilized, the robot can carry the 7 kg payload with no degradation in its performances. The maximum payload that can be carried by the robot when equipped with the active counterweight can be derived from equation 2.42.

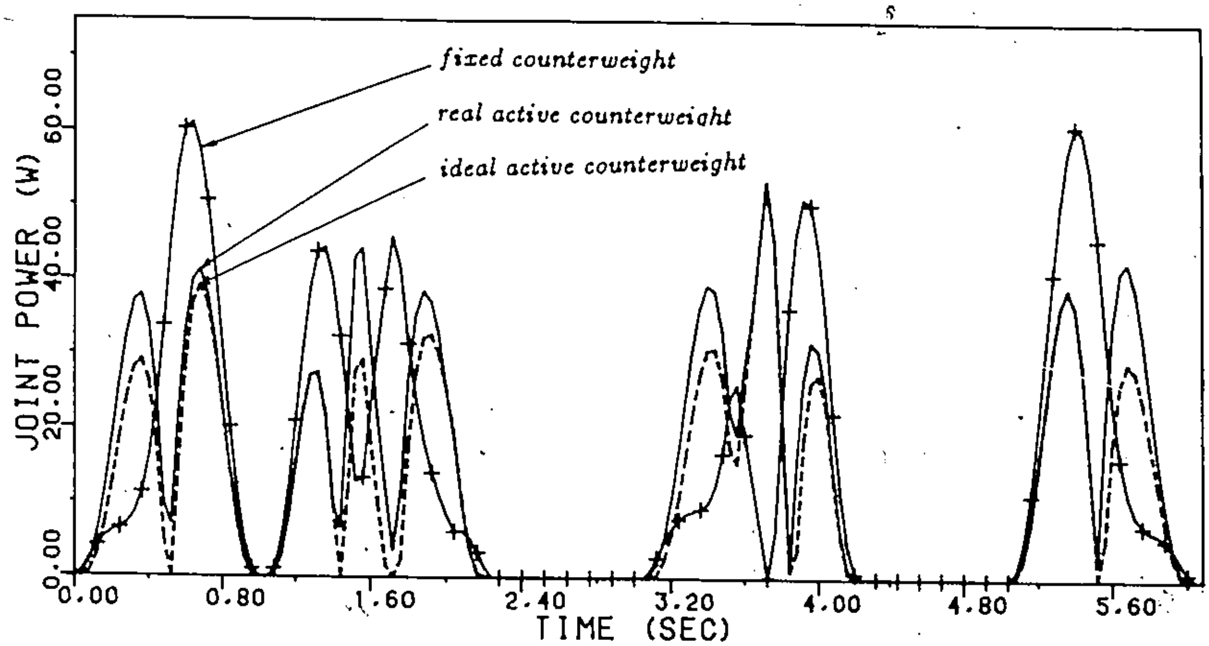

Figure 3.14. Power curves

Figure 3.14 shows the power consumption, for a payload of 6 kg, when the robot is equipped with the fixed counterweight and with the active counterweight system. With reference to the figure, the power consumption of the upper link drive, when the robot is equipped with the active counterweight system, is globally lower than for the case where the fixed counterweight is utilized.

3.5. Force required to drive the dynamic counterweight

Figure 3.15 shows the Free Body Diagram of the dynamic counterweight.

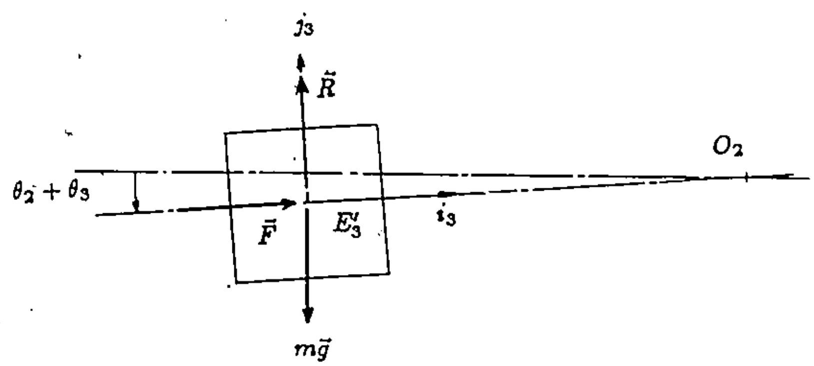

Figure 3.15. Active counterweight Free Body Diagram

With reference to the figure and assuming negligible friction in the i_3-direction, the sum of forces acting on the dynamic counterweight is given by:

$$m\vec{a} = m\vec{g} + \vec{F} + \vec{R} \qquad 3.3$$

where m is the mass of the dynamic counterweight.

The balance of forces for the components of Equation 3.3 along the i_3 -axis is given by:

$$ma_X = -mgS_{23} + F \qquad 3.4$$

With reference to Equation A.10 in Appendix A, the acceleration of the dynamic counterweight is expressed as follows:

$$\begin{aligned}\vec{a} = \quad & (-\ddot{r}_3 + r_3(\dot{\theta}_1^2 C_{23}^2 + \dot{\theta}_{23}^2))\vec{i}_3 \\ & - (r_3\ddot{\theta}_{23} + 2\dot{r}_3\dot{\theta}_{23} + r_3\dot{\theta}_1^2 C_{23} S_{23})\vec{j}_3 \\ & + (r_3(\ddot{\theta}_1 C_{23} - 2\dot{\theta}_1\dot{\theta}_{23}S_{23}) + 2\dot{r}_3\dot{\theta}_1 C_{23})\vec{k}_3 \qquad 3.5\end{aligned}$$

Substituting Equation 3.5 into Equation 3.4 gives:

$$F = -m(\ddot{r}_3 - r_3(\dot{\theta}_1^2 C_{23}^2 + \dot{\theta}_{23}^2) - gS_{23}) \qquad 3.6$$

Figure 3.16, 3.17 and 3.18 show the acceleration, force and power consumption of the dynamic counterweight as it traverses the trajectory of Figure 3.12.

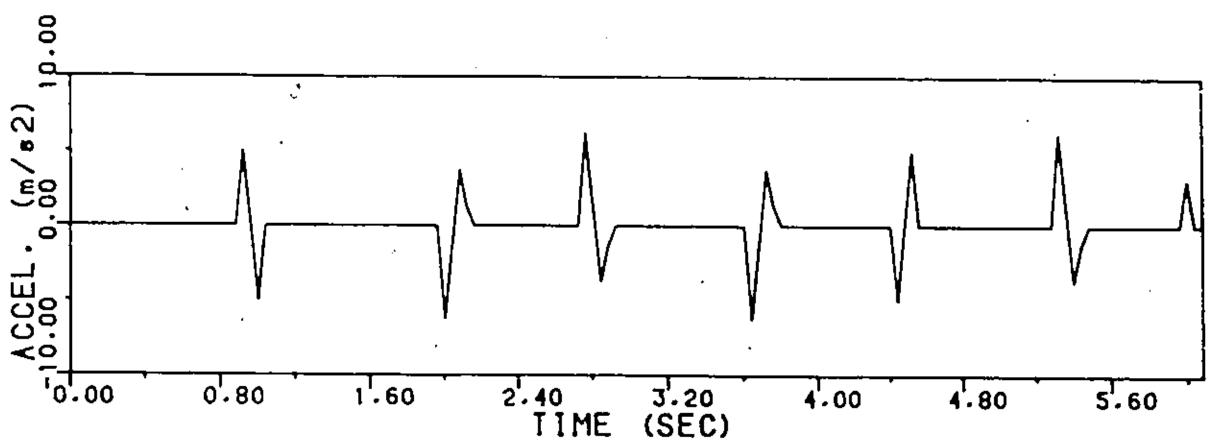

Figure 3.16. Acceleration of the dynamic counterweight

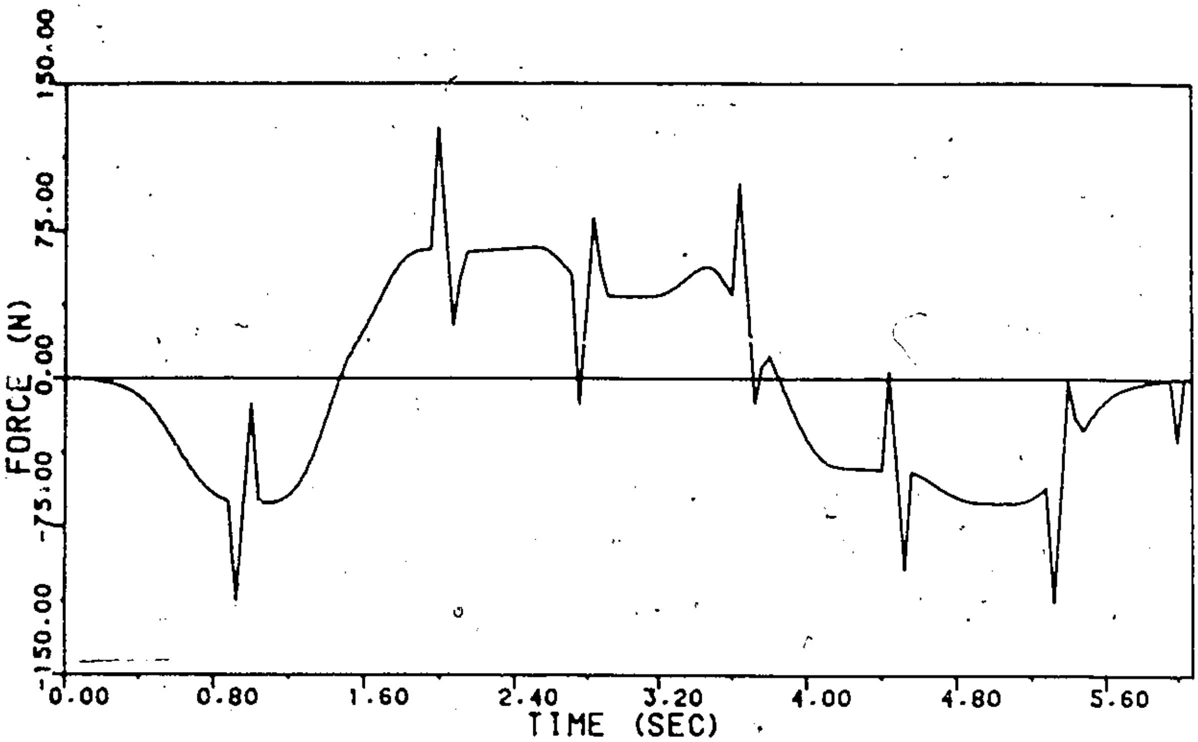

Figure 3.17. Force necessary to position the dynamic counterweight

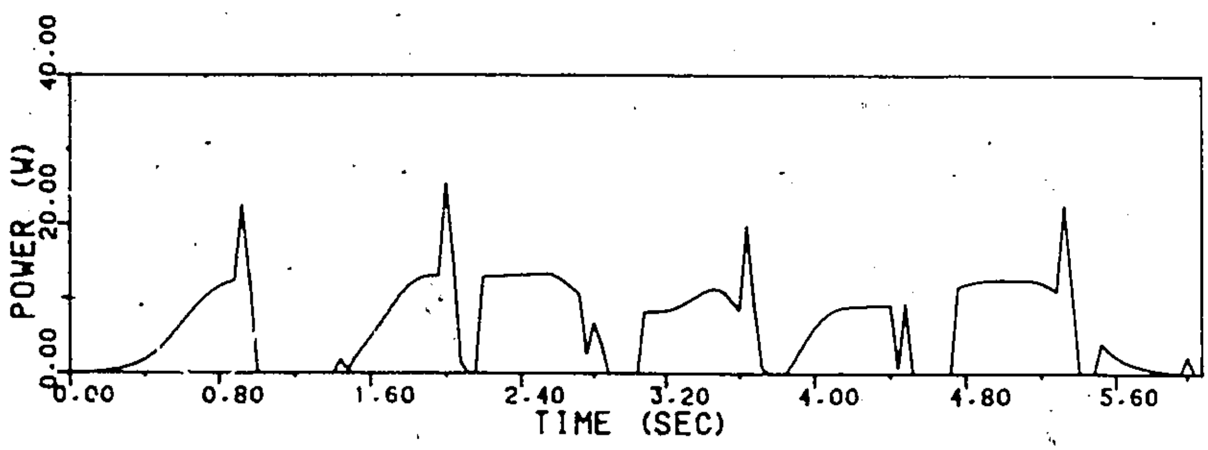

Figure 3.18. Power necessary to move the dynamic counterweight

The wave curve shown in Figure 3.17 is essentially due to the term ($m\,gS_{23}$) of Equation 3.6 that represents the effect of the inclination of the upper arm resulting from the motion of the robot along the trajectory. The sharp peacks, on the other hand, represent the force that result from the accelerations and decelerations of the dynamic counterweight which are shown in Figure 3.16. Power requirements for the dynamic counterweight drive remain reasonable as shown in Figure 3.18.

As a result of the dynamic study and the simulation, the characteristics of the active counterweight system for the ASEA Irb-6 robot are summarized as follows:

- The total mass of the counterweight system is 15 kg. This mass is equal to that of the fixed counterweight supplied by the manufacturer.
- The active counterweight system is composed of two parts:
  a) a quasistatic counterweight of 5 kg;
  b) a dynamic counterweight of 10 kg.
- The maximum acceleration of the dynamic counterweight is 7 m/s^2.
- The maximum velocity of the dynamic counterweight is 0.2 m/s.

4. PROTOTYPE DESIGN AND DESCRIPTION

A prototype of the active counterweight system has been designed and constructed so as to verify experimentally the concept and feasibility of such a counterbalancing system. The prototype has been installed on an ASEA Irb-6 robot. Figure 4.1 shows a schematic diagram of the prototype system.

The active counterweight system uses the dynamic model of the robot and counterweight to find the optimum location of the two counterweights. Feedback information about the kinematics, angular positions, velocities and accelerations of the three first links of the robot are fed into the model from the robot sensors. The system consists essentially of four distinct parts as follows:

1) The mechanical system, consisting of the dynamic and the quasistatic counterweights.
2) The data acquisition and processing system necessary to provide the balancing coordinator program with the kinematics of the robot arm.
3) The balancing coordinator program that defines the location of the counterweights, based upon the payload and robot trajectory, in order to minimize the torque required from the upper arm .
4) The control system for the quasistatic and dynamic counterweights.

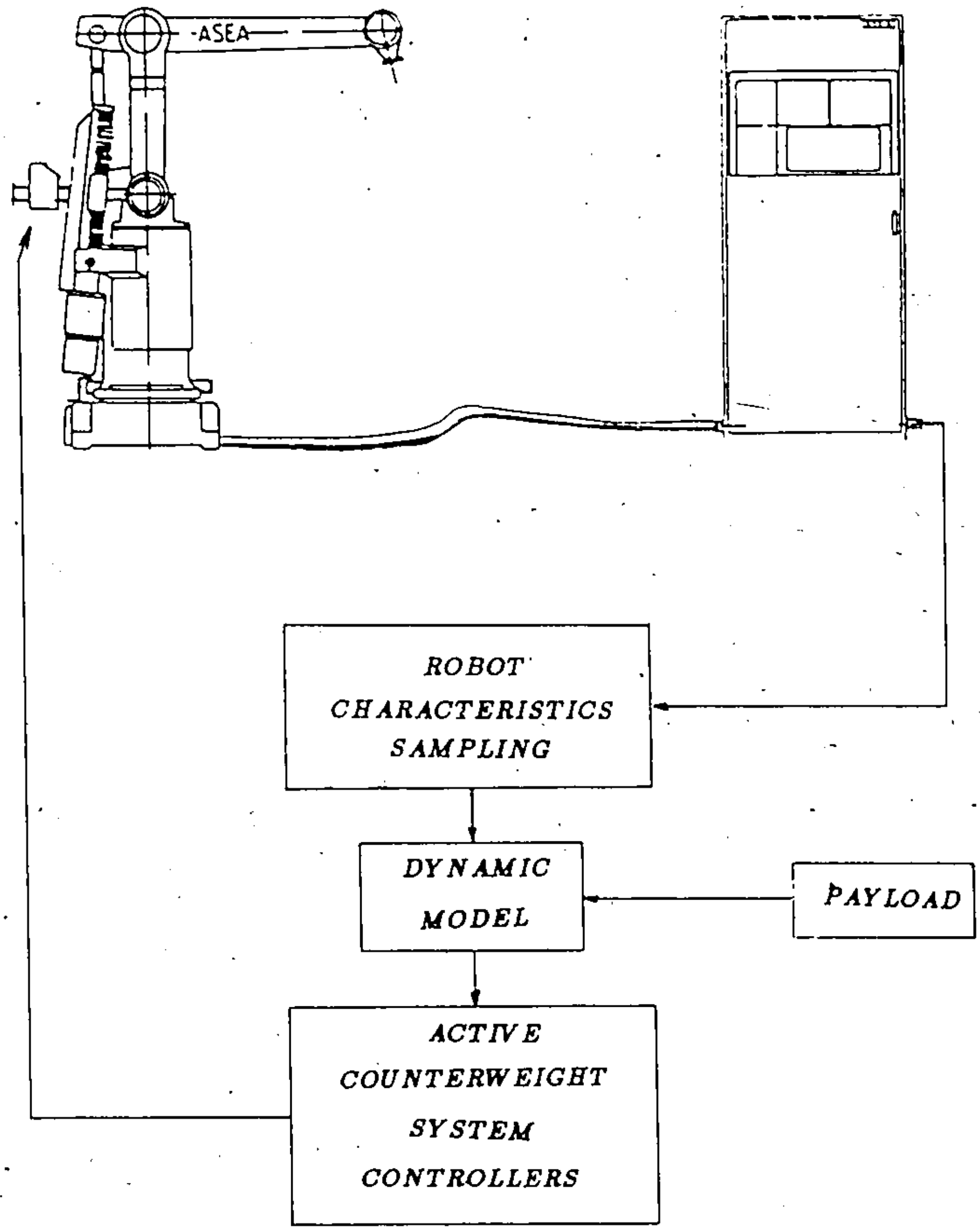

Figure 4.1. Active counterweight system

Detailed description of these four parts follows:

4.1. The mechanical system

As mentioned earlier, the active counterweight system is intended to be an add-on system to an existing robot arm. consequently, the system has to replace the fixed counterweight supplied by the manufacturer, and to operate within this tight space provided for the fixed counterweight.

Figure 4.2 shows the assembly drawing of the mechanical system. With reference to Figure 4.2, both the dynamic counterweight (M) and the quasistatic counterweight (N) slide along a pair of shafts (S) and (D) respectively. Guide shaft pair (S) for the dynamic counterweight are mounted on the quasistatic counterweight (N) as can be seen in the figure. Due to the rapid and frequent movements of the dynamic counterweight it is designed to ride guide shafts (S) on linear ball bearings (A) so as to minimize the friction forces. The quasistatic counterweight, however, rides guide shafts (D) on brass bushings (B) and slides with respect to the robot termination (C). Both counterweights are powered by electric DC motors through rack and pinion mechanisms. The rack (E) for the dynamic counterweight is fixed to the quasistatic counterweight system. A geared DC motor (F) rides on the dynamic and carries the pinion (G). The pinion (G) meshes with the rack (E) and causes the translation of the dynamic counterweight when it rotates.

The drive mechanism for the quasistatic counterweight is a similar system to that of the dynamic counterweight outlined above.

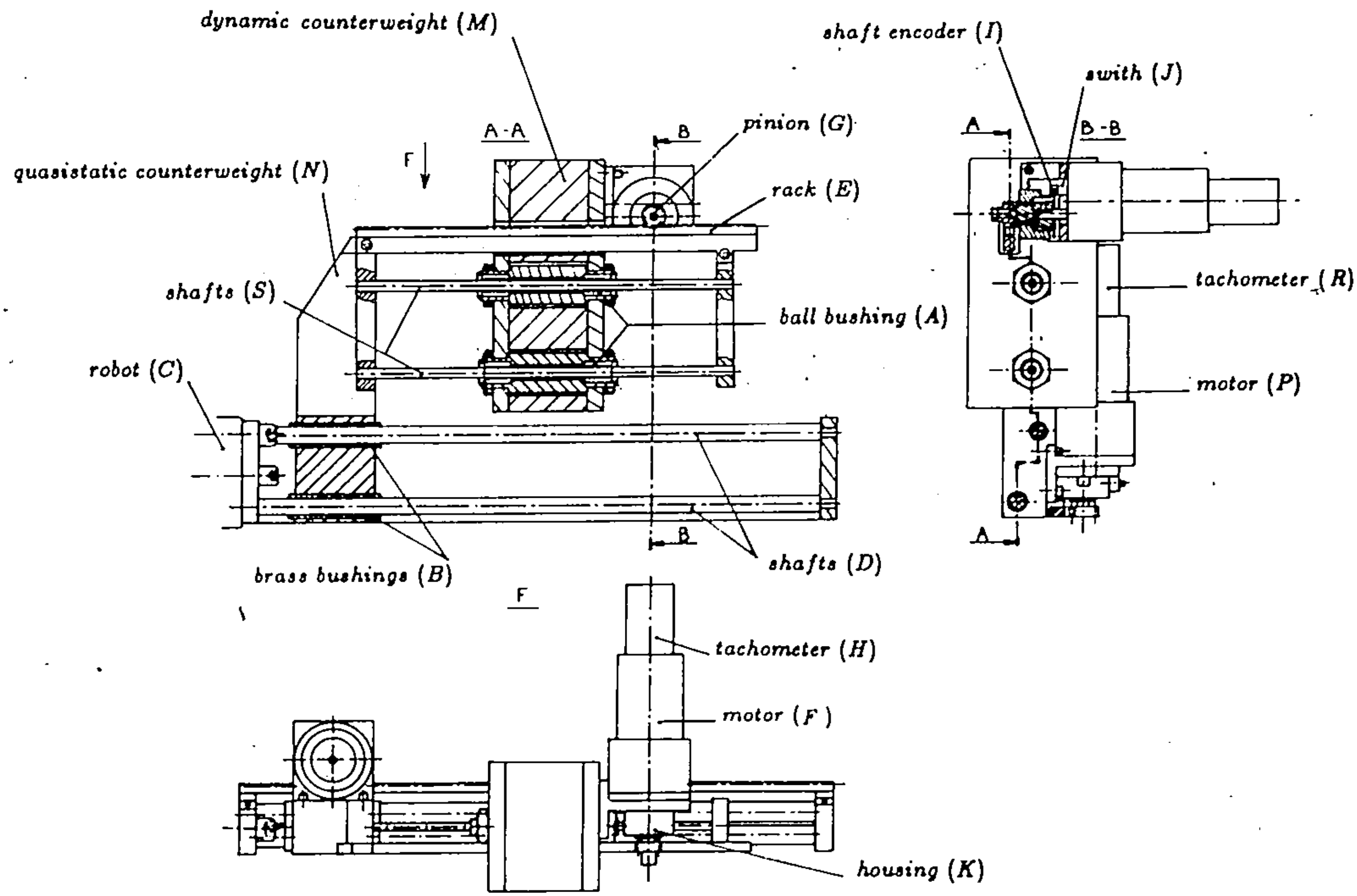

Figure 4.2. Assembly drawing

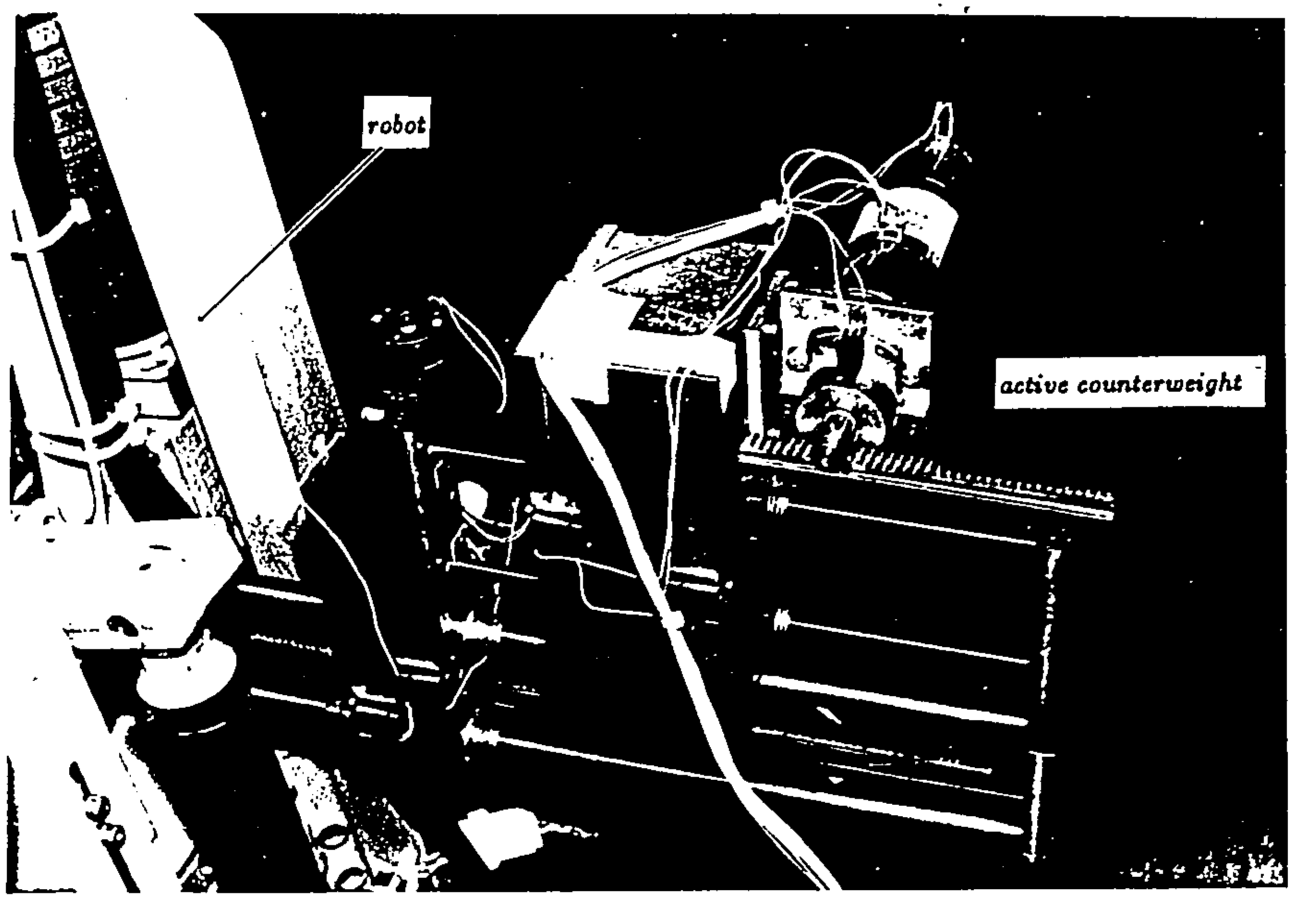

Figure 4.3. The active counterweight

The two counterweight systems use position and velocity feedback for motion control. The angular velocities of the motors (F) and (P) are measured by tachometers (H) and (R). The linear velocities of the counterweights are derived from these signals. Incremental shaft encoders are used to measure the angular displacement of the pinions. The linear displacements of the counterweights are calculated from these signals. Figure 4.3 shows the active counterweight system mounted on the ASEA Irb-6.

The complete set of design drawings and photographs of the components are given in Appendix B.

4.2. The data acquisition and processing system

The ASEA Irb-6 robot uses resolvers for measuring the angular position of the joint actuators [6]. Within one revolution the angular position of the actuators is represented by a phase shift between a reference input signal (Rref) and an output signal as shown on Figure 4.4. Both reference and output signals are available from the robot controller.

Since the angular displacements of the robot joints are not readily available from the robot controller, these displacements have to be calculated from the raw signals of the resolvers as follows:

The rising edge of the reference signal starts a counter/timer. The counter/timer stops when the rising edge of the shifted signal is encountered. The elapsed time during this period is directly proportional to the angular rotation of the motor within a revolution.

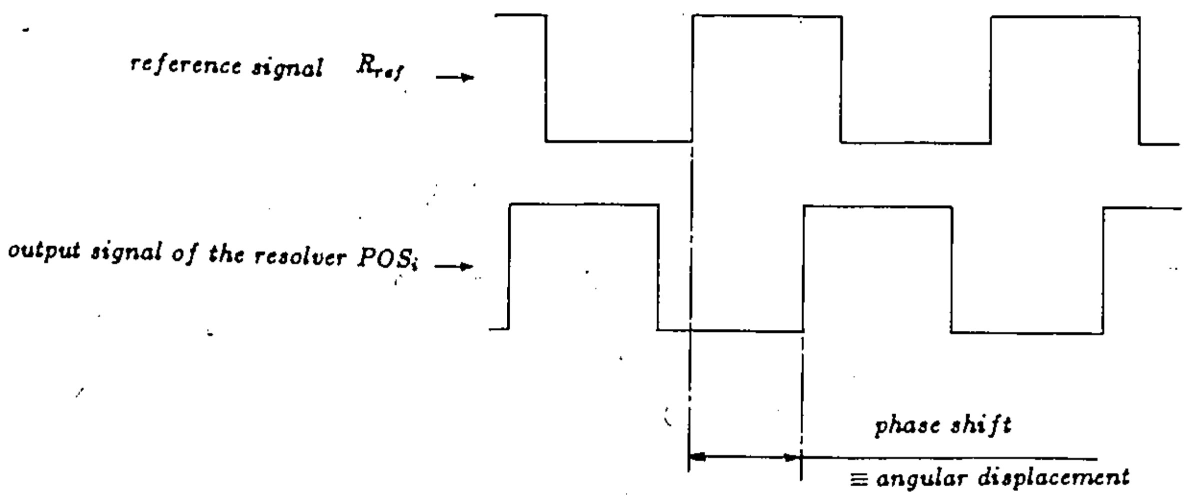

Figure 4.4. Resolver principle

Figure 4.5 shows the practical realization of the Z8 microprocessor based circuit for calculating the displacement. With reference to the figure, the reference and shifted signals are first converted into short pulses using monostable multivibrators in order to avoid undesired effects of overlap of the two signals. A JK Flip-Flop is set on the low to high transition of the reference signal. The output of the resolver resets the Flip-flop. The Flip-Flop signal is used to start and stop a counter in the microprocessor when configured in a "Gated Internal Clock Mode". The angular position of the robot joints are sampled one after the other. For the simplified model used in this work, the positions of the upper and lower arm joints only are required, and the microprocessor samples these two positions only.

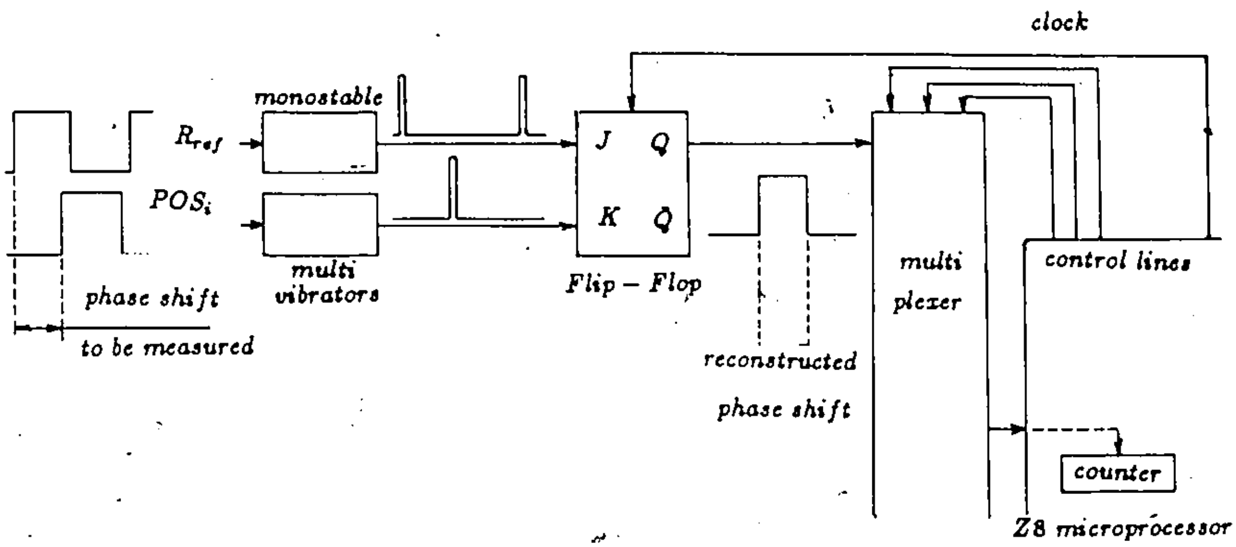

Figure 4.5. Position sampling

Full revolutions of the joint actuators are calculated from the resolver signals as follows:

Figure 4.6 shows the phase shift sequence when a joint motor is rotating at a constant velocity in a given direction. With reference to the figure, the sampling period 't' of the counter circuit discussed above is much smaller than the minimum period of one revolution of the joint motors. The maximum absolute change in phase shift within one revolution is calculated based on the maximum possible angular velocity of the joint motor and the sampling period. A recorded phase shift larger than this maximum indicates a boundary of one revolution has been crossed in a negative sense, and the full revolution counter has to be decremented. This situation is portrayed in Figure 4.6 by the transition B to A. On the other hand, a change in phase shift less than the negative of the maximum phase shift within a revolution indicates a boundary of one revolution has been crossed in a positive sense. This situation is portrayed in Figure 4.6 by the transition A to B.

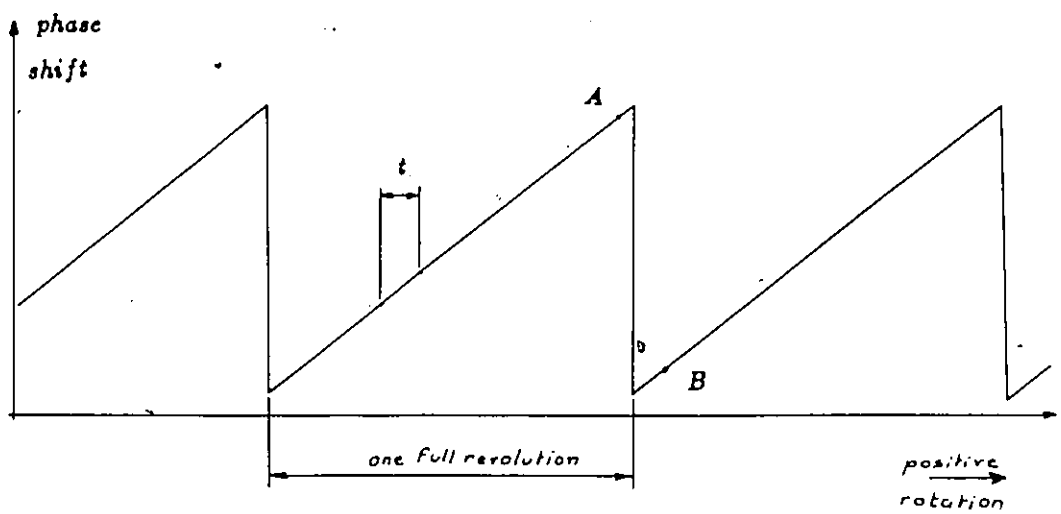

Figure 4.6. Determination of the angular position of the link

The velocity of each link actuator is fed-back through a tachometer that provide a voltage proportional to the velocity of the link itself. The velocities of the three first links are sampled using Analog to Digital Converters and are stored by the microprocessor. Figure 4.7 shows a block diagram of the structure of the software for the sampling process. As shown in Figure 4.7, the kinematics of the robot links are stored and are at the disposal of the counterweight system controlling computer for the computation of the dynamic model.

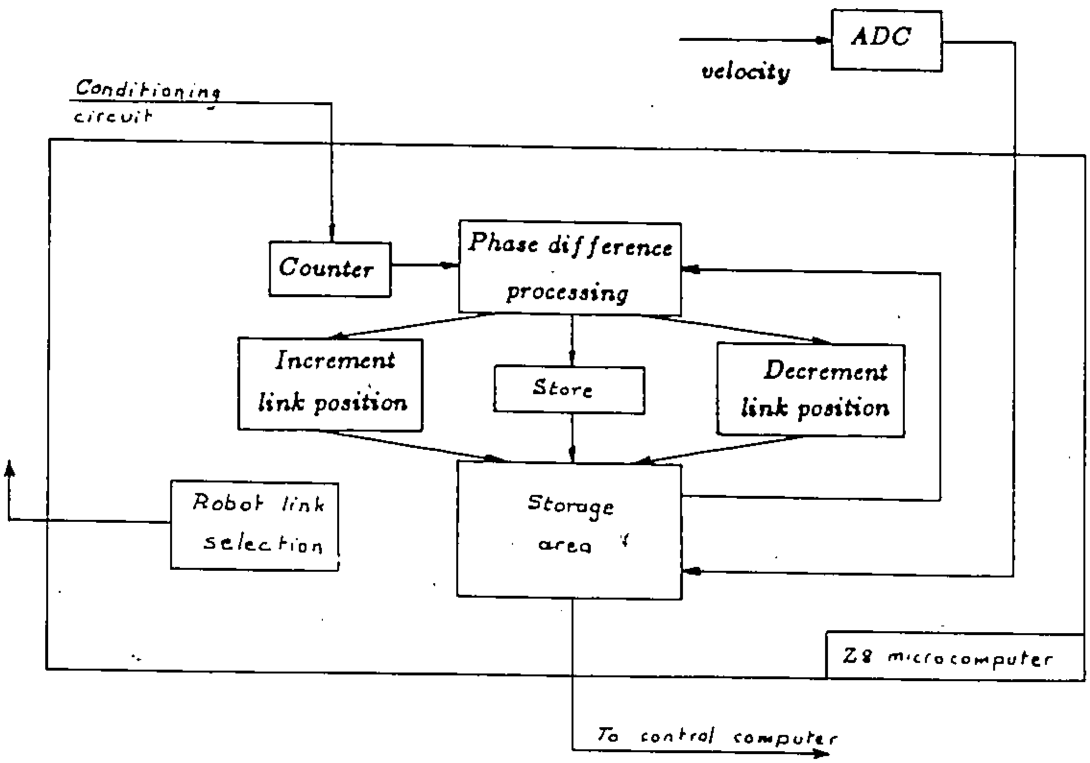

Figure 4.7. The Sampling Process flow chart

A detailed flow chart of the sampling process and the corresponding assembler program for the Z8 Basic/Debug microcomputer are presented in Appendix C.

4.3. The balancing coordinator program

The role of this program is to derive the optimum position of the active counterweight when the robot arm traverses its trajectory. The program also calculates the optimum location of the quasistatic counterweight for a given payload.

Figure 4.8. shows the flow graph of the program. The program is written in Fortran and runs on an 8 MHz microcomputer based on the 8088 microprocessor (IBM compatible) and equipped with an 8087 math coprocessor. With reference to the figure, the program mainly consists of one loop that is repeatedly executed. For every execution cycle, the program reads the positions and velocities of the first three links from the data acquisition and processing system. The angular displacement of the links are approximated to one full revolution of the link drive motor (i.e. 2 degrees) in order to increase processing speed. The 2 degrees inaccuracy results in a maximum error in the calculation of the transcendental functions of 1.8%.

The accelerations of the links are derived from the corresponding link velocities as follows:

$$\ddot{\theta}_i(k) = \frac{1}{T}[\dot{\theta}_i(k) - \dot{\theta}_i(k-1)] \qquad 4.1$$

where $\dot{\theta}_i(k)$ is the present angular velocity of the link,

$\dot{\theta}_i(k-1)$ is the previous angular velocity of the link,

$\ddot{\theta}_i(k)$ is the present angular acceleration of the link

and T is the period of the cycle.

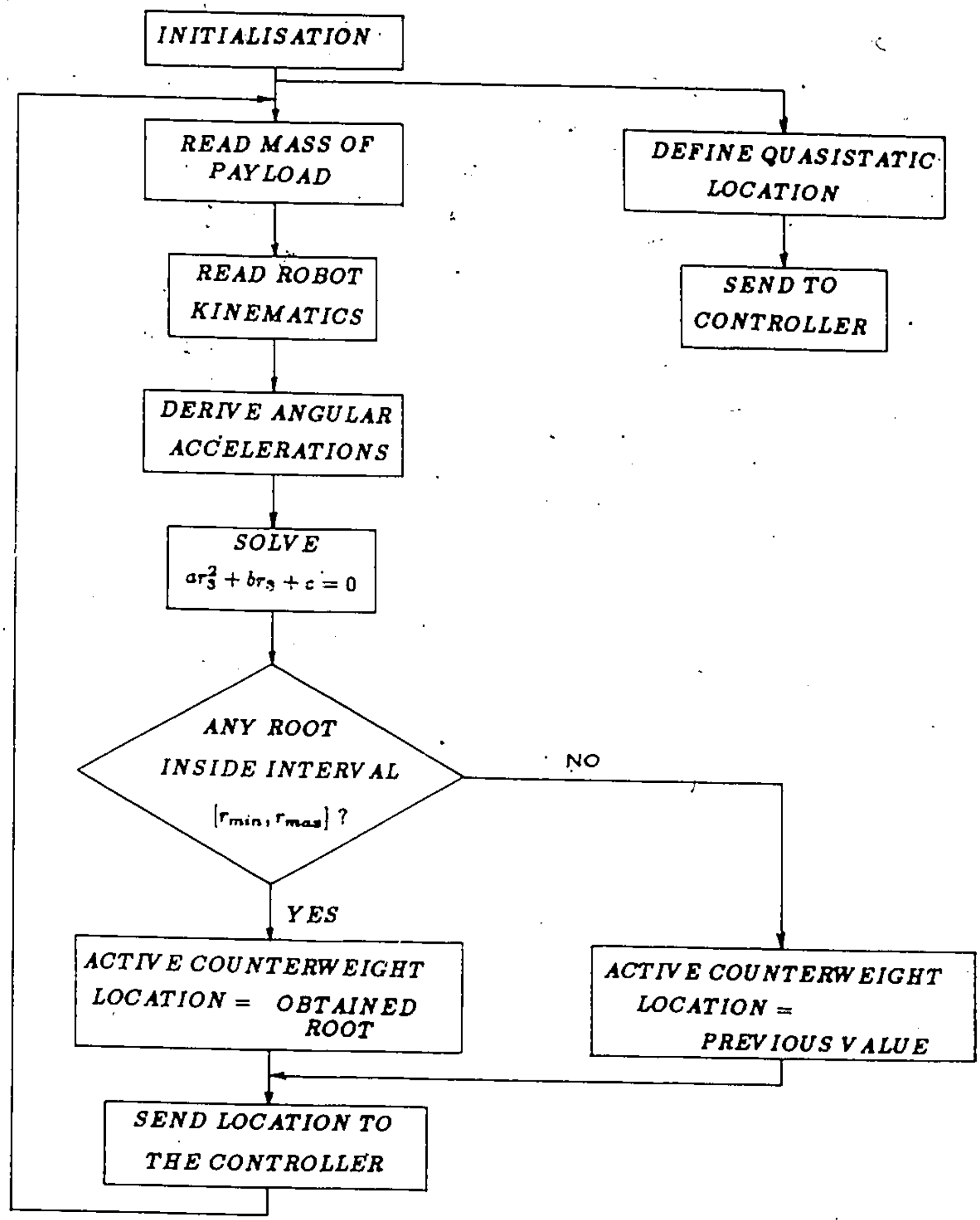

Figure 4.8. The balancing coordinator program

The optimum location of the active counterweight is then computed using Equations 2.42 to 2.46. The calculated location is then sent to the Z8 microcomputer based controller of the counterweights. Due to the high speed of motion of the robot links, the number of cycles of the balance coordinator program that have to be executed per second must be large so as to reduce the distortion due to the digital processing. In order to increase the speed of execution of the Fortran program, look-up tables are used to find transcendental functions, rather than calculating them.

The description and computer listing of the balance coordinator program are given in Appendix D.

4.4. The control system

The theoretical design of the control system for both the dynamic and quasistatic counterweights is identical. Both counterweights consist of a mass that is translated using a DC motor through a rack and pinion transmission system. Figure 4.9. shows a block diagram of the feedback control system for either counterweights. With reference to the figure, the control system consists of a digital part and an analog part. Analog to digital and digital to analog converters interface these parts together.

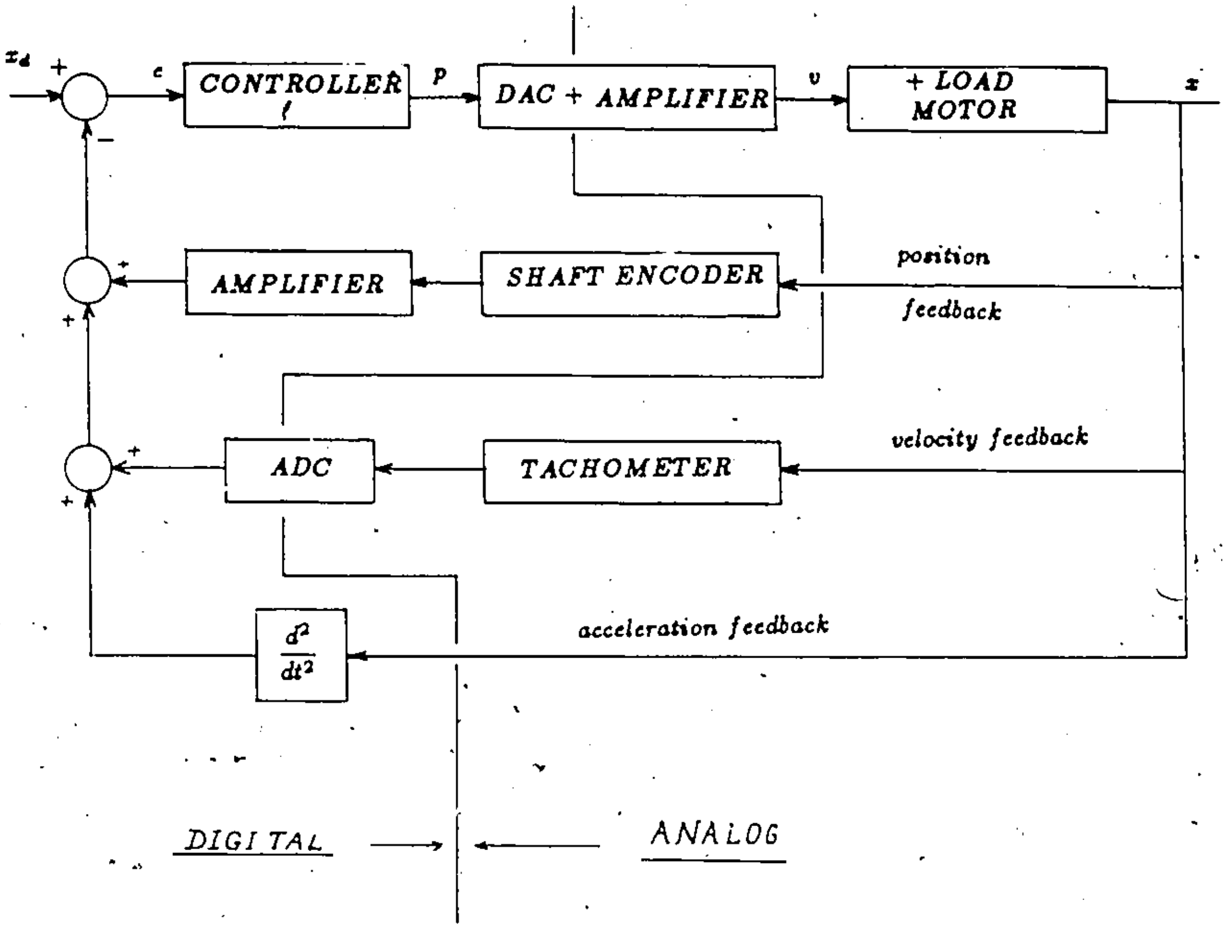

Figure 4.9. Control loop for the counterweights

The optimum location of the counterweight x_d is compared with the feedback signals and result in the error signal e. This error is processed by the controller and becomes a command signal p. These operations are digitally performed using a Z8 microcomputer. The command is then converted to an analog signal and amplified using a transistor circuit in order to power the motor. Detailed description of the mathematics and components of the control system follows:

4.4.1. Design of the controllers

Due to the similarity of both counterweight systems, the design procedure is presented in details for the dynamic counterweight, and only the final results for the quasistatic counterweight are given. A schematic diagram of the counterweight and its drive motor is shown on Figure 4.10.

A permanent magnet armature controlled DC motor is used to drive the counterweight.

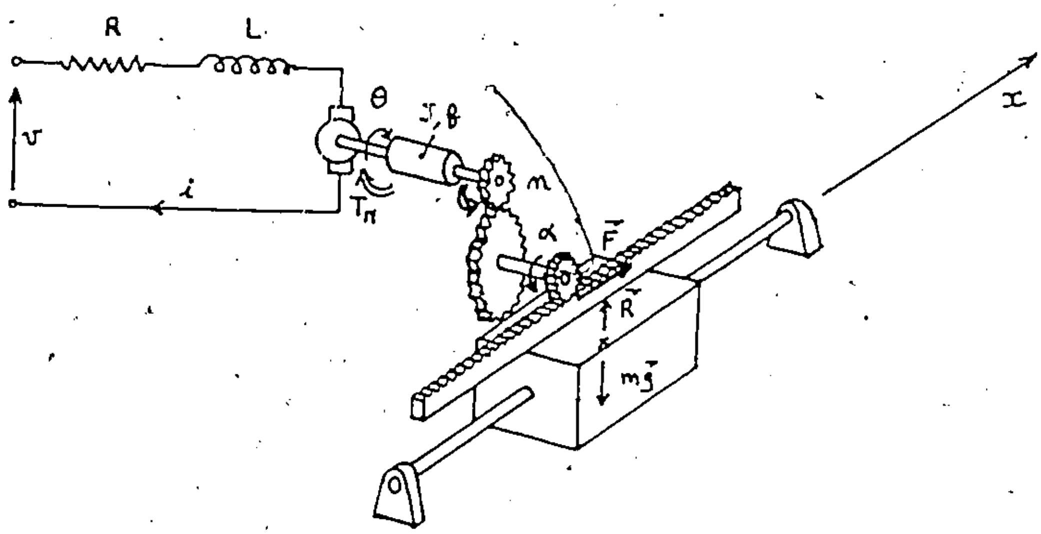

Figure 4.10. Schematic diagram for the counterweight and its drive motor system

With reference to Figure 4.10, the electromechanical relation for the motor is given as follows [9]:

$$T_M = k_M \frac{(V - k_b\theta s)}{R + Ls} \qquad 4.2$$

where T_M is the motor torque,

V is the applied voltage,

k_b is the back EMF constant,

θ is the angular position of the motor,

R is the armature resistance

and L is the armature inductance.

The moment equation for the motor rotor gives is given by:

$$T_M = (Js^2 + fs)\theta + \frac{r}{n}F \qquad 4.3$$

where J is the inertia of the rotor,

f is its friction coefficient,

r is the radius of the pinion,

n is the gear ratio

and F is the force transmitted by the pinion to the rack.

The angular position θ of the motor can be expressed as a function of the linear displacement X of the active counterweight as follows:

$$\theta = \frac{n}{r}X \qquad 4.4$$

The dynamic equation for the active counterweight along the x-axis is given by:

$$ms^2X + P(s) = F \qquad 4.5$$

where P(s) is a disturbance term that includes the effect of the inclination of the counterweight with respect to, the horizontal axis as well as its acceleration in the x-direction due to the motion of the robot itself.

Solving Equations 4.2 to 4.5 simultaneously and rearranging gives the position of the active counterweight as follows:

$$X(s) = \frac{rnk_M V(s) - (R + Ls)r^2 P(s)}{[(R + Ls)(Jn^2 + rm^2)s + (R + Ls)fn^2 + k_b k_M n^2]s} \qquad 4.6$$

Figure 4.11. shows the complete bloc diagram for the position controller of the active counterweight.

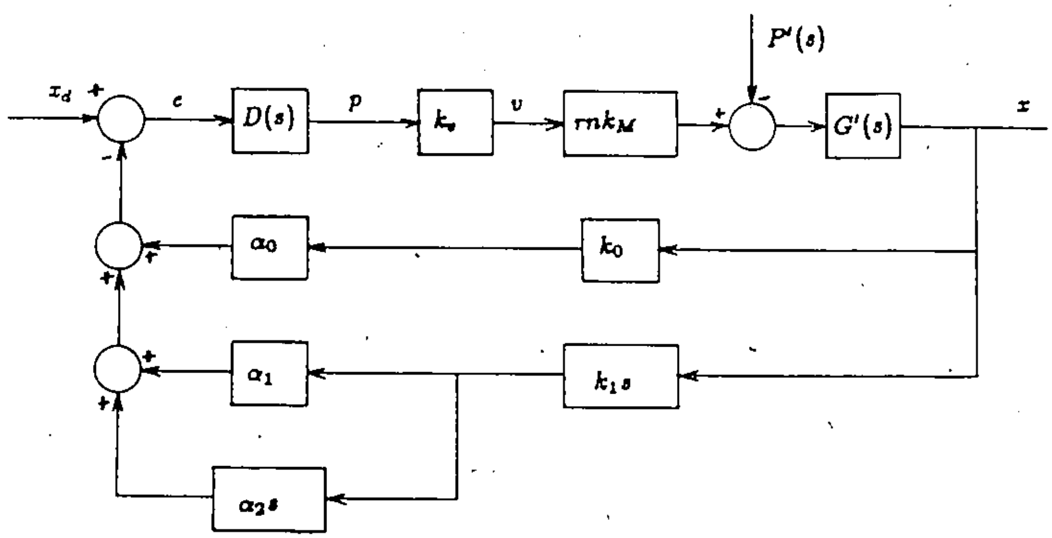

Figure 4.11. Complete block diagram of the dynamic counterweight

With reference to Figure 4.11:

D(s) is the transfer function of the controller which is still to be determined,

k_a is the gain of the power amplifier,

G'(s) refers to equation 4.6 and is expressed as follows:

$$G'(s) = \frac{1}{[(R+Ls)(Jn^2+r^2m)s+(R+Ls)fn^2+k_bk_Mn^2]s} \qquad 4.7$$

P'(s) is the equivalent disturbance given by:

$$P'(s) = r^2(R+Ls)P(s) \qquad 4.8$$

k_0 is the gain of the position feedback

k_1 is the gain of the velocity feedback

α_0, α_1 and α_2 are additional software adjustable gains for the position, velocity and acceleration feedbacks respectively.

The acceleration of the counterweight is calculated using the present and the previous velocities every sampling period as follows:

$$\ddot{x}(k) = \frac{1}{T}[\dot{x}(k) - \dot{x}(k-1)] \qquad 4.9$$

With reference to the superposition theorem, one can ignore for the time being the perturbation due to the disturbance P' and proceed with a preliminary design for the controller.

The design of the controller is conducted in the continuous time domain using the root-locus method [8-9]. The digital algorithm is obtained later from the analog transfer function using the Z-transform analogy. If the sampling period decreases, the discrete time transfer function obtained using this method become more accurate in representing the designed continuous time transfer function [7-10]. A sampling period of one tenth the smallest period in the input change is chosen. According to the simulation results, the minimum time required by the counterweight to move from one extreme position to the other is about 0.3 second. The sampling period is chosen to be 30 milliseconds.

The controller is designed to be a Proportional-Integral (P-I) one in order to improve the steady state error and to reduce the effect of disturbances. The derivative action is not necessary in the controller itself since the velocity and acceleration in the feedback loop introduce an effect similar to that of a derivative component [7].

The transfer function of the controller is expressed as follows:

$$D(s) = k_P\left(1 + \frac{k_I/k_P}{s}\right) \qquad 4.10$$

Figure 4.12 shows a reduction of the entire system block diagram with values of the system parameters.

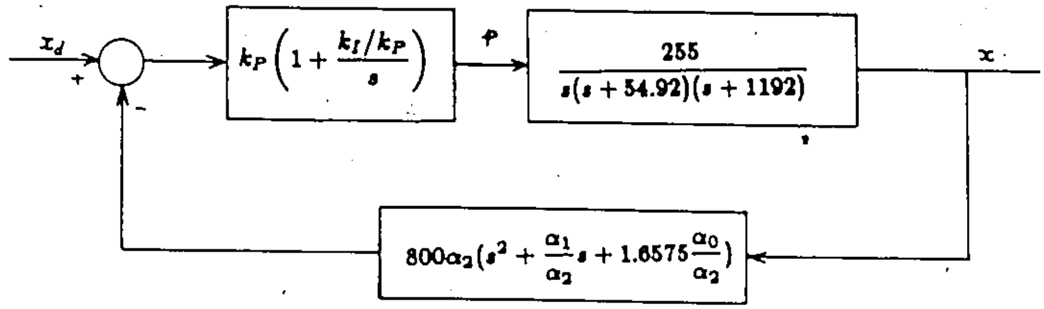

Figure 4.12. Reduced block diagram of the dynamic counterweight

The choice of the values for the feedback sensor gains is made so as to allow maximum range of adjustment, yet would minimize round off errors during calculations. This yields the following numerical values:

$$\alpha_0 = 1$$

$$\alpha_1 = 0.5 \qquad 4.11$$

$$\alpha_2 = 0.015$$

The feedback transfer function is factorized to give:

$$F(s) = 12(s+3.73)(s+29.6) \qquad 4.12$$

All the poles and zeros of the system fall inside the region $\sigma = 0$ to $\sigma = -55$ in the σ versus jw plane, except for one of the poles of the motor and load transfer function. This pole is located at s=-1192 and can be neglected.

The ratio between the integral and proportional gains in the transfer function of the controller k_I/k_P is kept small so as to

minimize the integral effect and thus reduce eventual oscillations. The following ratio is chosen: $k_I / k_P = 0.1$
The bloc diagram of Figure 4.12 thus reduces to that in Figure 4.13:

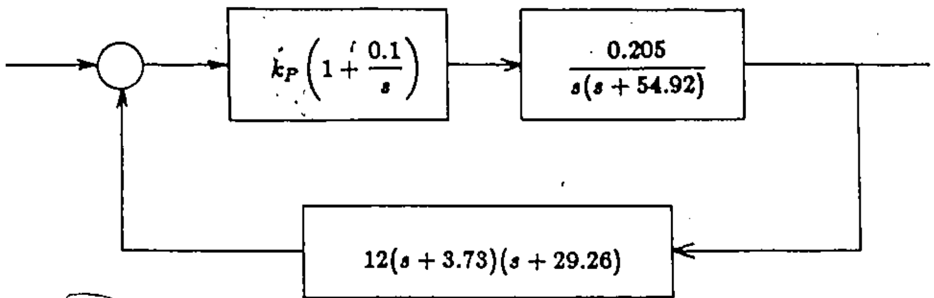

Figure 4.13. Final block diagram of the dynamic counterweight

With reference to Figure 4.13, the characteristic equation of the system can be expressed as follows:

$$1+K\frac{(s+0.1)(s+3.73)(s+29.6)}{s^2(s+54.92)}=0 \qquad 4.13$$

where

$$K = 2.465 k_P \qquad 4.14$$

The root-locii for the zeros and poles of the system as K varies from 0 to ∞ are shown in Figure 4.14. With reference to the figure, the break-away points occur at $s = 0$ $(K = 0)$ and s

$= -0.19$ $(K = 0.21)$.

Hence, for K greater than 0.21, the system will not oscillate. The gain K can thus be chosen so as to satisfy the minimum settling time fixed by the maximum velocity of the counterweight.

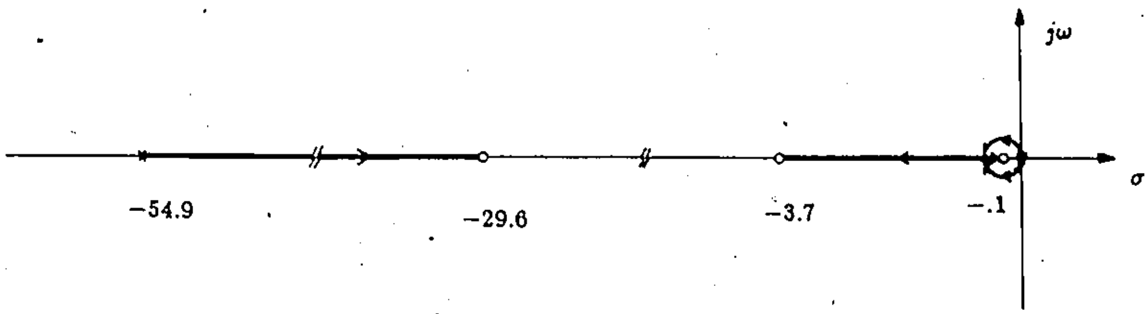

Figure 4.14. Root-locii for the dynamic counterweight

A gain $K = 5$ is chosen. This yields a proportional gain $k_p = 2.03$ for the controller transfer function. The roots of the characteristic equation corresponding to this gain are:

$p_1 = -0.101$ $p_2 = -2.66$ $p_3 = -34.25$

The pole $p_1 = -0.101$ and the zero $z_1 = -0.1$ can be ignored since they are too close to one an other and tend to cancel. The overall transfer function is thus given as follows:

$$H(s) = \frac{0.0695}{(s + 34.25)(s + 2.66)} \qquad 4.15$$

If a unit step input 1/s is considered, the output, or the actual position of the counterweight is expressed as follows:

$$x(t) = 1.011(1 - 1.084e^{-2.66t} + .084e^{-34.2t}) \qquad 4.16$$

The response to a step input is shown on Figure 4.15.

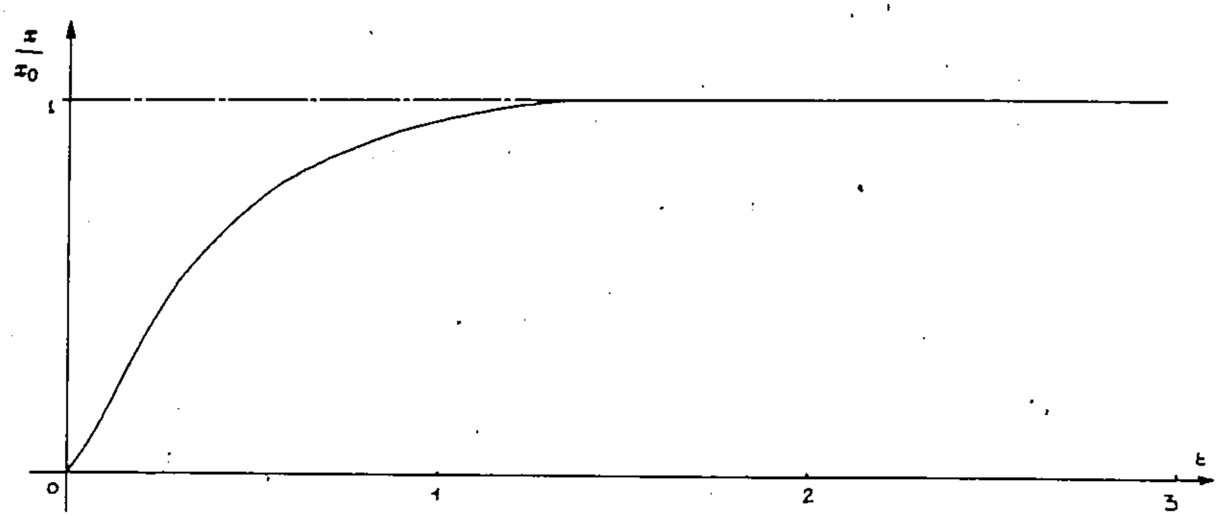

Figure 4.15. Step response of the dynamic counterweight

Figure 4.16 shows the entire bloc diagram for the dynamic counterweight, including the disturbance P'(s). For the chosen controller, the effect of a disturbance P'(s) is as follows:

$$\frac{X(s)}{P'(s)} = \frac{0.205s}{s^2(s+54.9) + k'(s+0.1)(s+3.73)(s+29.6)} \qquad 4.17$$

The error due to the disturbance is given by:

$$E(s) = -X(s)F(s) \qquad 4.18$$

where F(s) is the feedback transfer function.

Using Equation 4.17 into Equation 4.18 and rearranging gives:

$$E(s) = \frac{-2.46s(s+3.73)(s+29.6)P'(s)}{s^2(s+54.9)+k'(s+0.1)(s+3.73)(s+29.6)} \qquad 4.19$$

The steady state error being expressed as follows:

$$e_{ss}(\infty) = \lim_{s \to 0} \left(sE(s)\right) \qquad 4.20$$

the steady state error due to a step disturbance P'(s)=1/s is calculated using Equations 4.19 and 4.20:

$$e_{ss}(\infty) = \lim_{s \to 0} s \frac{-2.46s(s+3.73)(s+29.6)\frac{1}{s}}{s^2(s+54.9)+k'(s+0.1)(s+3.73)(s+29.6)}$$

$$= 0 \qquad 4.21$$

The designed system is thus not affected by step disturbances.

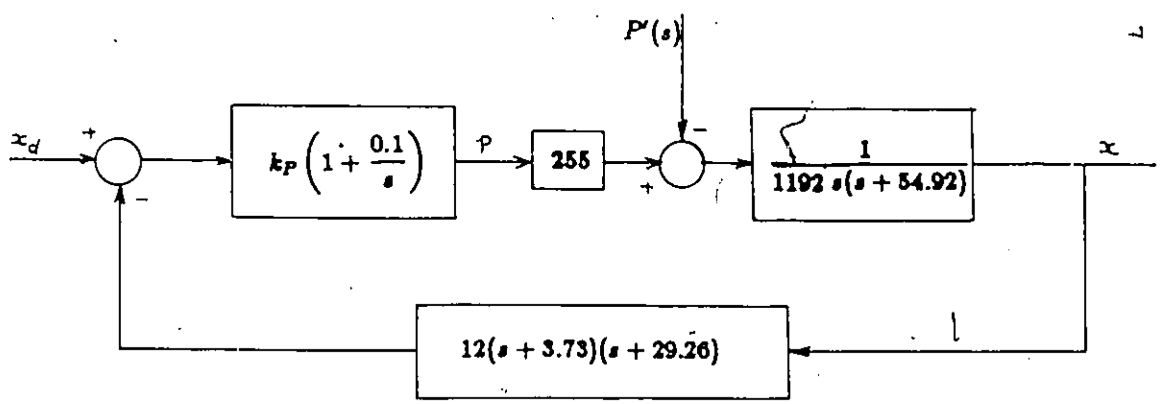

Figure 4.16. Block diagram for the entire dynamic counterweight

The transfer function of the chosen controller is given by:

$$D(s) = 2.03\left(1+\frac{0.1}{s}\right) \qquad 4.22$$

The digital controller is obtained by writing Equation 4.22 in the Z-domain as follows:

$$D(z) = 2.03\frac{(1.1 - z^{-1})}{(1 - z^{-1})} \tag{4.23}$$

The output of the controller p(k) in Equation 4.23, can be expressed as follows:

$$p(k) = p(k-1) + 2.23e(k) - 2.02e(k-1) \tag{4.24}$$

For a microprocessor, mathematical operations are executed much faster in binary base than in decimal base. Rewriting the coefficients of p(k) gives the desired controller equation for the active counterweight as follows:

$$p(k) = p(k-1) + \frac{9}{4}e(k) - \frac{65}{32}e(k-1) \tag{4.25}$$

A similar design process is carried out for the quasistatic counterweight. Figure 4.17 shows the bloc diagram for the quasistatic counterweight control loop.

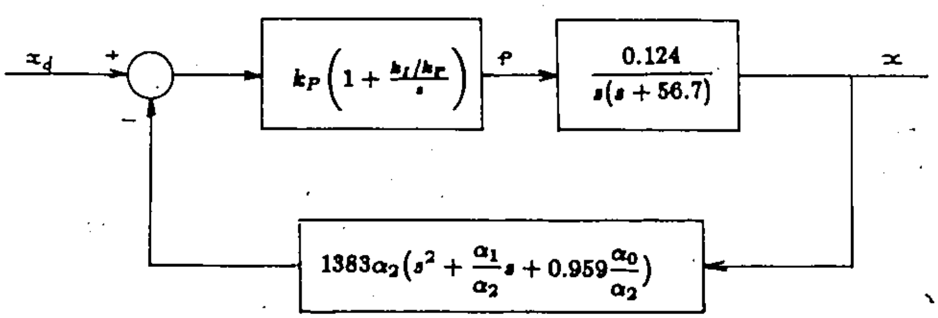

Figure 4.17. control loop for the quasistatic counterweight

The adjustable gain for the feedbacks are the same for the quasistatic counterweight as those for the dynamic one with the exception of α_1 which takes a value of α_1=0.75 here.
The characteristic equation is hence given as follows:

$$q(s) = 1 + K\frac{(s+0.1)(s+1.31)(s+48.7)}{s^2(s+56.7)} \qquad 4.26$$

The root-locii for Equation 4.26 are shown in Figure 4.18.

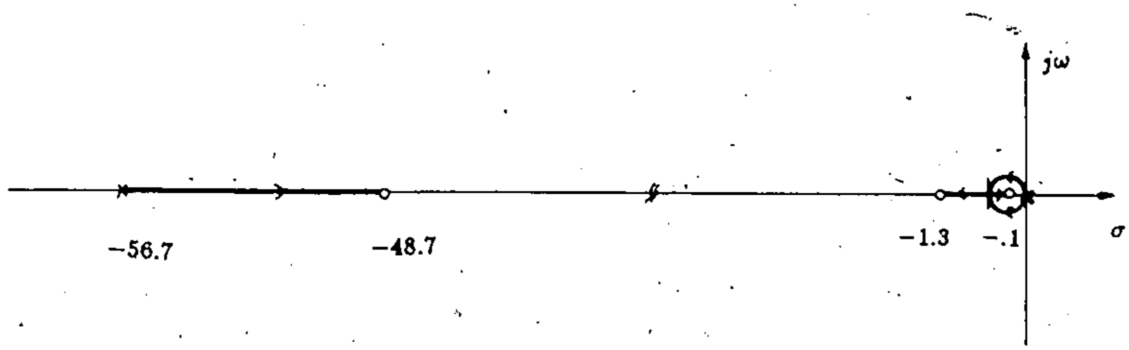

Figure 4.18. Root-locii for the quasistatic counterweight

The gain K is chosen to be 5 in this case as well. This results in the proportional gain for the controller k_p= 1.944.
The overall transfer function is hence given as follows:

$$H(s) = \frac{0.04}{(s+50)(s+1.04)} \qquad 4.27$$

The response of the quasistatic counterweight to a step input is shown on Figure 4.19, and is represented by the following equation:

$$x(t) = 1.02(1 - 1.02e^{-1.04t} + 0.021e^{-50t}) \qquad 4.28$$

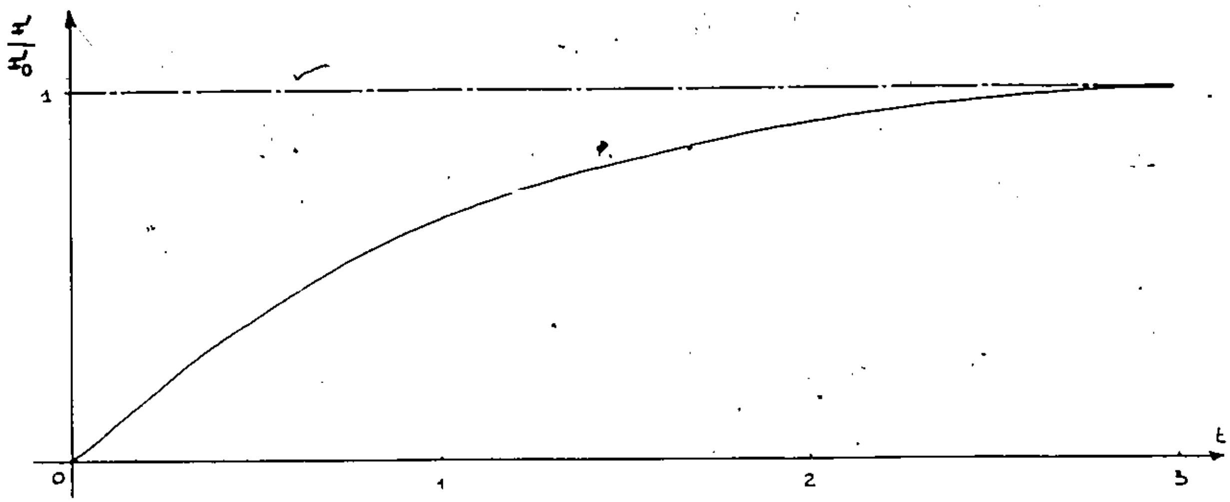

Figure 4.19. Step response of the quasistatic counterweight

The discrete-time controller is given as follows:

$$D(z) = 1.94\frac{(1.1 - z^{-1})}{(1 - z^{-1})} \qquad 4.29$$

The expended form of Equation 4.29 is given by:

$$p(k) = p(k-1) + 2.138e(k) - 1.944e(k-1) \qquad 4.30$$

The controller equation is expressed in binary form for ease of implementation and speed execution as follows:

$$p(k) = p(k-1) + \frac{17}{8}e(k) - \frac{31}{16}e(k-1) \qquad 4.31$$

4.4.2. The associated electronics

This section describes the two circuits that are necessary to implement the two control loops, namely:

A) The feedforward circuit, that converts the digital commands of the microprocessor into the appropriate voltage to be applied on the corresponding motor.

B) The feedback circuit that gives the controller the necessary information about the actual state of the corresponding load and motor system.

A) The feedforward circuit

The feedforward circuit is composed of with the following subcircuits: 1) An Digital to Analog Converter as a direct interface with the microprocessor; 2) A Sampling and Holding stage for proper distribution of information between both motors; 3) A bi-directional servo amplifier for both motors.

1) The Digital to Analog Converter (DAC)

Figure 4.20 shows the DAC circuit configured for bipolar offset binary operation. This is necessary in order to command the counterweight motor to rotate in either directions. With reference to Figure 4.20, the output voltage v can be expressed as a function of the input byte provided by the microprocessor as shown in table 4.1.

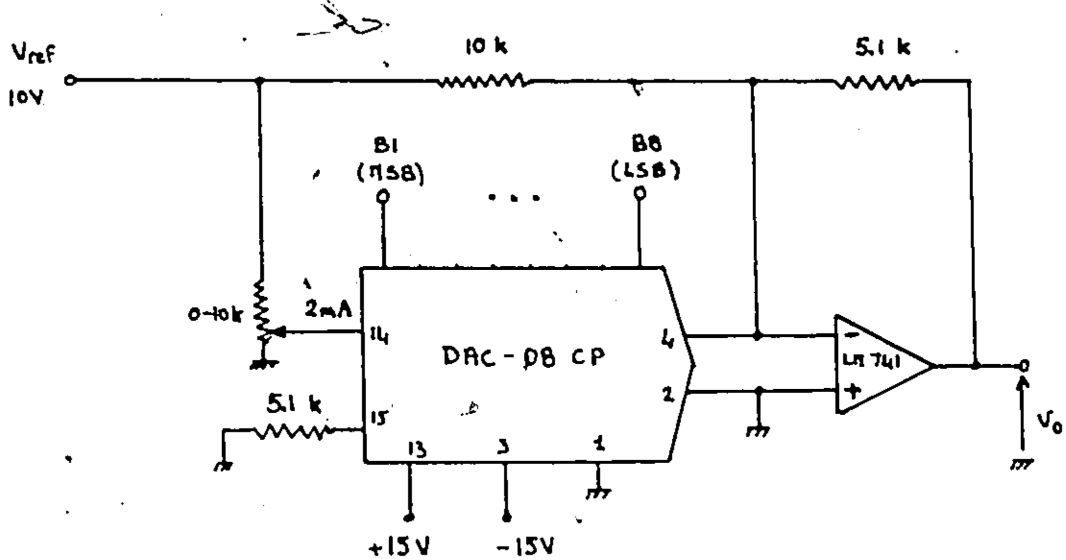

Figure 4.20. Digital to Analog Converter circuit

Table 4.1 shows the bit assignment and the output voltage for the DAC. As can be seen from the table, a zero byte corresponds to full negative voltage while an FF byte corresponds to full positive voltage.

	B1	B2	B3	B4	B5	B6	B7	B8	V_o
Pos. Full Scale	1	1	1	1	1	1	1	1	5.06
Zero Scale	1	0	0	0	0	0	0	0	0.00
Neg. Ful Scale + 1 LSB	0	0	0	0	0	0	0	1	- 5.06
Neg. Ful Scale	0	0	0	0	0	0	0	0	- 5.10

Table 4.1. Analog output

2) <u>The sample and hold (SH) circuit</u>

One DAC is used to convert the command signals for both the dynamic and the quasistatic counterweight motors. The digital information and its corresponding analog voltage v_o is sent from the microcomputer to either of the two motors at a time. Hence, the digital output of the microprocessor is sent to the DAC simultaneously with control logic signals that select which motor is to receive the command.

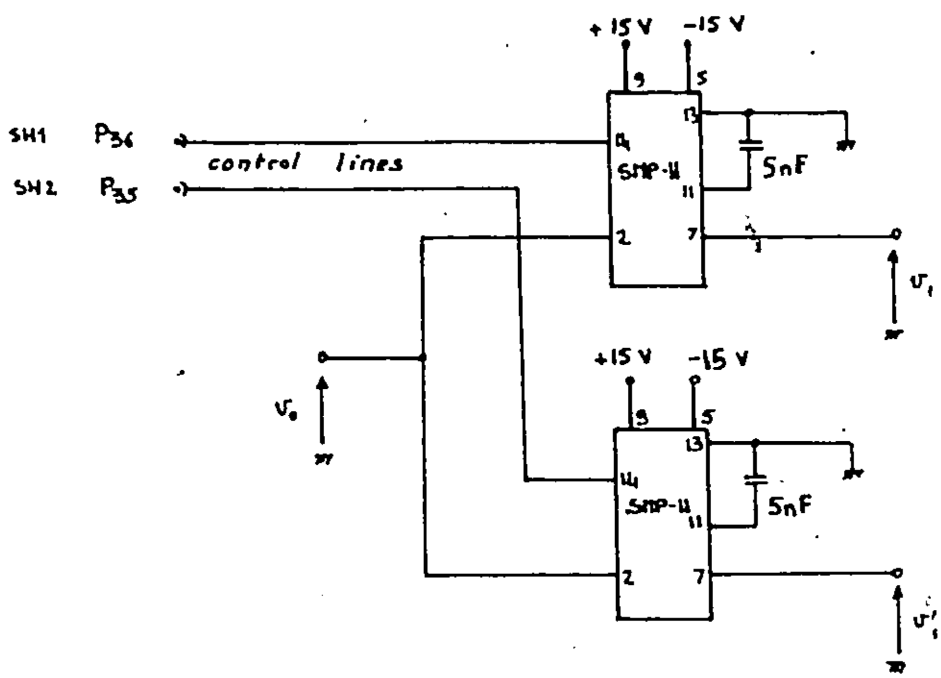

Figure 4.21. Sample and hold circuit

While a command is sent to one of the motor, the information necessary for the other motor is held at its previous value by a unity gain SH amplifier allows such operations. The information is alternatively given to both motors: when one is selected for sampling, the other one is asked to hold and vice versa. A fast switching sequence is necessary to prevent loss of signal or drifting when change over from one SH to the other, or during the holding periods. The control microcomputer switches from one motor to the other every 150 microseconds. Figure 4.21 shows the circuit with its two SH amplifiers.

3) Bidirectional servo amplifier

The bidirectional servo amplifiers for both motors consists in a linear bipolar output transistor circuit as shown on Figure 4.22. The bipolar amplifier uses dual power supplies for forward and reverse operations. The voltage applied to the motor is equal to the difference between the supply voltage and the drop across the collector emitter of Q_1 or Q_2, whichever is conducting. The V_{CEO} rating of the power transistors must be greater than the sum of the two power supplies. Free wheeling diodes are connected across Q_1 and Q_2. The diodes clamp the transistor reverse voltage to one diode voltage drop when reversal of voltage occur due to the motor inductance current transients [11]. The specifications for the linear amplifier bipolar circuit are as follows:

1) Supply voltage: ±15 V;

2) Output voltage: ±12 V;

3) Peak output current: ±5 A.

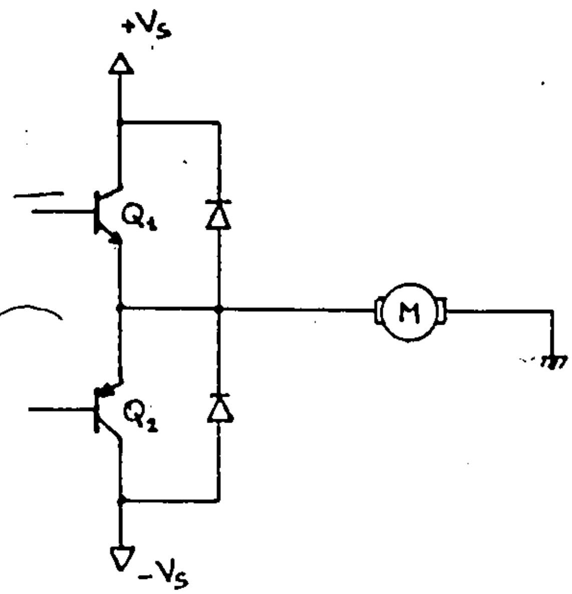

Figure 4.22. Bipolar output stage

The 2N6387 and 2N6667 complementary pair of Darlington transistors is used in this circuit. These are rated at 60 Volts 10 Amperes and their current gain is approximately 10,000 . The maximum driving current is thus 1 mA which can be easily obtained from a one stage operational amplifier circuit.

In order to avoid undesirable transient overcurrents particularly during starting, the operational amplifier driving the power transistors includes both current and voltage feedbacks. This requires a composite voltage source and current source amplifier circuit as shown on Figure 4.23.

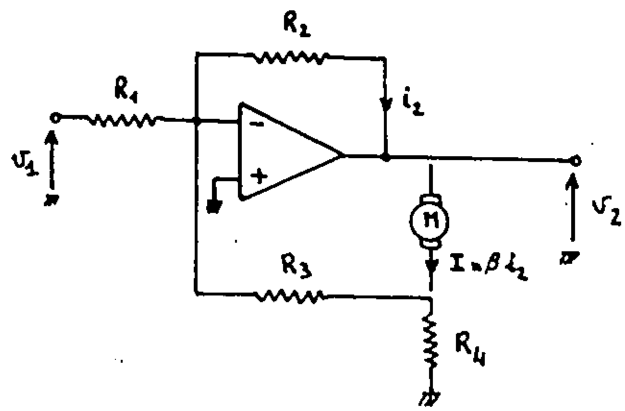

Figure 4.23. Composite voltage source and current source amplifier

With reference to Figure 4.23, solving for the output voltage of the amplifier v_2 and for the motor current I gives:

$$v_1 = R_1\left(\frac{1}{\beta} - \frac{R_4}{R_3 + R_4}\right) I \qquad 4.32$$

and

$$v_2 = -\frac{R_2}{R_1}\left(\frac{R_3}{R_4} + 1\right)\frac{1}{\beta}\, v_1 \qquad 4.33$$

where β is the current gain of the transistors.

For practical purposes, R_1, R_2 and R_3 are selected in the kilohms range. R_4 is selected very small, $R_4 = 0.1$ ohm, in order to maintain a low voltage drop across it, and that v_2 may be considered as the actual voltage applied on the motor itself.

Hence, Equations 4.32 and 4.33 may be approximated by:

$$\frac{I}{v_1} = -\frac{R_3}{R_1 R_4} \qquad 4.34$$

and

$$\frac{v_2}{v_1} = -\frac{R_2 R_3}{\beta R_1 R_4} \qquad 4.35$$

Since v_1 is in the ±5 V range, a unit voltage-current gain is required to match the ±5 Amps specification. The values of R_1 to R_4 are as follows:

R_1 = 10 kohms R_2 = 100 kohms

R_3 = 1 kohm R_4 = 0.1 ohm.

A very sensitive voltage amplifier is necessary to achieve a fast response to the position input changes, and to reduce the crossover distortion around the zero volt region. Figure 4.24 shows the voltage and current gains of the amplifier, and the voltage saturation that results from the large voltage gain.

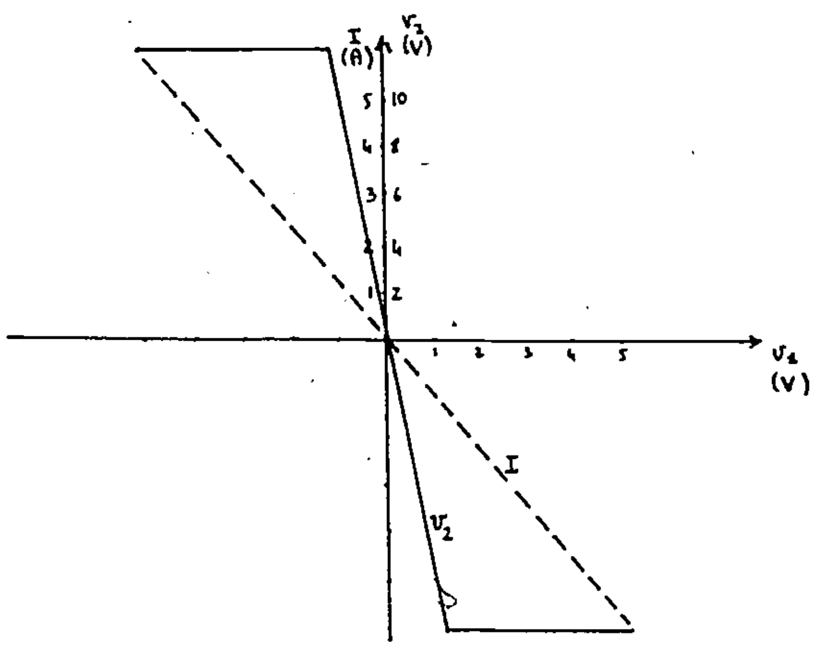

Figure 4.24. Current and voltage gains

Figure 4.25 shows the complete circuit of the servo amplifier which is used to drive each of the two motors.

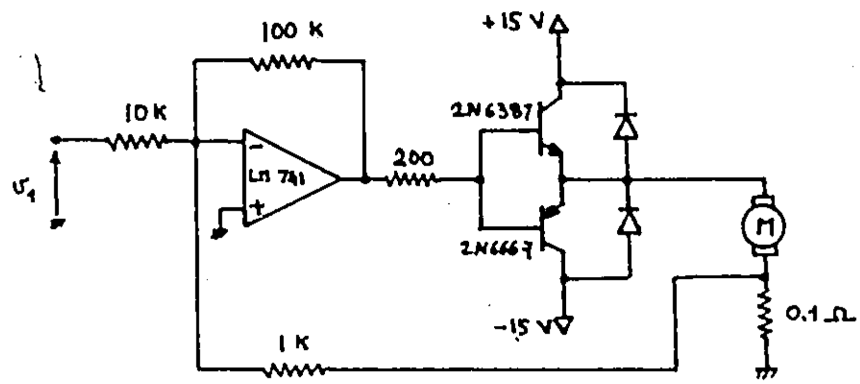

Figure 4.25. servo amplifier

The entire feedforward circuit for each of the two motors is shown on Figure 4.26.

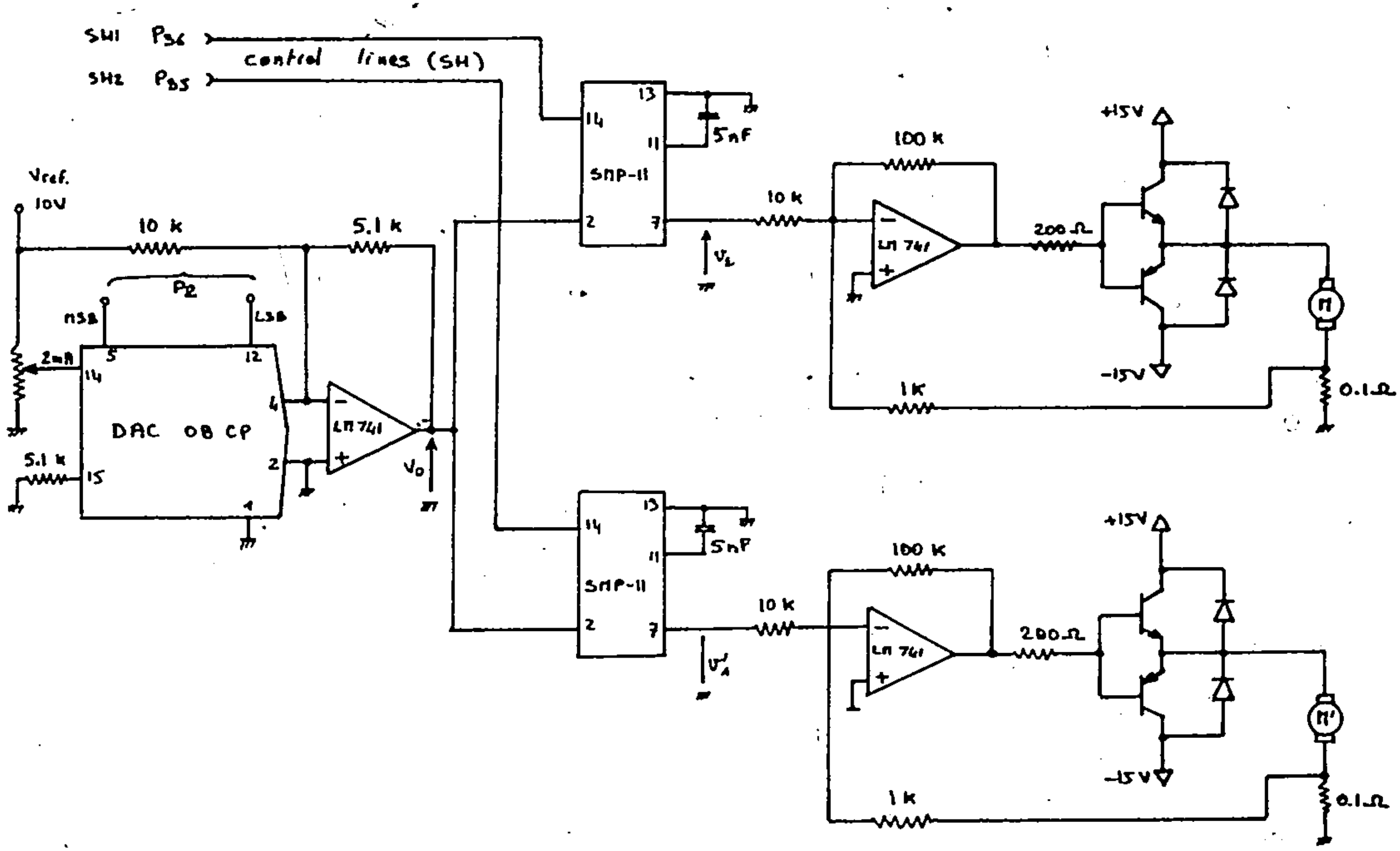

Figure 4.26. The feedforward circuit

B) <u>The feedback circuit</u>

Both position and velocity are feedback to the control microcomputer to close the control loop. Figure 4.27 shows the entire circuit.

As mentioned earlier, the position is sensed using a shaft encoder. The 50 equally distributed holes on the encoder disk are picked up by an optical switch. Ideally, the optical switch should provide a pulse every time a hole is encountered. However, due to the specifications of the switch and the small dimensions of the holes, the resulting voltage is a positive sine-wave with a maximum voltage of 0.2 Volt. The output voltage of the photo transistor is amplified from 0.2 Volt to about 6 Volts using the LM 741 Op-Amp as shown on Figure 4.27. The amplified voltage is then squared using a voltage comparator circuit utilizing an LM 311 Op-Amp. The capacitor on the feedback of the comparator amplifier is necessary to prevent glitches that occur when the input to the comparator is close to the reference voltage.

The comparator digital signal is used to initiate a counting interrupt in the control microcomputer every time a hole is detected. In order to know the direction of motion of the counterweight, a voltage comparator is used to detect the zero voltage crossover of the output voltage of the tachometer.

One such signal is necessary for each counterweight motor. However, one input line only is available on the control microcomputer. A selecting cicuit, also shown in Figure 4.27 is used to chanel the two signals one at a time.

The output voltage of the tachometers is filtered in order to suppress undesired ripple noise. The filtered signal is then converted into an 8-bits digital word using an Analog to Digital board which is directly interfaced with the control microcomputer.

The assembler program for the digital controller of the counterweights drives and the feedback processing is given in Appendix E.

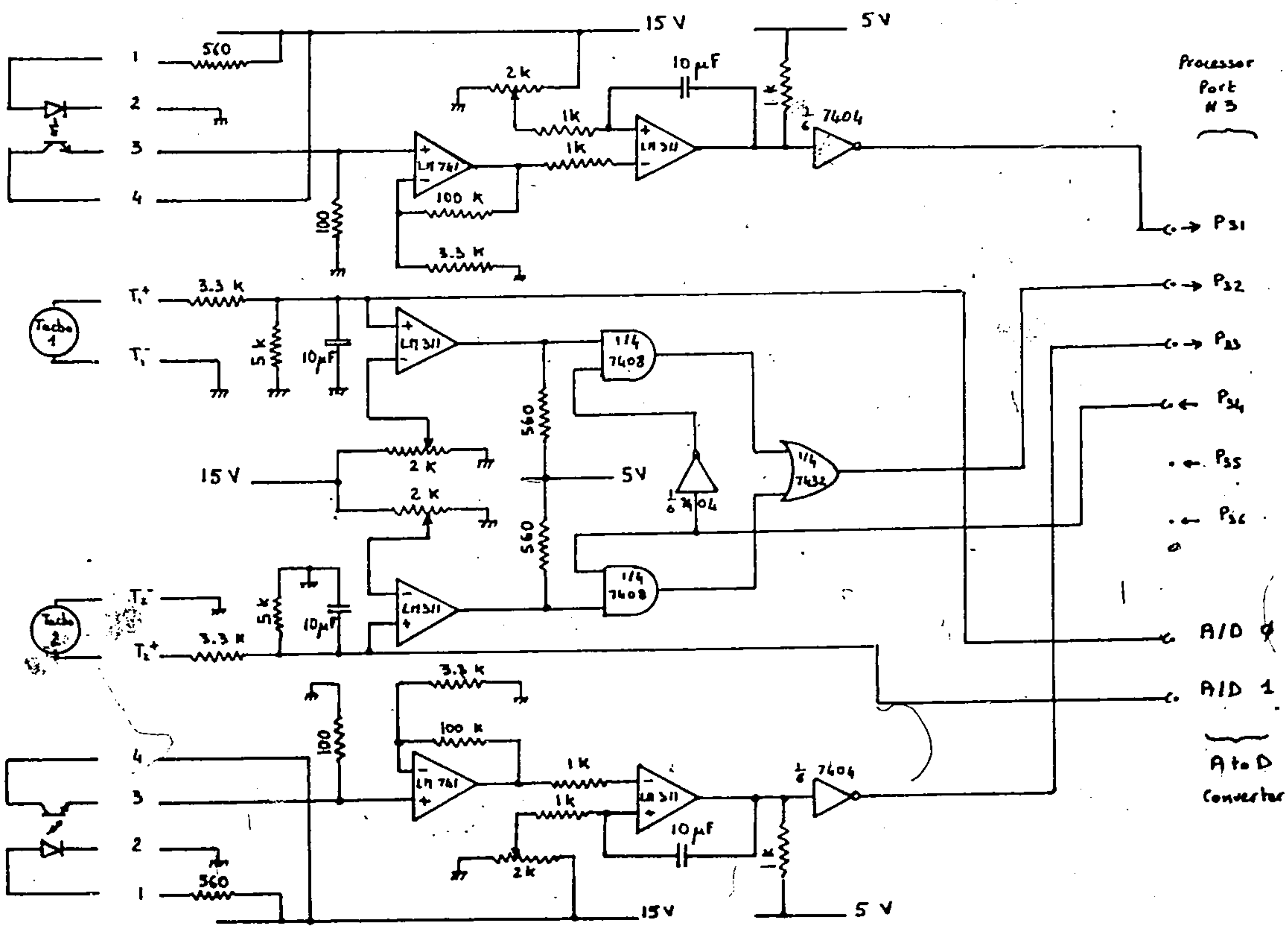

Figure 4.27. The feedback circuit

5. EXPERIMENTAL RESULTS OF THE ACTIVE COUNTERWEIGHT SYSTEM PROTOTYPE

Experiments have been conducted to verify that the theoretical results that show the torque necessary to move the upper arm can be reduced by using the active counterweight system. Furthermore that the savings in torque may be used to enable the robot arm to carry more load than the specified maximum payload.
The experiments were conducted using the ASEA Irb-6 revolute robot, described in Chapter 3, and the active counterweight system prototype described in Chapter 4. In these experiments the robot arm was guided over a number of trajectories while carrying different payloads, and the current to the different joint motors recorded. The motor current is used as an indication of the joint motors torques.

5.1. Experimental conditions

The torque required by the upper arm drive motor while the robot arm traverses its trajectory is directly proportional to the current fed into the motor, with the proportionality factor being the motor torque constant. Thus, the current of the motor is used as an indication of that motor torque.

Due to the inherent operating limitation of the ASEA Irb-6 robot used in the experiments, two modifications had to be made to the operating conditions that was used in the simulation work.

First, the experiments were conducted at a lower than the maximum possible velocity of the link for the following two reasons:

1) For the particular case of the ASEA Irb-6 industrial robot, it is not possible to control the speed of each joint individually. Only a maximum velocity for the end effector may be specified to the program and the robot controller computes the necessary velocity profile for each link so as to coordinate the overall motion and adhere to the specified velocity. The second and third link drive motors are identical, however the second link drive motor carries a much heavier load. consquently, the maximum velocity of the third link could not be reached for the trajectory used for the simulation.
2) The current for each drive motor of the robot is limited to a maximum value by the ASEA robot controller. Therefore, any reduction in torque, i.e. current, as a result of using the active counterweight system cannot be shown by these experiments, if a high velocity is used, as depicted in Figure 5.1. The velocities are thus chosen such that the current limitation is not encountered in order to be able to show the effect of the active counterweight system.

Secondly, the motion of the dynamic counterweight is anticipated before it occurs, and action is taken so that it is properly located when critical accelerations and decelerations occur. Modification of the balancing coordinator program were thus made to predict in advance the location of the dynamic counterweight.

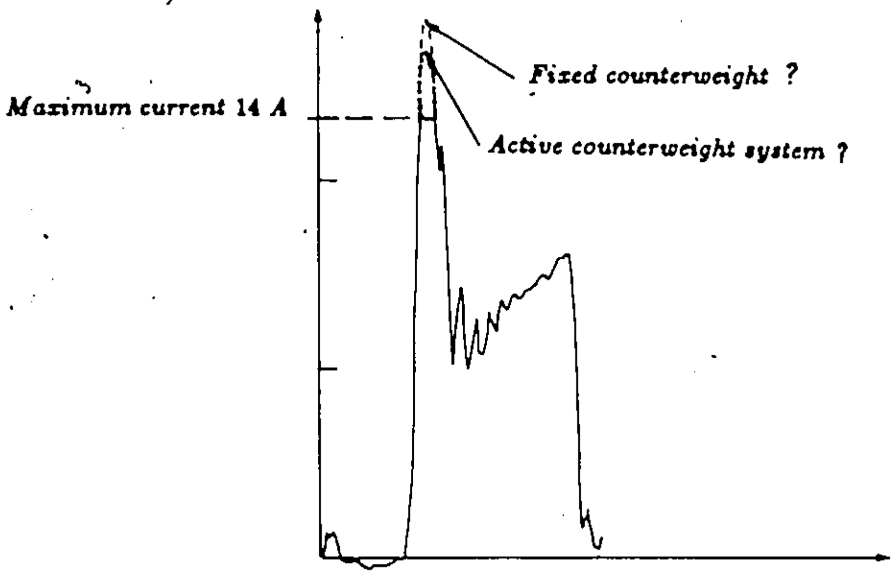

Figure 5.1. Joint motor current limiting in ASEA Irb-6 robot controller

5.2. Results of the experiments and discussion

Two different trajectories were utilized. The first trajectory is identical to the trajectory used in the simulation. The second trajectory was defined in such a way that it involves only the up and down motion of the upper arm.

5.2.1. <u>Experimental results utilising the trajectory used for the simulation</u>

Figure 5.2 shows the current curves for the upper arm drive for the cases where the upper link is balanced with the fixed counterweight, and when it is balanced with the active counterweight system. The identified points on the figure correspond to the points of the trajectory given in Figure 3.2. The payload carried by the robot in both cases is 6 kg. With reference to the figure, the overall effect of the active counterweight system as predicted by the simulation is apparent here. The entire current curve is centered around the zero ampere, and a maximum reduction of 12% in the first positive peak current is obtained versus a 25% theoretical reduction in torque predicted by the simulation. This discrepancy is due in large to the difference in link velocity between the simulation and the experiments.

Figure 5.3 shows the effect of the motion of the dynamic counterweight. With reference to the figure, a comparison is made between current curves when the dynamic counterweight is at rest, fully retracted, and when it moves as the robot traverses its trajectory. In the case where the dynamic counterweight is at rest, the center of mass of the active counterweight system corresponds approximately to the one of the fixed counterweight provided by the manufacturer. The following describes the effect of the motion of the dynamic counterweight:

At points A and C on the figure, the accelerations are in the positive direction (i.e. the upper link has to move upwards, against the gravitational forces). During such a motion, the dynamic counterweight is fully extended so as to assist the link drive motor. On the other hand, at points B and D, the accelerations of the upper arm are in the negative direction (i.e. the upper arm is moving in the direction of the gravitational pull). The dynamic counterweight in this case is fully retracted so as to limit the increase in current in the negative region.

One of the results concluded from the dynamic study of the revolute parallelogram type robot is that the location and the motion of the active counterweight system do not affect the torque necessary to move the second link. Figure 5.4 shows the current curves for both the fixed counterweight, and the active counterweight system. The traces show no significant difference between the two current curves. Thus, the motion of the second link of the parallelogram type robot configuration is almost independent of the location or the weight of the counterweight system that balances the upper arm.

For the first link, no theoretical study was conducted in the dynamic analysis to evaluate the effect of weight or motion of the counterweight system on the torque required to drive the link. By intuition, however, one can expect an increase in the torque necessary to rotate the base of the robot as the inertia of the system increases. The increase in the inertia of the system results from the increase in the radial location of the active counterweight system and from the increase in the mass of the payload. Figure 5.5 shows experimentally the extend to which the torque of the base link is affected by the active counterweight system. A slight increase in the torque required by the base link occurs particularly during accelerations and decelerations of the link. During constant velocity motion, however, there is practically no difference between both curves.

The robot was further tested with a one kg overload, 7 kg payload, in order to show the ability of the active counterweight system to boost up the load carrying capacity of a robot system. Figure 5.6 shows the curves of the third link motor current when the robot carries the 7 kg payload for the case where the robot arm is equipped with the active counterweight and the case where it is carrying its maximum designed payload, 6 kg, and equipped with the fixed counterweight supplied by the manufacturer. The plots show that, as a result of the action of the active counterweight system, the positive peaks of the current curve for the upper arm drive have been reduced to the level of those of the 6 kg payload current curve, or slightly below at some points. The maximum peak for the 7 kg payload and active counterweight occurs when the robot accelerates upward from point P_2 on the trajectory of Figure 3.2, and has a value of 13.1 amperes as compared to 13.6 amperes for the 6 kg payload and fixed counterweight. The minimum negative peaks for the case of 7 kg payload and active counterweight, however, have been increased to 11.8 amperes from 10.3 amperes for the case of 6 kg payload and fixed counterweight. The values of these peak currents show that the active counterweight approximately equalises the torque demand in both directions around the zero current. As a result, a trajectory that would cause saturation in one direction in the case of a fixed counterweight can be traversed when the robot is equipped with an active counterweight .

5.2.2. Experimental results for the motion of the upper arm alone

In this experiment, both the first and the second links remain at rest and the upper arm moves up and down, traversing its entire range of motion. Figure 5.7 shows the effect of the active counterweight system when the robot is traversing this special trajectory. Three curves are displayed in the graph; two curves for the case where the robot is equipped with the fixed counterweight and carries 6 and 7 kg respectively, and the curve for the case where the robot is equipped with the active counterweight system and carries a 7 kg payload. The plots show a reduction of approximately 10.4% in the positive peak current values as a result of using the active counterweight system. Consequently, peak currents for the case of 7 kg payload and active counterweight system, and the case of 6 kg and fixed counterweight system coincide. The drive for the upper arm link is not affected by the 1 kg overload when accelerating in the positive direction. The figure also shows that the active counterweight system has an effect on the negative peaks when the upper arm accelerates in the negative direction, similar to the results of the simulation. The minimum negative peak, however, remains lower than the maximum positive peak. If the active counterweight position had been further optimised, the peaks would have been symmetric around the zero current and a further gain in the load carrying capacity would have been achieved.

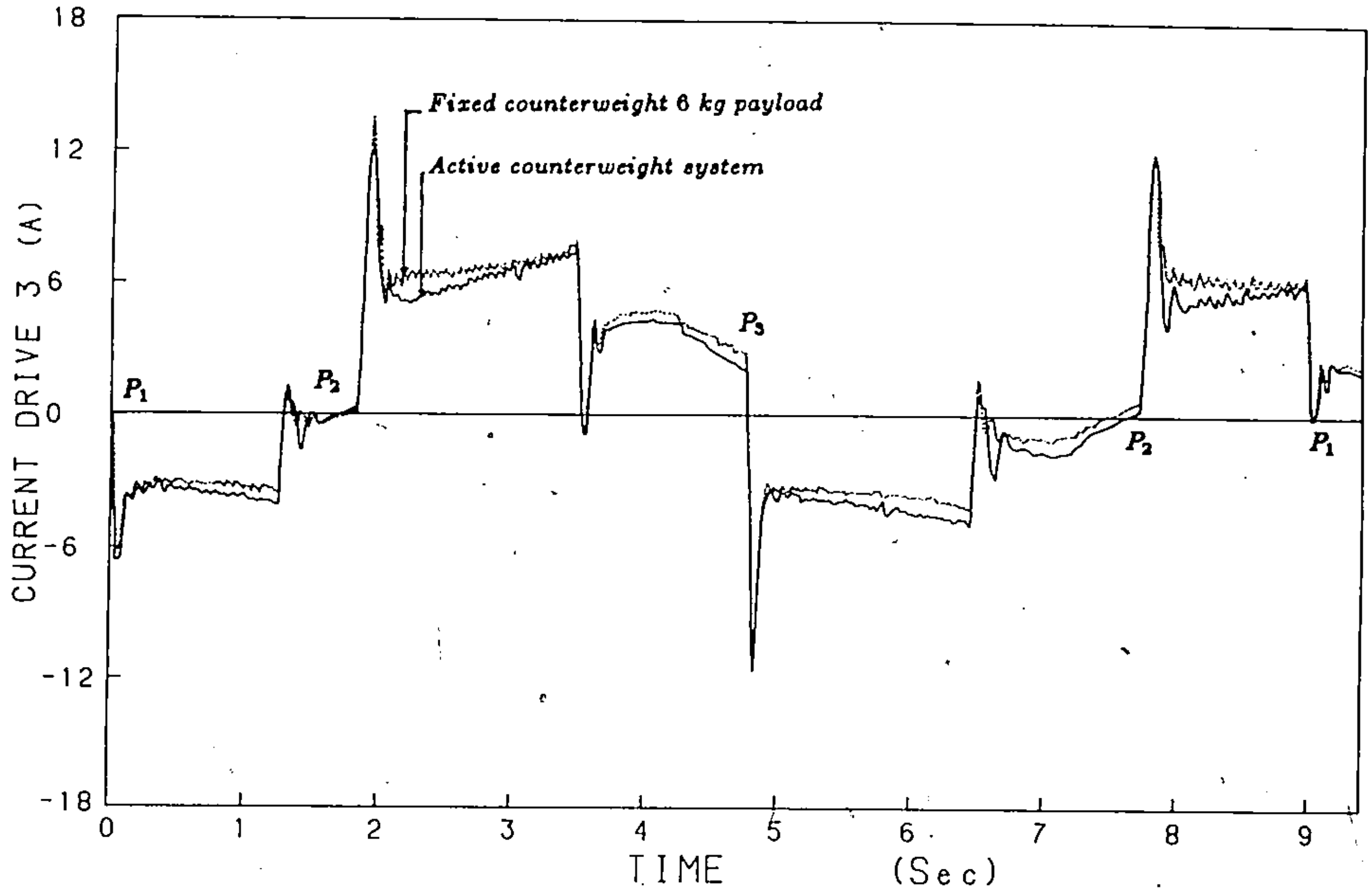

Figure 5.2. Current curves for the active and fixed counterweight systems

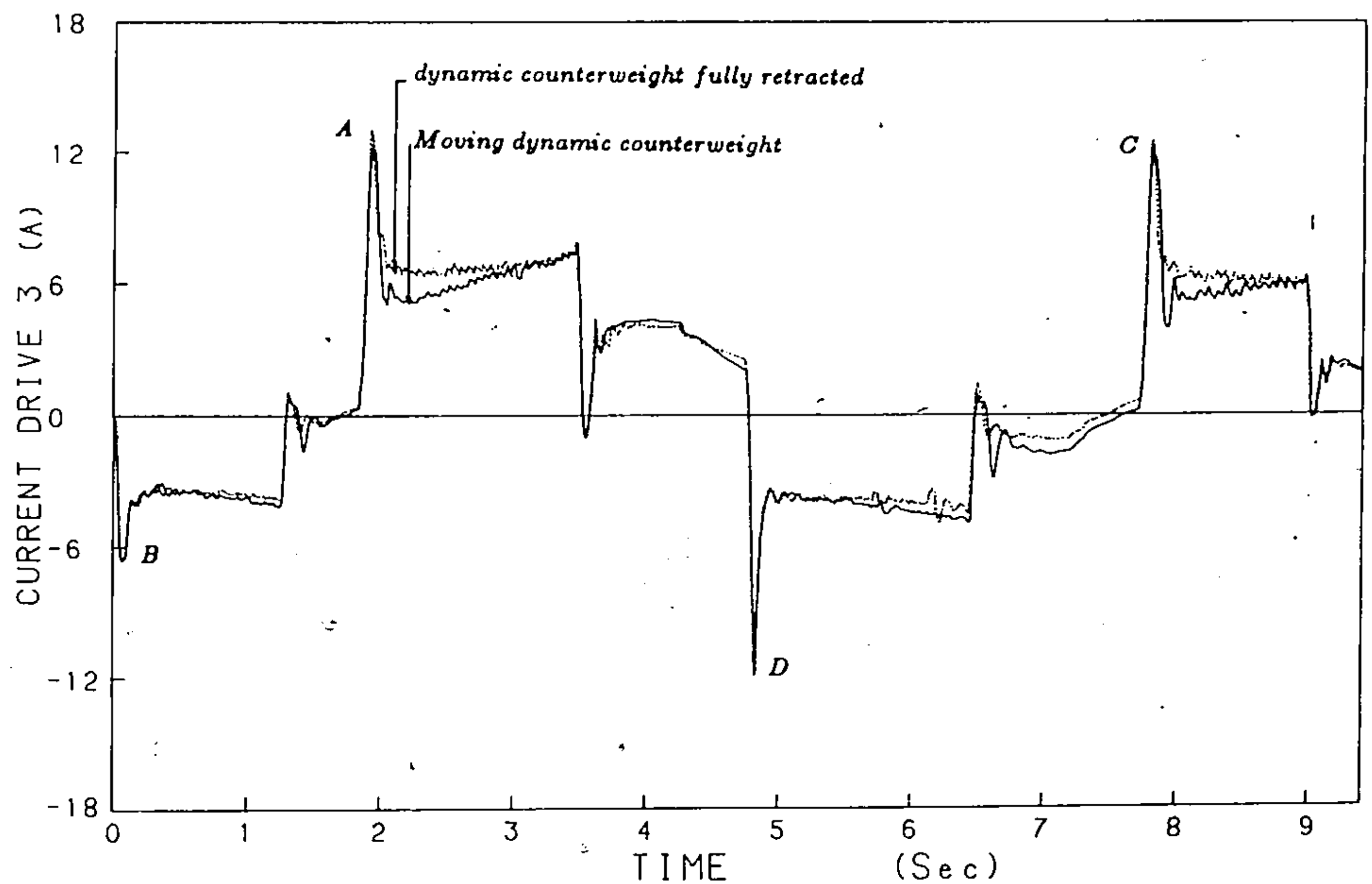

Figure 5.3. Isolated effect of the dynamic counterweight system

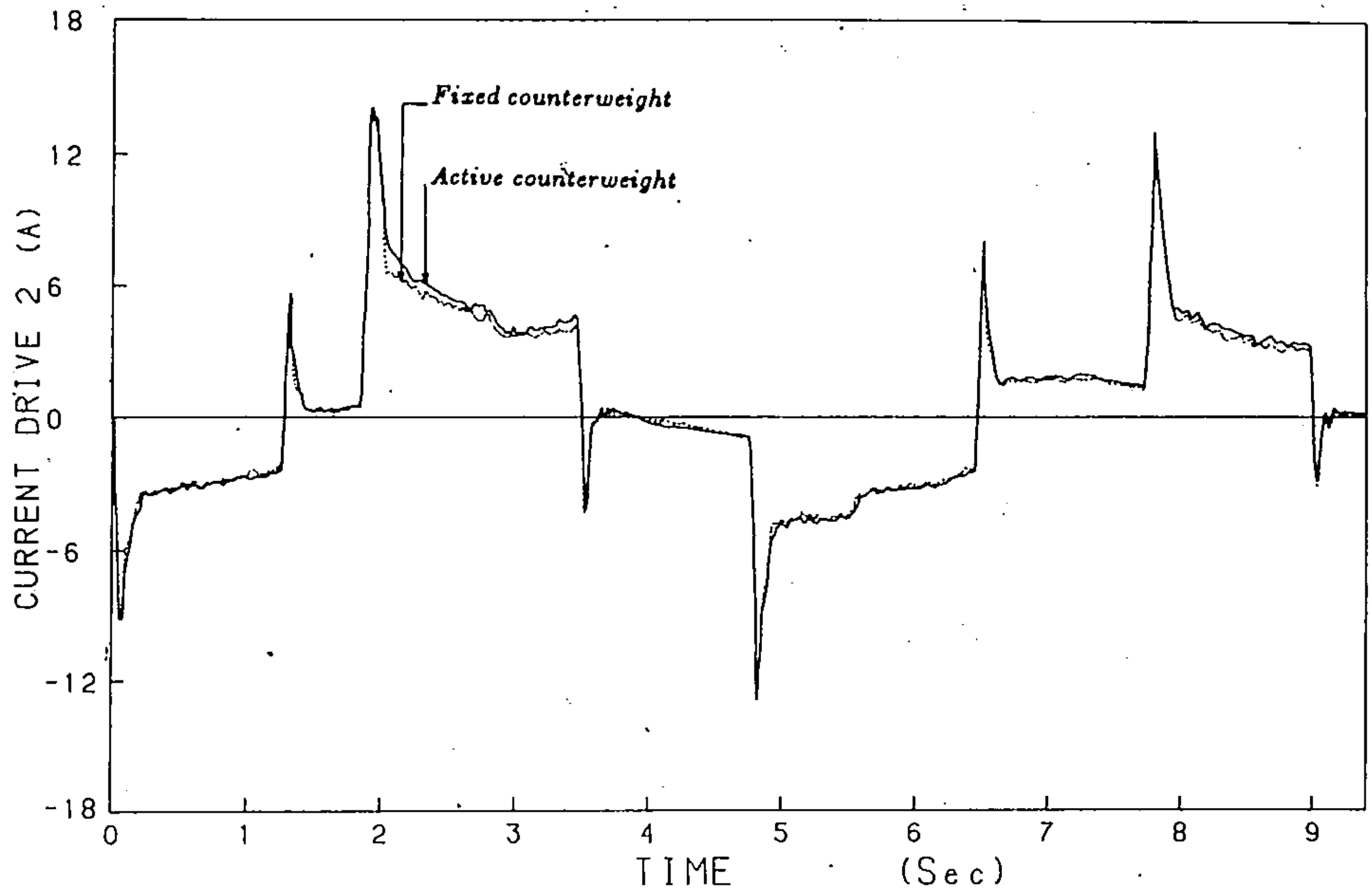

Figure 5.4. Effect of the active counterweight system on the second link drive motor current

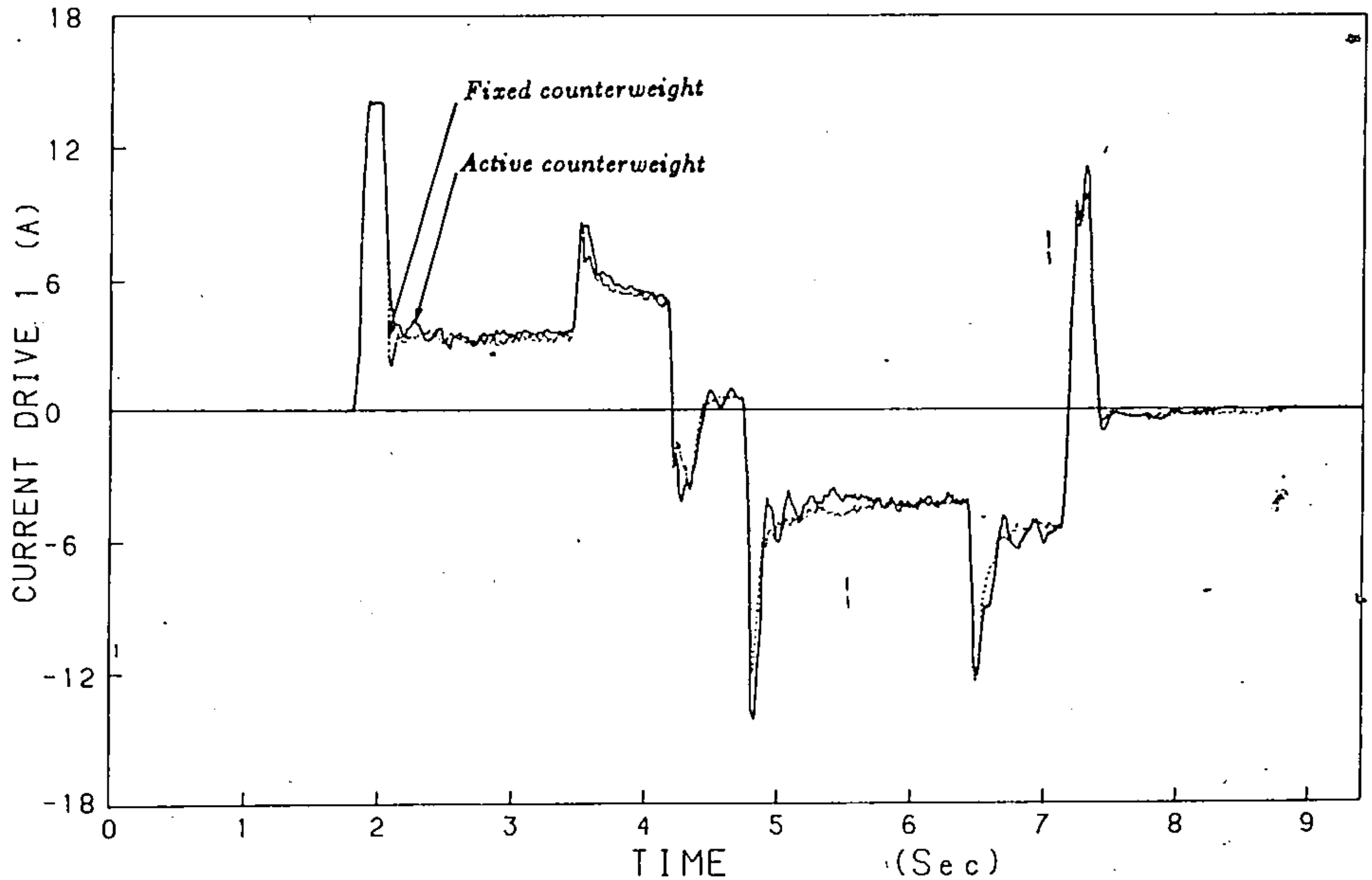

Figure 5.5. Effect of the active counterweight system on the first link drive motor current

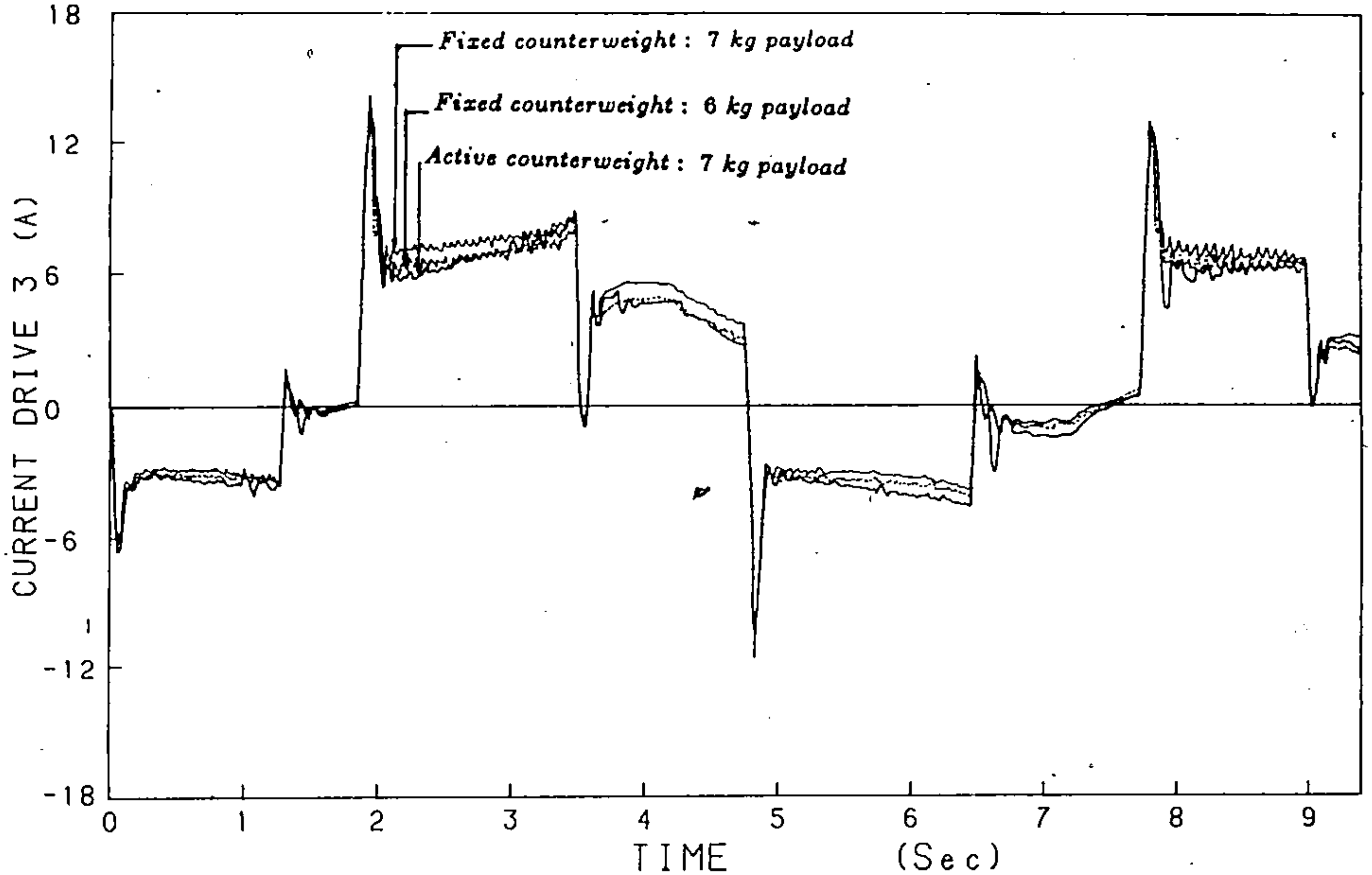

Figure 5.6. Comparison between the third link motor current for the case of: 6 & 7 kg payload & fixed counterweight, and 7 kg payload & active counterweight

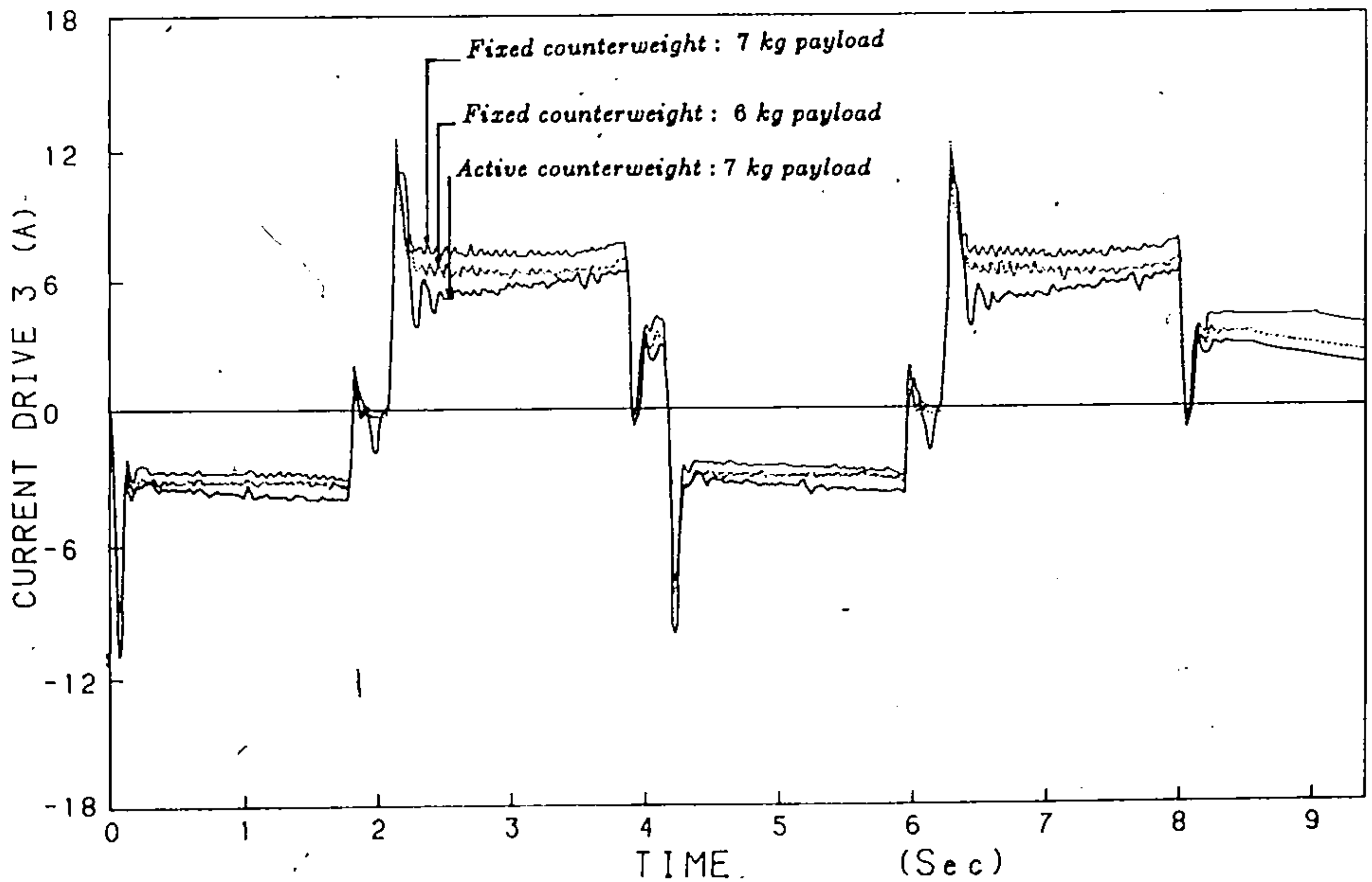

Figure 5.7. Comparison between active and fixed counterweight systems for 6 & 7 kg payloads, and upper arm movement only

6. CONCLUSION AND EXTENSIONS

The fixed counterweight approach currently used by robot manufacturers to counterbalance robot links only provides static balancing of these links. A new approach for balancing revolute-type robot arms is presented in this thesis. An "active counterweight system" is developed in order to achieve dynamic balancing of the robot links. The active counterweight masses are capable of changing their location as the robot arm traverses its trajectory. The counterweights movements are controlled in such a way to minimize the torque necessary to move the counterbalanced link. As a result of better balancing, more torque is available from the link drive to carry extra load.

A simplified dynamic analysis is developed for a robot arm equipped with the active counterweight system. This analysis is conducted under the following conditions:

1) The counterweight motion is assumed to be quasistatic. Thus, the dynamic effects due to the translation motion of the counterweight are neglected.
2) When compared with the 3 first links, the orientation of the wrist of the manipulator is assumed to have negligible effect on the dynamics of the system. Furthermore, The wrist and payload are assumed to be point mass and the dynamics of their motion with respect to their reference frames ignored.

3) The robot links are assumed to be symmetric along their longitudinal axis thus reducing the inertia matrices to diagonal ones.

A simulation based on this simplified dynamic analysis shows that the active counterweight system decreases the torque necessary to move the balanced link. For an active counterweight mass equal to that of the fixed counterweight supplied by the manufacturer, the savings in torque improves the payload carrying capacity of the arm by 17% above the maximum limit fixed by the robot manufacturer.

An active counterweight system prototype as well as the control scheme necessary for its operation is designed and built. The overall mass of the active counterweight system prototype is split among two counterweight subsystems; a) A quasistatic counterweight that can move with respect to the arm joint so as to statically balance the arm and payload, and b) A dynamic counterweight that translates with respect to the quasistatic counterweight to dynamically balance the arm and payload.

A 'balancing coordinator program' uses the kinematics of the robot arm to find the optimum position for both counterweights as the arm traverses its trajectory. Digital controllers utilizing closed loop control position the quasistatic and dynamic counterweights at the optimum locations.

Experiments were conducted with a parallelogram type revolute robot utilizing the prototype active counterweight system to balance the robot's upper arm. The experiments show good agreement with the simulation. As predicted, the active counterweight system enables the robot arm to carry a 17 % extra payload.
The experimental results were obtained for velocities up to 60 % of the maximum velocity of the particular robot. Joint motor current limiting built into the robot controller by the manufacturer prevented experimentation and drawing of conclusions at higher operating velocities.
The experiments confirmed one of the main advantages of the parallelogram robot configuration over the other revolute robots configurations, namely: the position and motion of the active counterweight system balancing the upper arm of the robot has no effect on the torque of the lower arm.

Further extensions on the topic of this thesis should include the following:

- Assumptions used in the dynamic analysis could be reconsidered and possibly a full dynamic model of the robot arm with active counterweight developed. This extended work would take into account the motion of the counterweight, the orientation of the payload and its inertial effects.
- Optimization of the balancing coordinator program could be carried out so as to predict more efficiently the correct

necessary position, velocity and acceleration profiles for the motion of the dynamic counterweight, thus reducing the peaks in negative torque experienced using the current program.

- The actual design of the active counterweight system could be enhanced for example by having both the quasistatic and dynamic counterweights physically independent from each other, thus increasing the span of motion of the overall active counterweight system.

REFERENCES

[1] Martins G.: 'Flexible manufacturing cells for small batch production'; ASEA AB Sweden ; p. 149 of the '14th International Symposium on Industrial Robots'; Edited by Prof. N. Martensson; Gothenburg; 1984.

[2] C. S.George Lee: 'Robot Arm Kinematics, Dynamics and Control'; IEEE Paper 0018-9162/82/1200-0062500.75; 1982.

[3] El-Zorkany H. I.: 'Basic Motion and Control of Robots'; National Research Council, Ottawa, Ontario; Paper for the Canadian Conference on Industrial Computer Systems; Mc Master H.; May 1982.

[4] Euvrard P. & Fernandez M.: 'Montage Automatique Flexible d'une Planche de Bord'; ENSAM Paris; 1985.

[5] Paul R.: 'Robot Manipulator, Mathematical Programming and Control'; MIT press; Cambridge, Mass; 1981.

[6] Kafrissen Edward & Stephans Mark: 'Industrial Robots and Robotics' Reston Publishing Compagny; 1984.

[7] William J. Palm III: 'Modelling, Analysis and Control of Dynamic Systems'; John Wiley and Sons, Inc; 1983.

[8] Kuo Benjamin C.: 'Automatic Control Systems'; Prentice-Hall; 1982.

[9] Dorf Richard C.: 'Modern Control Systems'; Addison-Wesley Publishing compagny, Inc; 1983.

[10] Katz Paul: 'Digital Control Using Microprocessors'; Prentice-Hall International, Inc; 1981.

[11] Kuo B. C. & Tal J.; 'Incremental Motion Control: DC Motors and Control Systems'; S.R.L. Publishing Compagny; 1978.

[12] Gvozdev Y.F.; 'New Balancing Mechanisms For The Links Of Robot Arms'; Vestnik Mashinostroeniya, Vol. 63, Issue 8; 1983.

[13] Asada Haruhiko; 'Analysis And Design Of A Direct-Drive Arm With A Five-Bar-Link Parallel Drive Mechanism'; MIT; ASME Paper; 1984.

APPENDIX A

Acceleration vectors for the important points of the robot arm

Equation 2.3 gives the acceleration for the end point of the upper arm, $\vec{a}_{O_4}$ as follows:

$$\vec{a}_{O_4} = -[\ddot{\theta}_2 b_2 S_2 + \ddot{\theta}_{23} b_3 S_{23} + \dot{\theta}_1^2(b_2C_2 + b_3C_{23}) + \dot{\theta}_2^2 b_2 C_2 + \dot{\theta}_{23}^2 b_3 C_{23}]\vec{i}_1$$
$$+ [\ddot{\theta}_2 b_2 C_2 + \ddot{\theta}_{23} b_3 C_{23} - \dot{\theta}_2^2 b_2 S_2 - \dot{\theta}_{23}^2 b_3 S_{23}]\vec{j}_1$$
$$+ [-\ddot{\theta}_1(b_2C_2 + b_3C_{23}) + 2\dot{\theta}_1\dot{\theta}_2 b_2 S_2 + 2\dot{\theta}_1\dot{\theta}_{23} b_3 S_{23}]\vec{k}_1 \qquad \text{A.1}$$

The acceleration of the center of mass of the upper arm, $\vec{a}_{G_3}$, is derived from Equation A.1 by replacing the term b_3 by e_3 :

$$\vec{a}_{G_3} = -[\ddot{\theta}_2 b_2 S_2 + \ddot{\theta}_{23} e_3 S_{23} + \dot{\theta}_1^2(b_2C_2 + e_3C_{23}) + \dot{\theta}_2^2 b_2 C_2 + \dot{\theta}_{23}^2 e_3 C_{23}]\vec{i}_1$$
$$+ [\ddot{\theta}_2 b_2 C_2 + \ddot{\theta}_{23} e_3 C_{23} - \dot{\theta}_2^2 b_2 S_2 - \dot{\theta}_{23}^2 e_3 S_{23}]\vec{j}_1$$
$$+ [-\ddot{\theta}_1(b_2C_2 + e_3C_{23}) + 2\dot{\theta}_1\dot{\theta}_2 b_2 S_2 + 2\dot{\theta}_1\dot{\theta}_{23} e_3 S_{23}]\vec{k}_1 \qquad \text{A.2.a}$$

The three components of $\vec{a}_{G_3}$ in the frame $(\vec{i}_1, \vec{j}_1, \vec{k}_1)$, $a^X_{G_3}$, $a^Y_{G_3}$ and $a^Z_{G_3}$ can thus be expressed as follows:

$$a^X_{G_3} = -[\ddot{\theta}_2 b_2 S_2 + \ddot{\theta}_{23} e_3 S_{23} + \dot{\theta}_1^2(b_2C_2 + e_3C_{23}) + \dot{\theta}_2^2 b_2 C_2 + \dot{\theta}_{23}^2 e_3 C_{23}] \qquad \text{A.2.b}$$

$$a^Y_{G_3} = [\ddot{\theta}_2 b_2 C_2 + \ddot{\theta}_{23} e_3 C_{23} - \dot{\theta}_2^2 b_2 S_2 - \dot{\theta}_{23}^2 e_3 S_{23}] \qquad \text{A.2.c}$$

$$a^Z_{G_3} = [-\ddot{\theta}_1(b_2C_2 + e_3C_{23}) + 2\dot{\theta}_1\dot{\theta}_2 b_2 S_2 + 2\dot{\theta}_1\dot{\theta}_{23} e_3 S_{23}] \qquad \text{A.2.d}$$

The acceleration $\vec{a}_{E_3}$ of the center of mass of the counterweight, when it is aligned with the upper arm, is obtained by replacing b_3 by $-r_3$ in Equation A.1:

$$\vec{a}_{E_3} = -[\ddot{\theta}_2 b_2 S_2 - \ddot{\theta}_{23} r_3 S_{23} + \dot{\theta}_1^2(b_2C_2 - r_3C_{23}) + \dot{\theta}_2^2 b_2 C_2 - \dot{\theta}_{23}^2 r_3 C_{23}]\vec{i}_1$$
$$+ [\ddot{\theta}_2 b_2 C_2 - \ddot{\theta}_{23} r_3 C_{23} - \dot{\theta}_2^2 b_2 S_2 + \dot{\theta}_{23}^2 r_3 S_{23}]\vec{j}_1$$
$$+ [-\ddot{\theta}_1(b_2C_2 - r_3C_{23}) + 2\dot{\theta}_1\dot{\theta}_2 b_2 S_2 - 2\dot{\theta}_1\dot{\theta}_{23} r_3 S_{23}]\vec{k}_1 \qquad \text{A.3}$$

Considering now the parallelogram-type configuration for the robot arm, the counterweight is located on the first link as shown on Figure 2.6. In such a case, the acceleration of the counterweight $\vec{a}_{B_3'}$ is derived from Equation A.3 by setting the length b_2 to zero as follows:

$$\begin{aligned}\vec{a}_{B_3'} = \quad & [\ddot{\theta}_{23} r_3 S_{23} + \dot{\theta}_1^2 r_3 C_{23} + \dot{\theta}_{23}^2 r_3 C_{23}]\vec{i}_1 \\ & + [-\ddot{\theta}_{23} r_3 C_{23} + \dot{\theta}_{23}^2 r_3 S_{23}]\vec{j}_1 \\ & + [\ddot{\theta}_1 r_3 C_{23} - 2\dot{\theta}_1 \dot{\theta}_{23} r_3 S_{23}]\vec{k}_1\end{aligned} \qquad \text{A.4.a}$$

The three components of $\vec{a}_{B_3'}$ in the frame $(\vec{i}_1\ \vec{j}_1\ \vec{k}_1)$, $a^X_{B_3'}$, $a^Y_{B_3'}$ and $a^Z_{B_3'}$ are thus written as follows:

$$a^X_{B_3'} = \ddot{\theta}_{23} r_3 S_{23} + \dot{\theta}_1^2 r_3 C_{23} + \dot{\theta}_{23}^2 r_3 C_{23} \qquad \text{A.4.b}$$

$$a^Y_{B_3'} = -\ddot{\theta}_{23} r_3 C_{23} + \dot{\theta}_{23}^2 r_3 S_{23} \qquad \text{A.4.c}$$

$$a^Z_{B_3'} = \ddot{\theta}_1 r_3 C_{23} - 2\dot{\theta}_1 \dot{\theta}_{23} r_3 S_{23} \qquad \text{A.4.d}$$

Expressed in the frame of the upper arm, $(\vec{i}_3, \vec{j}_3, \vec{k}_3)$, the acceleration $\vec{a}_{E_3'}$ becomes:

$$\begin{aligned}\vec{a}_{B_3'} = & (\dot{\theta}_1^2 r_3 C_{23}^2 + \dot{\theta}_{23}^2 r_3)\vec{i}_3 \\ & - (\ddot{\theta}_{23} r_3 + \dot{\theta}_1^2 r_3 C_{23} S_{23})\vec{j}_3 \\ & + (\ddot{\theta}_1 r_3 C_{23} - 2\dot{\theta}_1 \dot{\theta}_{23} r_3 S_{23})\vec{k}_3\end{aligned} \qquad \text{A.5}$$

As far as the counterweight is concerned, a quasistatic approach is considered in the second chapter and the translation of the active counterweight along the axis of the upper arm is ignored. In the simulation, however, the complete acceleration of the active counterweight system is required so as to derive the force necessary to translate the dynamic counterweight.

Let $\vec{r}_3$, $\dot{\vec{r}}_3$ and $\ddot{\vec{r}}_3$ be the relative position, velocity and acceleration of the counterweight respectively, and $\vec{\Omega}_3$ and $\dot{\vec{\Omega}}_3$ be the absolute angular velocity and acceleration of the counterweight. The general form of the absolute acceleration of the active counterweight system is as follows:

$$\vec{a} = \ddot{\vec{r}}_3 + \dot{\vec{\Omega}}_3 \times \vec{r}_3 + \vec{\Omega}_3 \times (\vec{\Omega}_3 \times \vec{r}_3) + 2\vec{\Omega}_3 \times \dot{\vec{r}}_3 \qquad \text{A.6}$$

where

$$\begin{aligned} \vec{r}_3 &= -r_3\vec{i}_3 \\ \dot{\vec{r}}_3 &= -\dot{r}_3\vec{i}_3 \\ \ddot{\vec{r}}_3 &= -\ddot{r}_3\vec{i}_3 \end{aligned} \qquad \text{A.7}$$

and

$$\vec{\Omega}_3 = \dot{\theta}_1 S_{23}\vec{i}_3 + \dot{\theta}_1 C_{23}\vec{j}_3 + \dot{\theta}_{23}\vec{k}_3 \qquad \text{A.8}$$

$$\begin{aligned} \dot{\vec{\Omega}}_3 = \quad & (\ddot{\theta}_1 S_{23} + \dot{\theta}_1\dot{\theta}_{23}C_{23})\vec{i}_3 \\ & + (\ddot{\theta}_1 C_{23} - \dot{\theta}_1\dot{\theta}_{23}S_{23})\vec{j}_3 \\ & + \ddot{\theta}_{23}\vec{k}_3 \end{aligned} \qquad \text{A.9}$$

Substituting Equations A.7 to A.9 into Equation A.6, and rearranging gives:

$$\begin{aligned} \vec{a} = \quad & [r_3(\dot{\theta}_1^2 C_{23}^2 + \dot{\theta}_{23}^2) - \ddot{r}_3]\vec{i}_3 \\ & - [2\dot{r}_3\dot{\theta}_{23} + r_3(\ddot{\theta}_{23} + \dot{\theta}_1^2 C_{23}S_{23})]\vec{j}_3 \\ & + [2\dot{r}_3\dot{\theta}_1 C_{23} + r_3(\ddot{\theta}_1 C_{23} - 2\dot{\theta}_1\dot{\theta}_{23}S_{23})]\vec{k}_3 \end{aligned} \qquad \text{A.10}$$

APPENDIX B

Design drawings of the active conterweight system

prototype

Part description and list

23	GEARED DC MOTOR		2	PITTMAN GMT9414 12VDC
22	OPTICAL SWITCH		2	TI XL 143
21	BRONZE BUSHING	BRONZE	2	ID 1/2, OD 5/8, L 2 1/4
20	BRONZE BUSHING	BRONZE	2	ID 3/8, OD 1/2, L 3/8
19	BALL BUSHING		4	ID 1/4, OD 1/2, L 3/4
18	LOWER SHAFTS	STEEL	2	DIA = 1/2 "; L = 14.97 "
17	UPPER SHAFTS	HARDND STEEL	2	DIA = 1/4 "; L = 9.46 "
16	SPUR GEAR	STEEL	2	H 2412 PITCH 24; 14.5 PA
15	RACK	BRASS	1	G 579-2 14.5 PRESS. ANGLE
14	LOWER HOLDER	STEEL	1	
13	UPPER HOLDER	STEEL	1	
12	ENCODER	ALUMINIUM	2	
11	COUPLING	STEEL	2	
10	HOUSING	STEEL	2	
9	BRACKET	STEEL	2	
8	LEAD BLOCK	LEAD	1	
7	LEFT COVER	STEEL	1	
6	RIGHT COVER	STEEL	1	
5	CASING	STEEL	2	
4	UPPER PLATE	STEEL	1	
3	SHAFT HOLDER	STEEL	1	
2	SUPPORT	STEEL	1	
1	SPACER	STEEL	2	
NO	DESIGNATION	MATERIAL	QTY	REMARKS

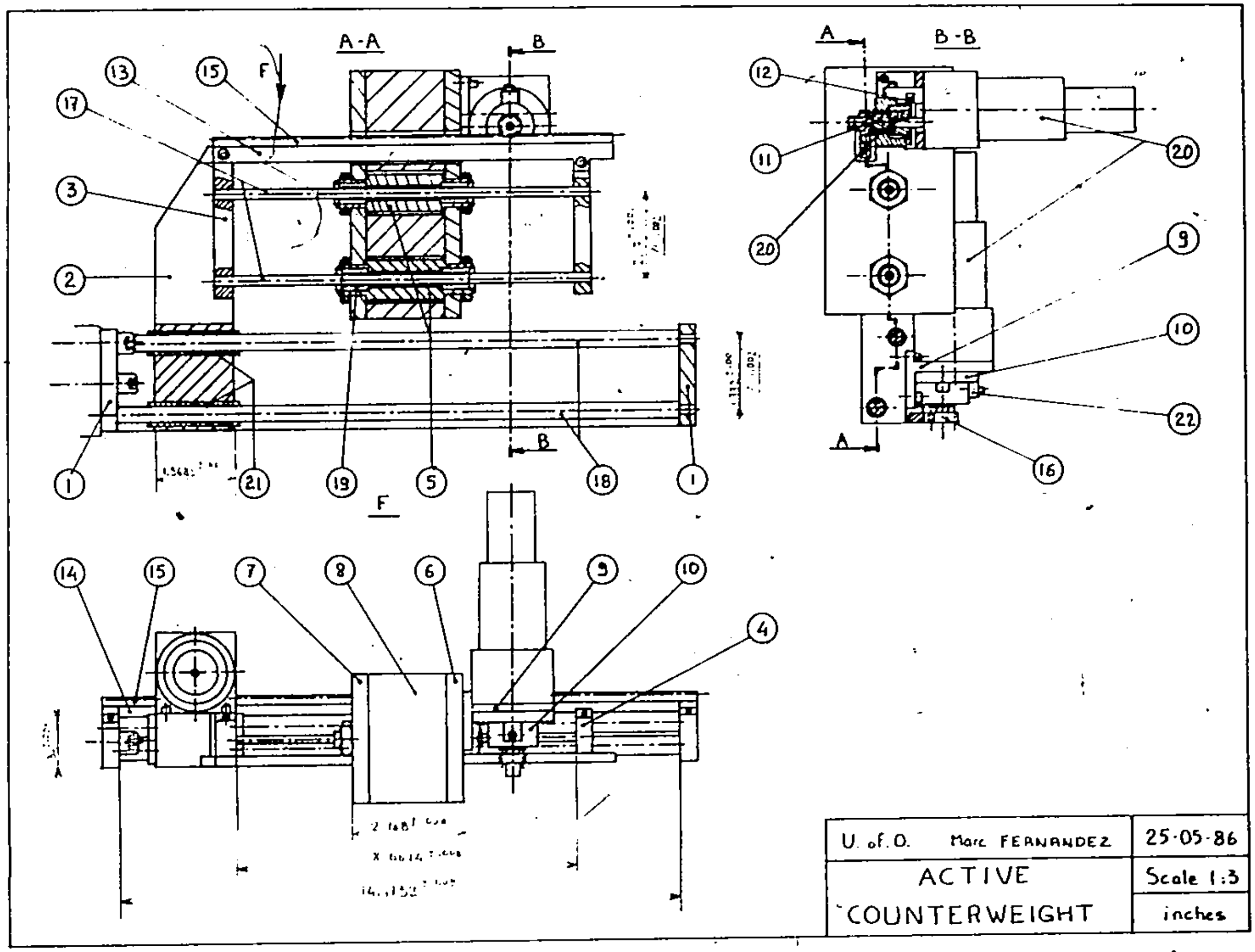

Figure B.1. Design drawings of the active counterweight system prototype (continued)

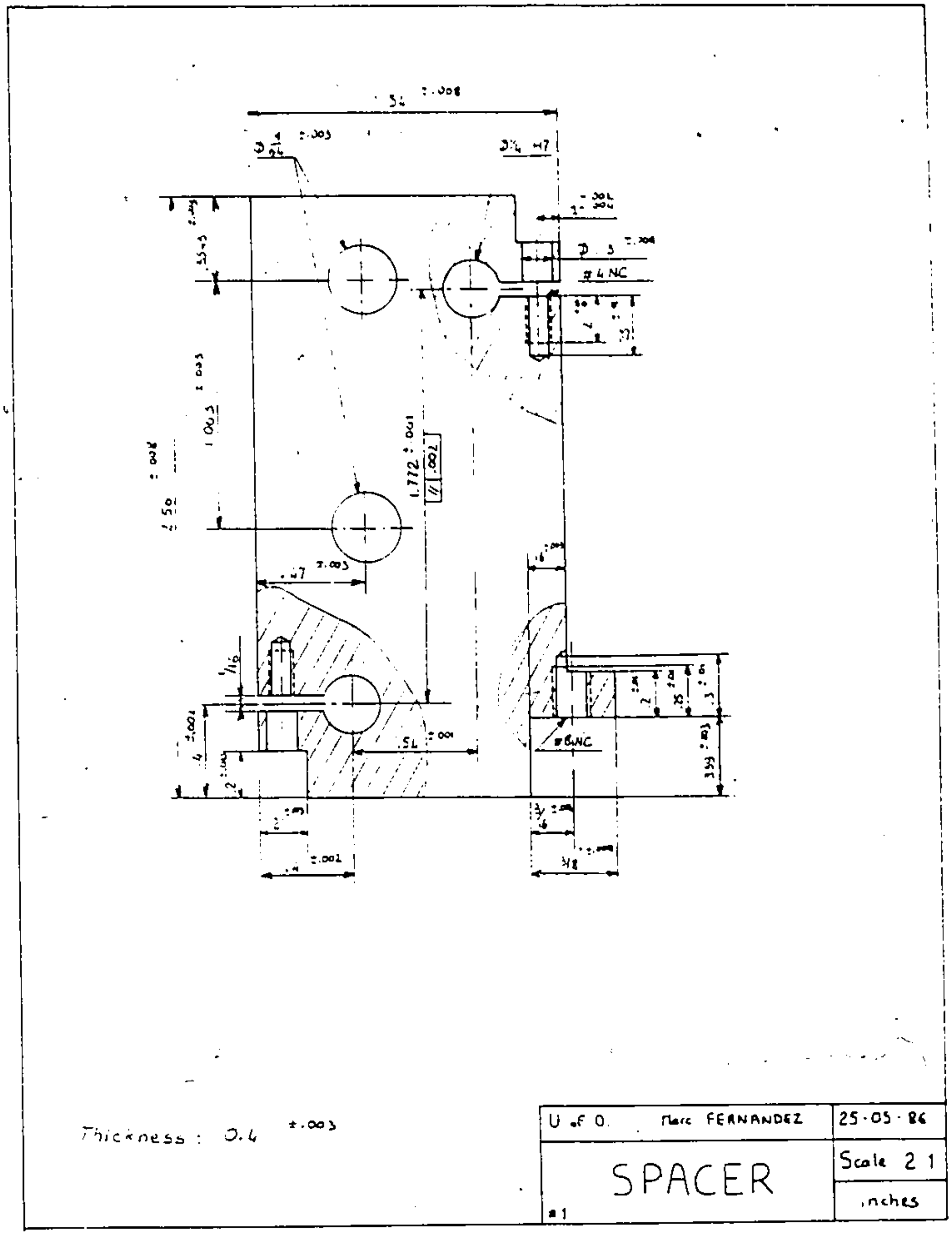

Figure B.2. Design drawings of the active counterweight system prototype (continued)

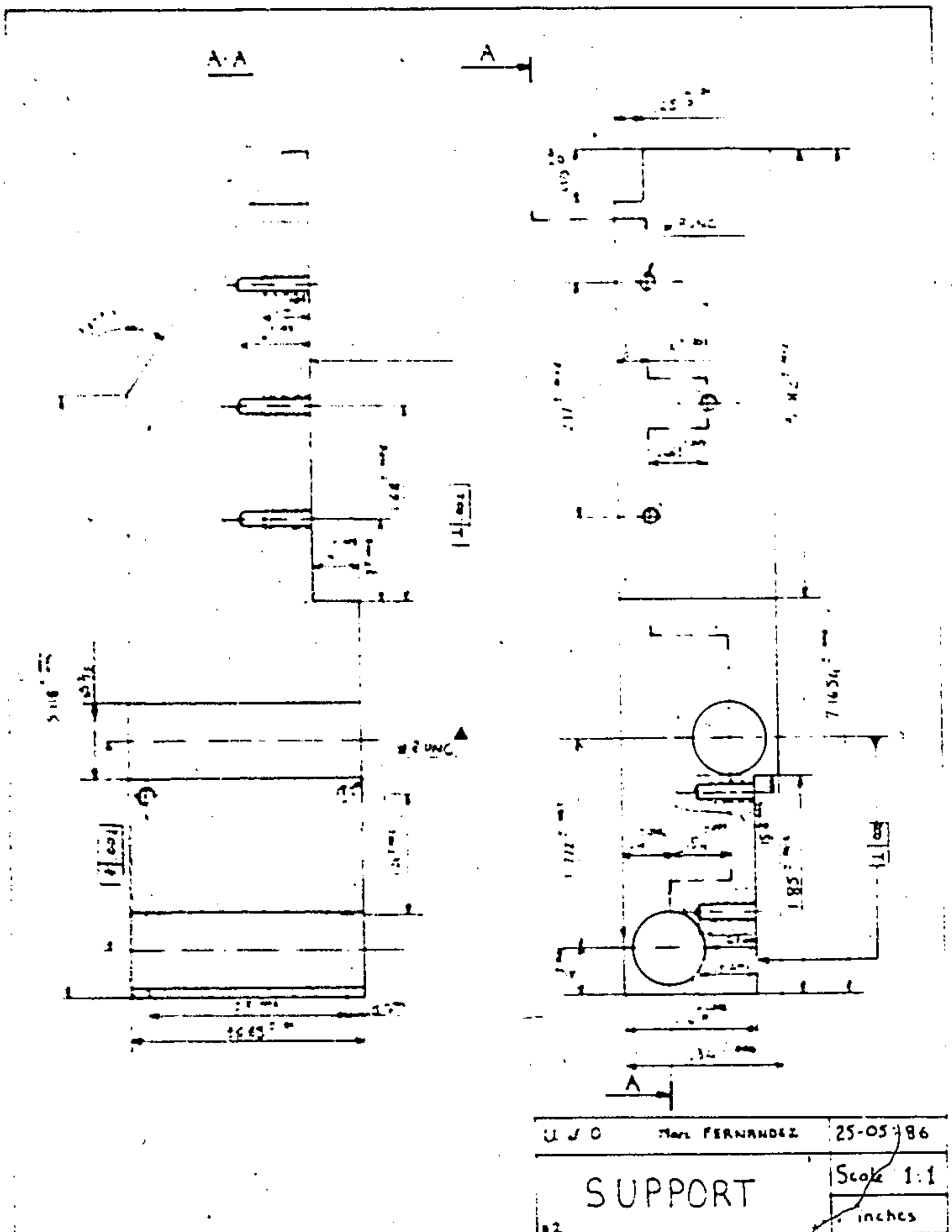

Figure B.3. Design drawings of the active counterweight system prototype (continued)

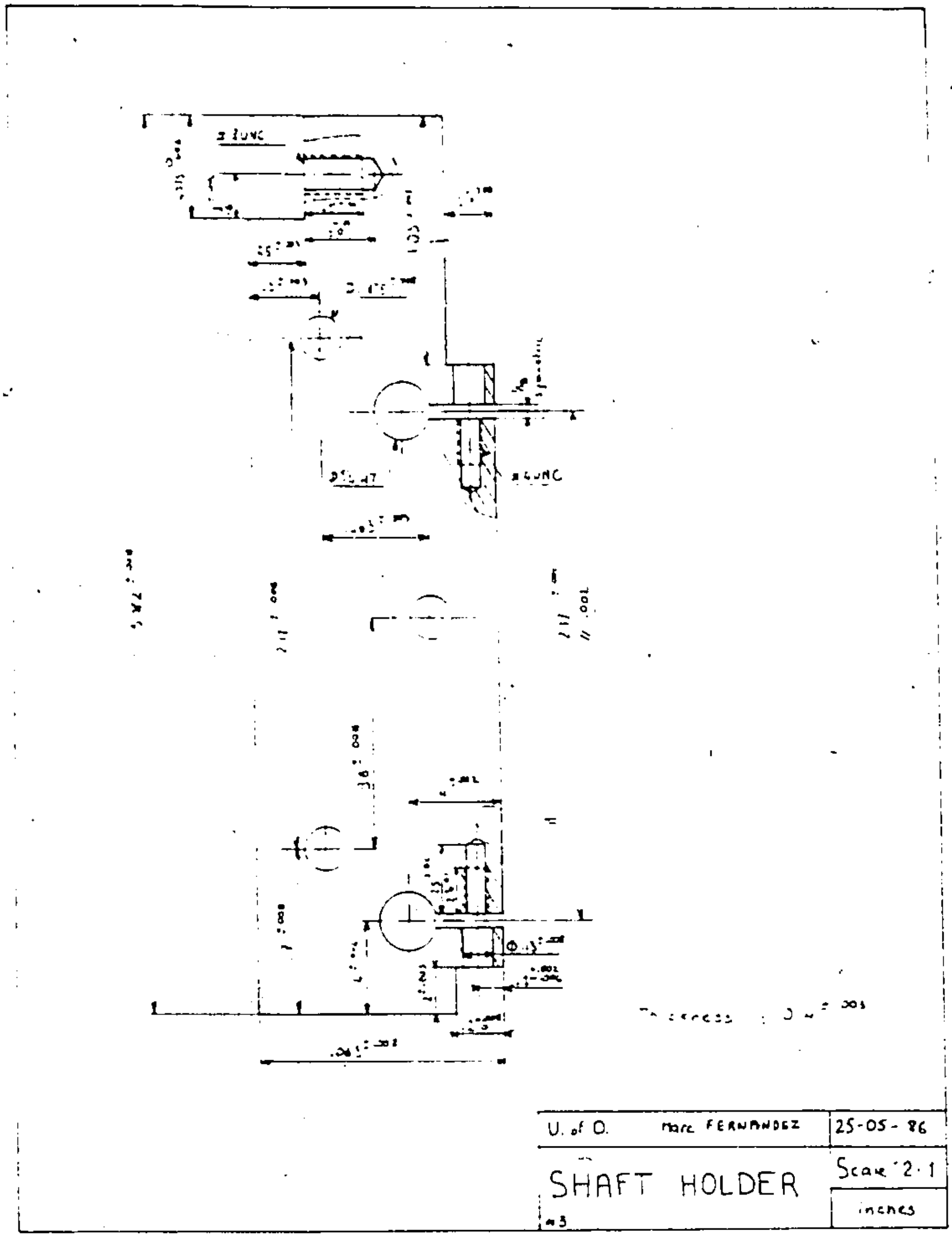

Figure B.4. Design drawings of the active counterweight system prototype (continued)

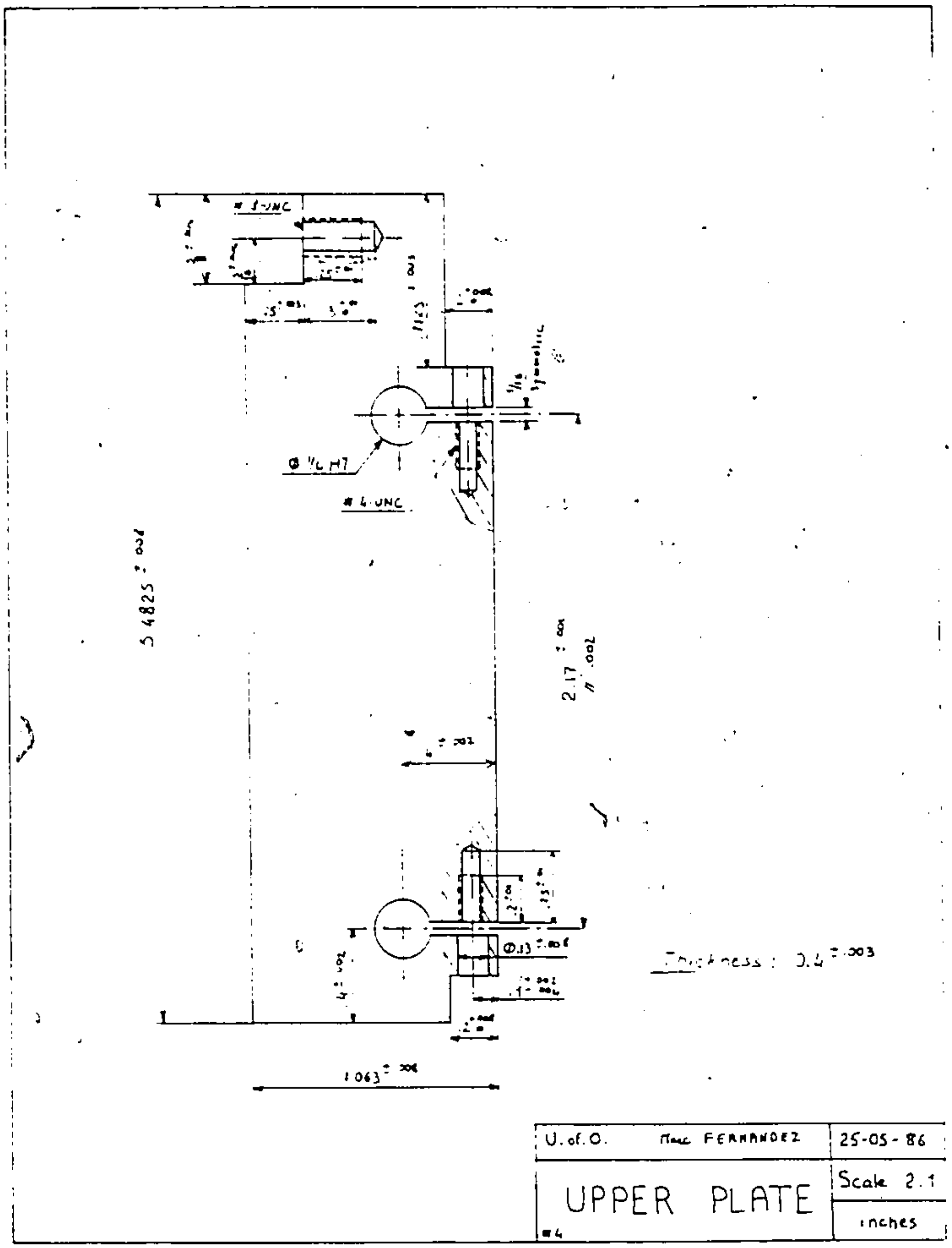

Figure B.5. Design drawings of the active counterweight system prototype (continued)

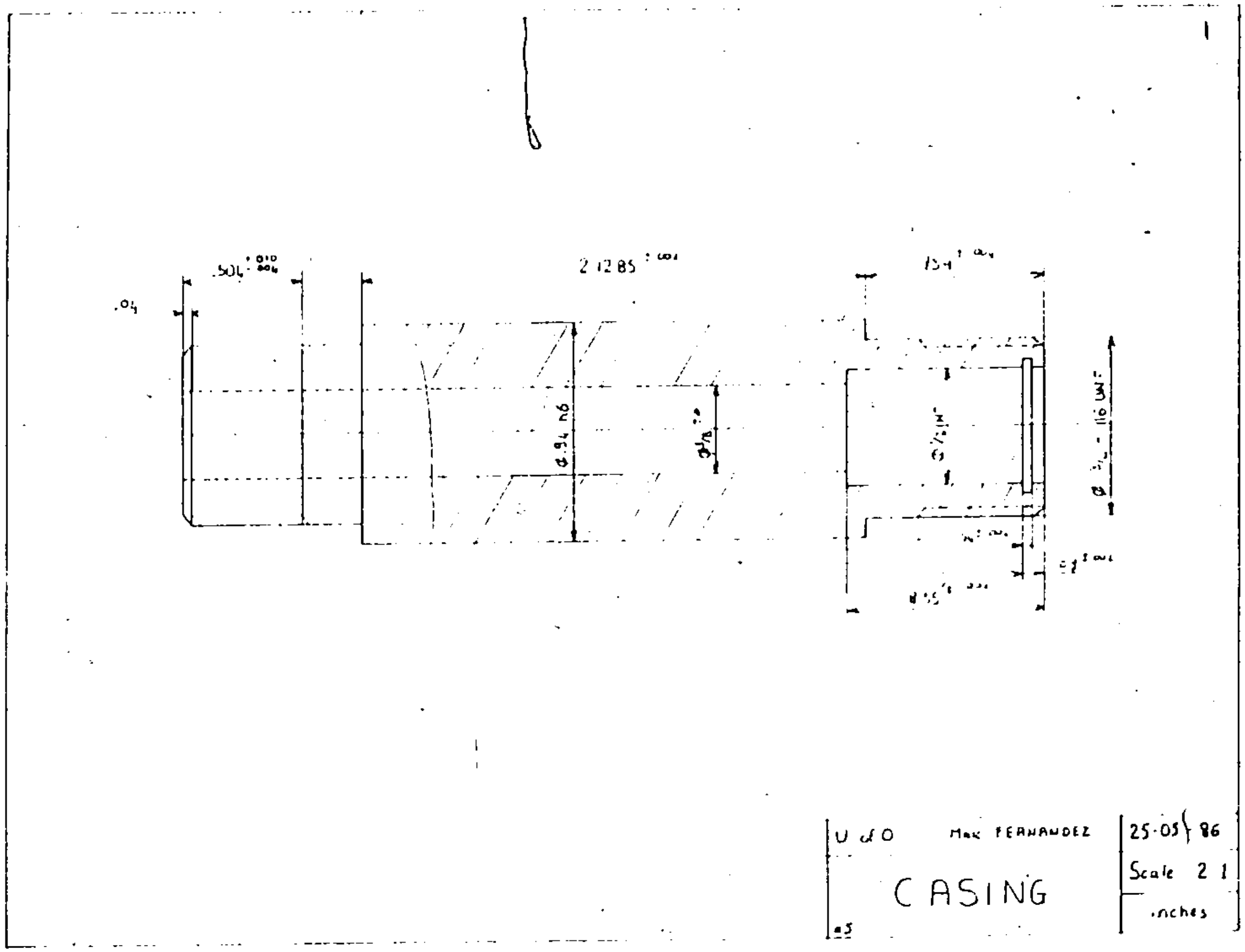

Figure B.6. Design drawings of the active counterweight system prototype (continued)

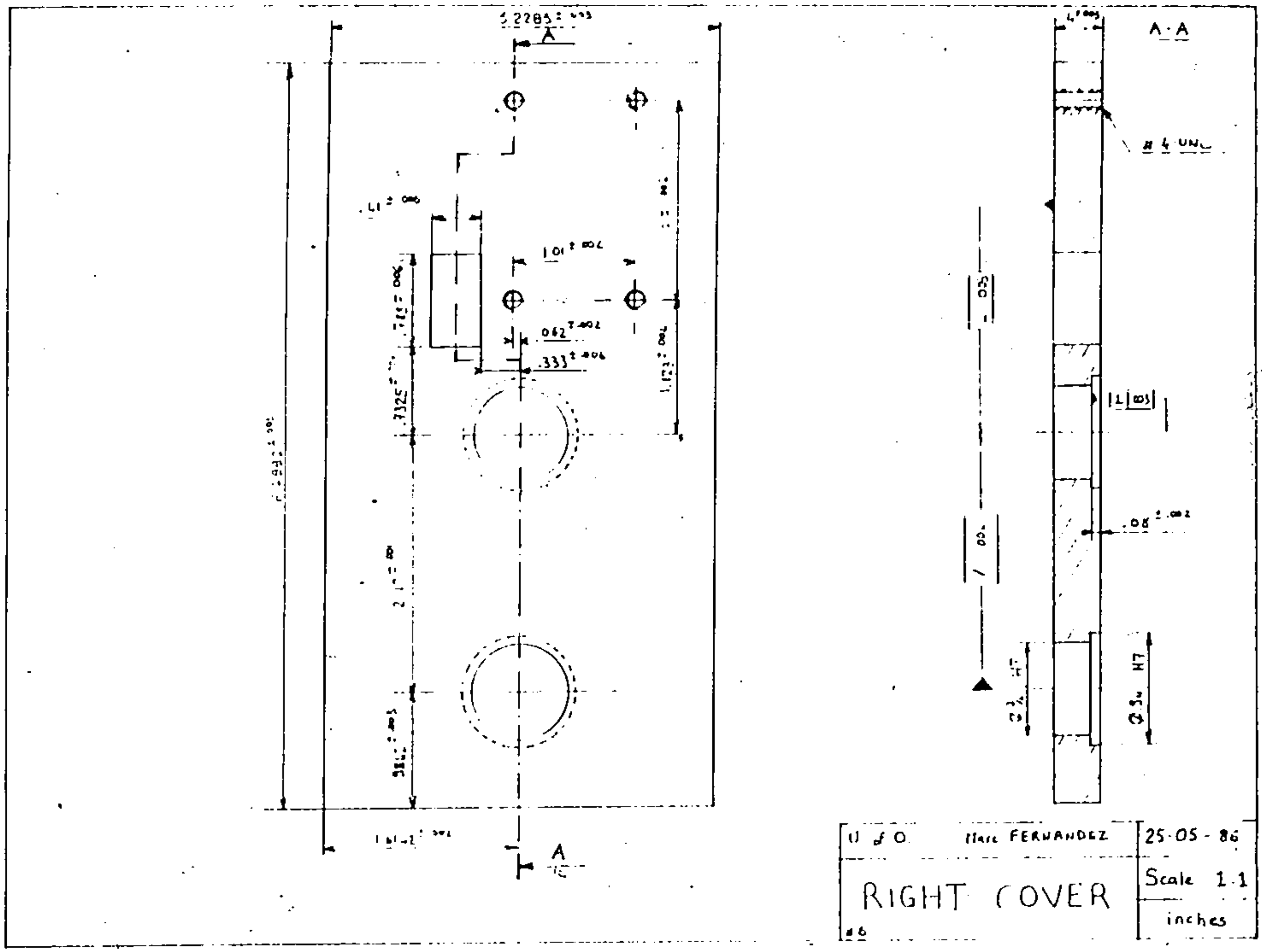

Figure B.7. Design drawings of the active counterweight system prototype (continued)

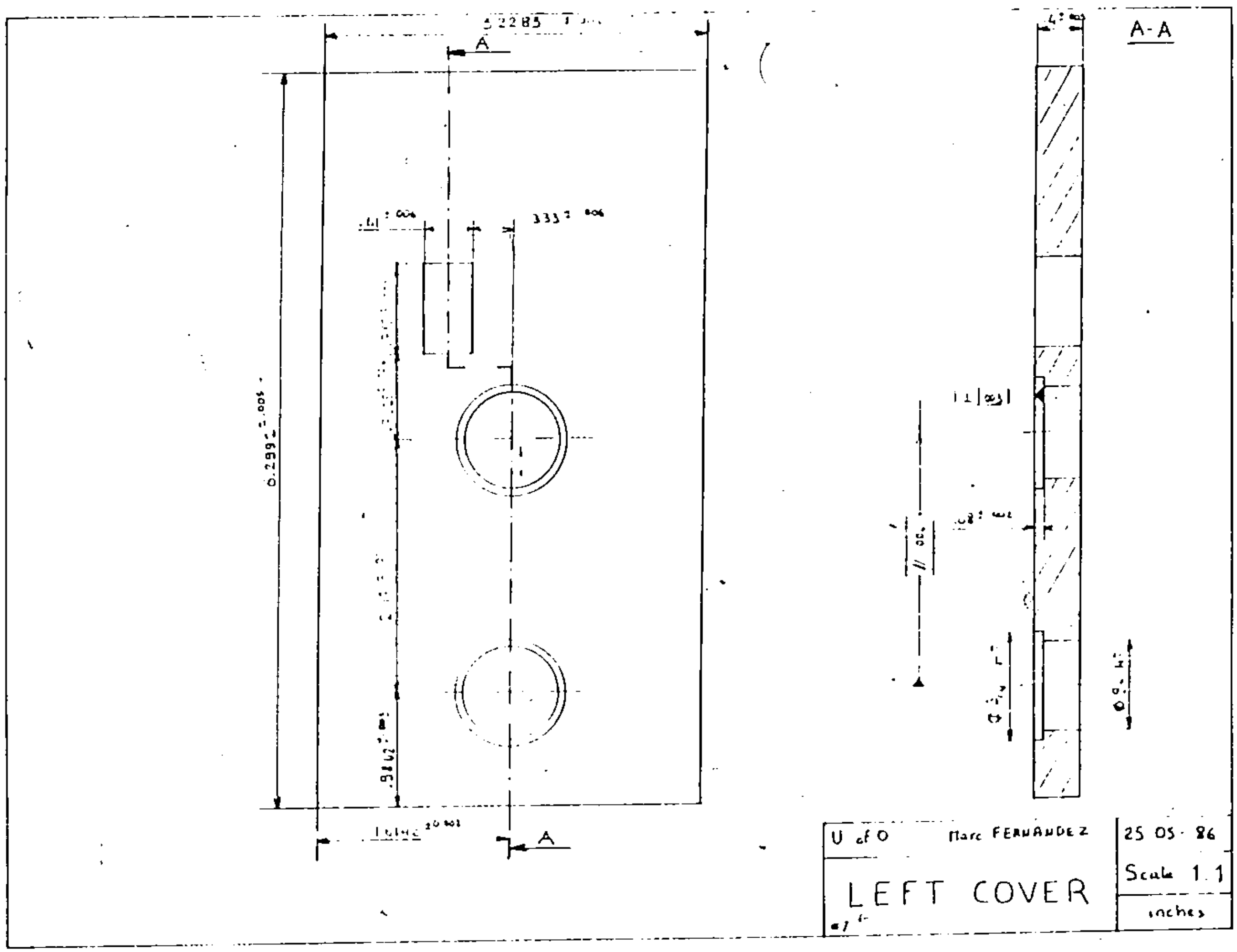

Figure B.8. Design drawings of the active counterweight system prototype (continued)

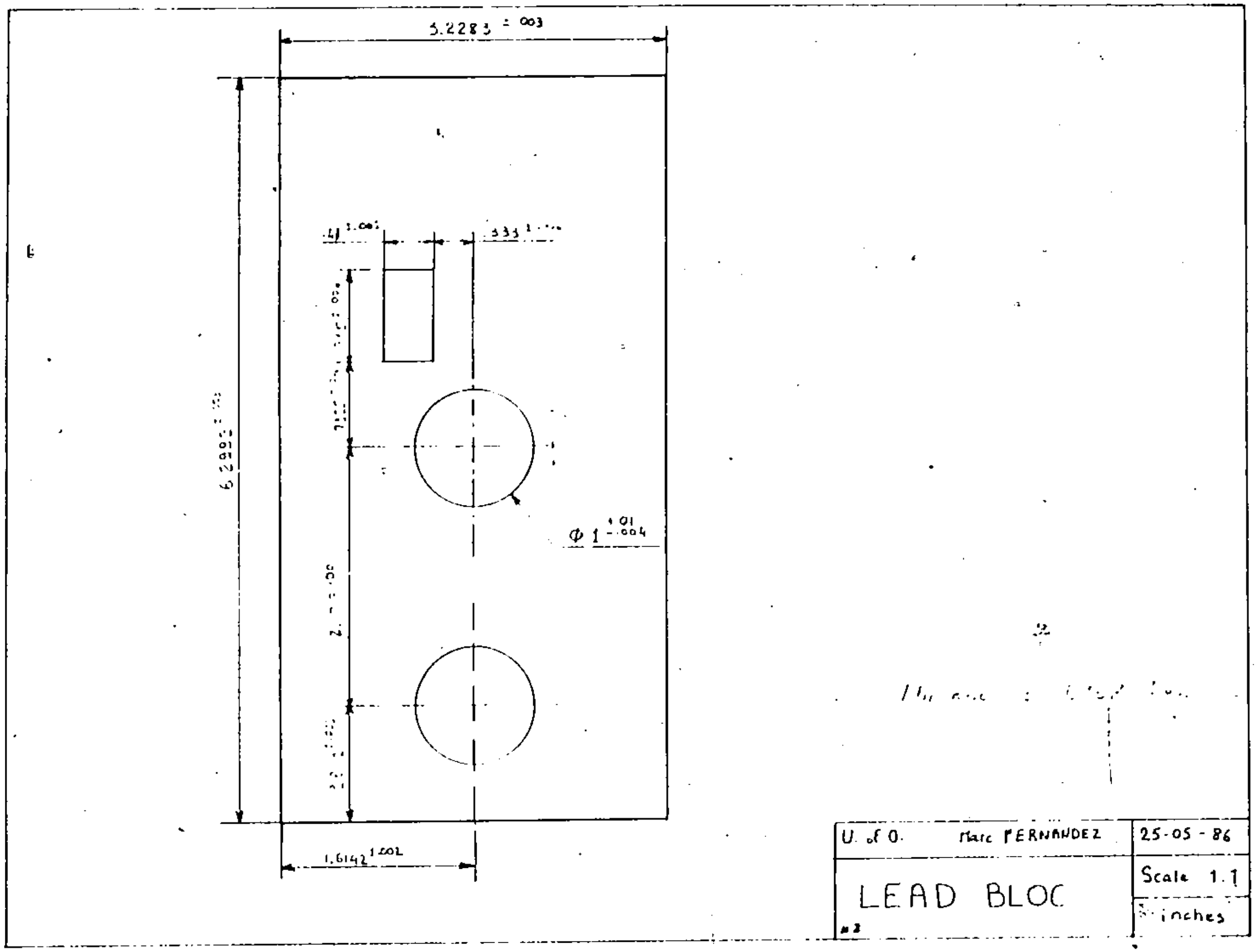

Figure B.9. Design drawings of the active counterweight system prototype (continued)

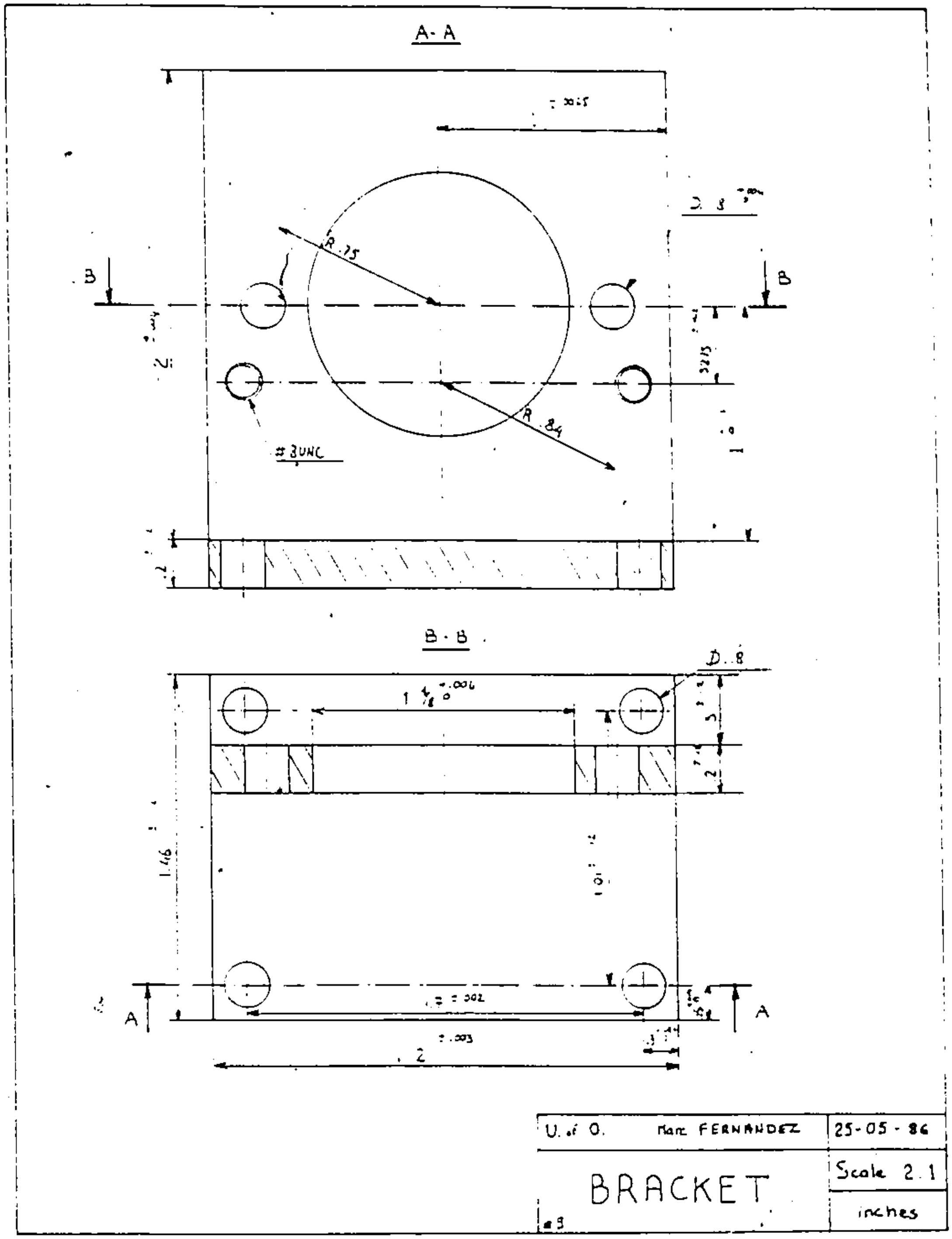

Figure B.10. Design drawings of the active counterweight system prototype (continued)

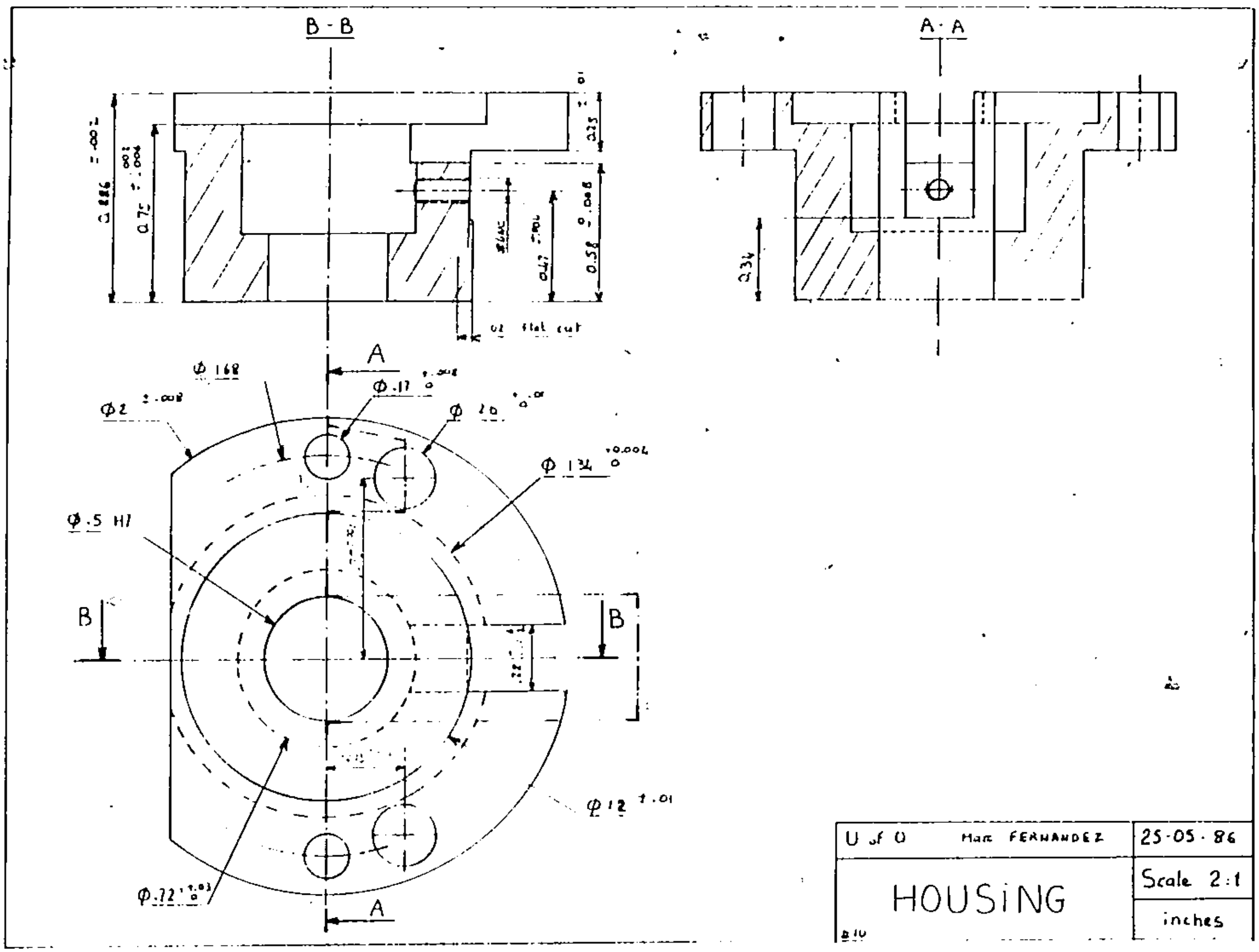

Figure B.11. Design drawings of the active counterweight system prototype (continued)

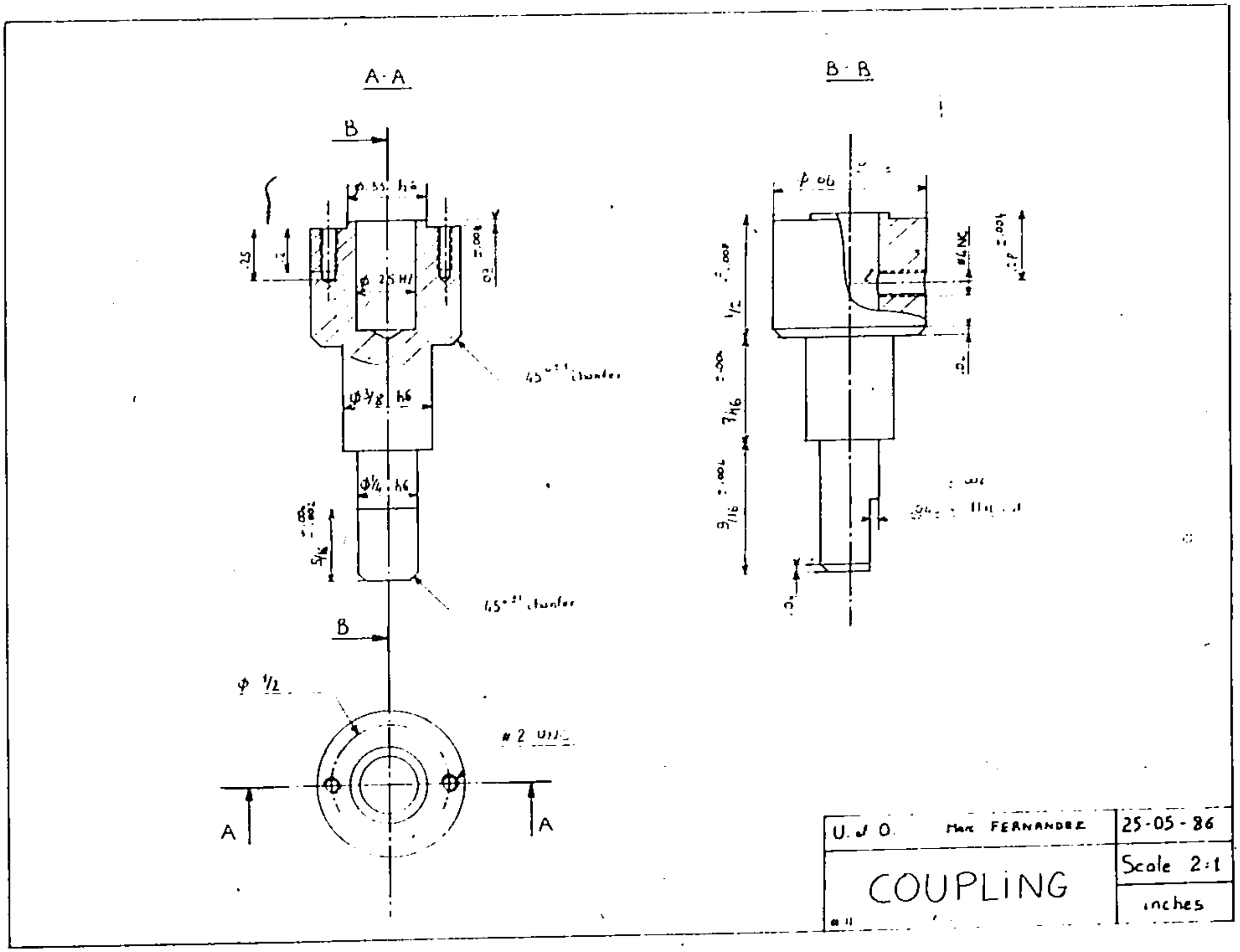

Figure B.12. Design drawings of the active counterweight system prototype (continued)

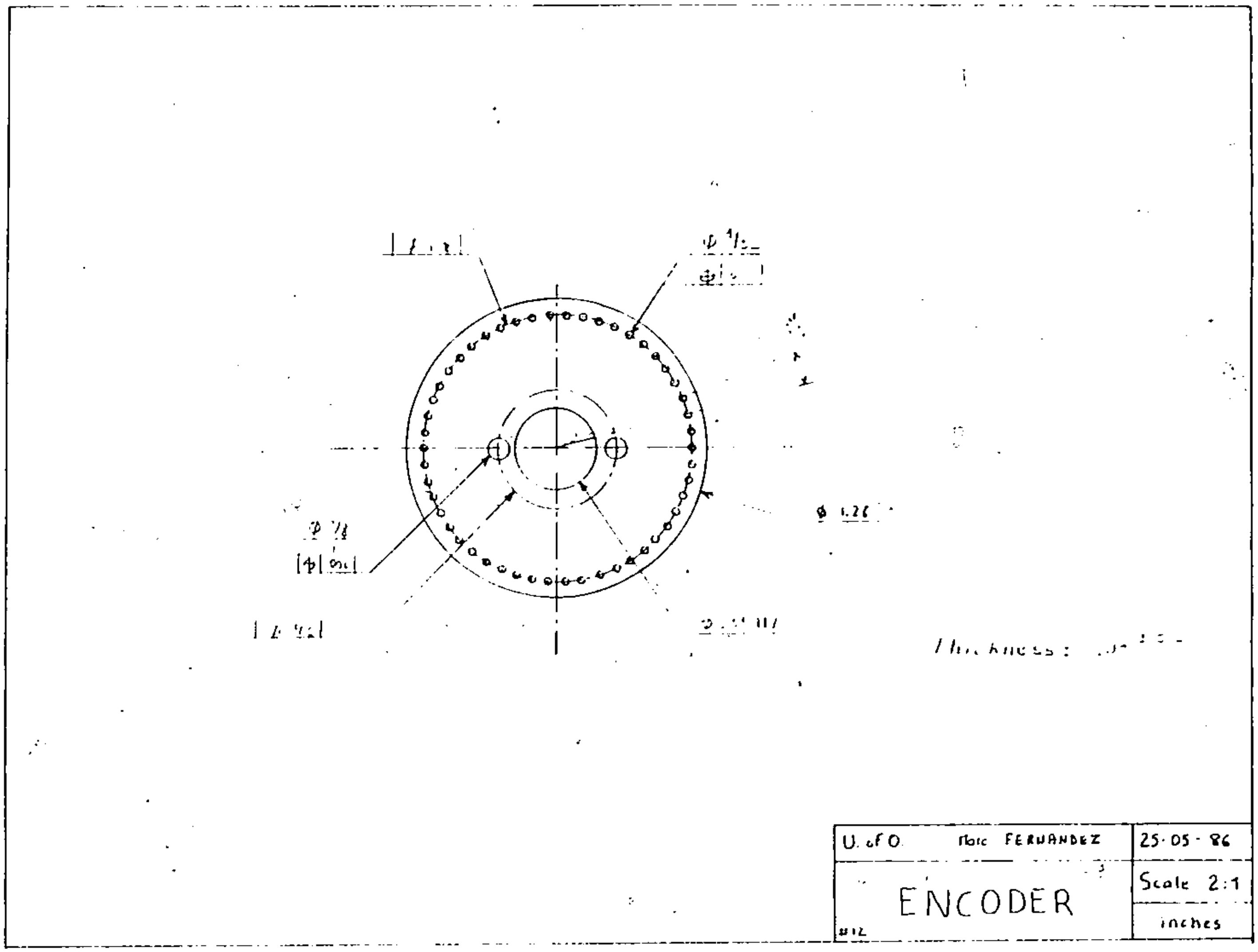

Figure B.13. Design drawings of the active counterweight system prototype (continued)

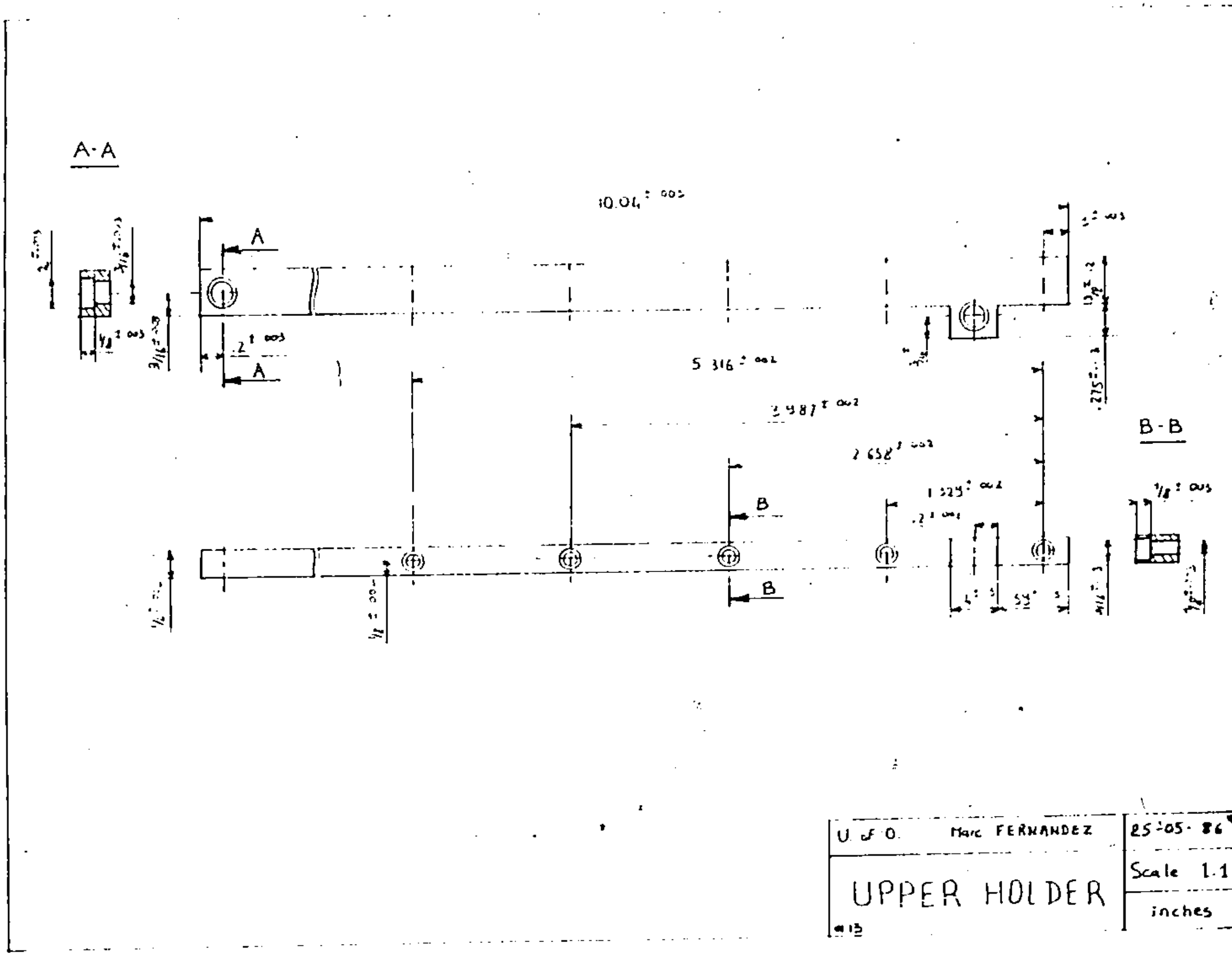

Figure B.14. Design drawings of the active counterweight system prototype (continued)

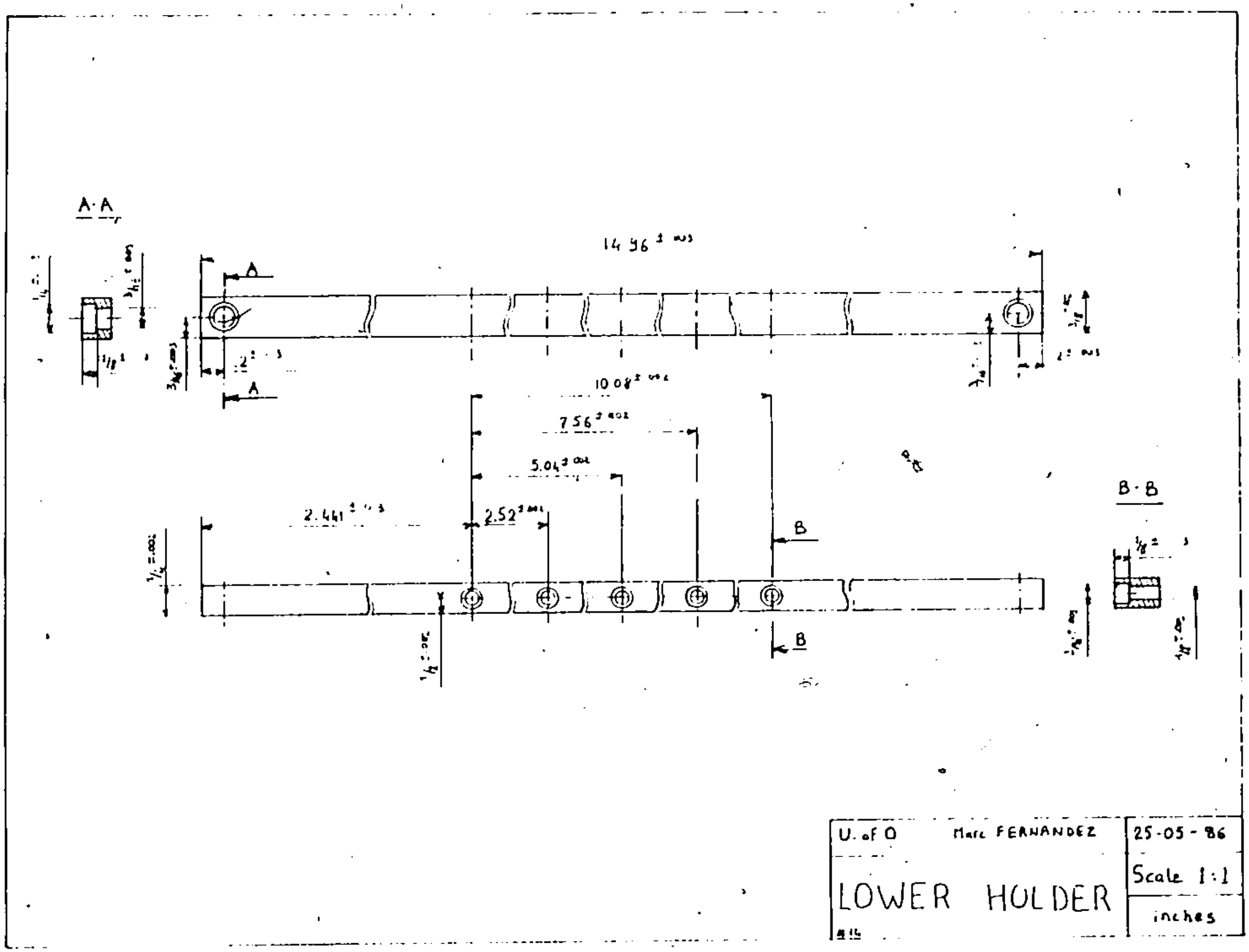

Figure B.15. Design drawings of the active counterweight system prototype (continued)

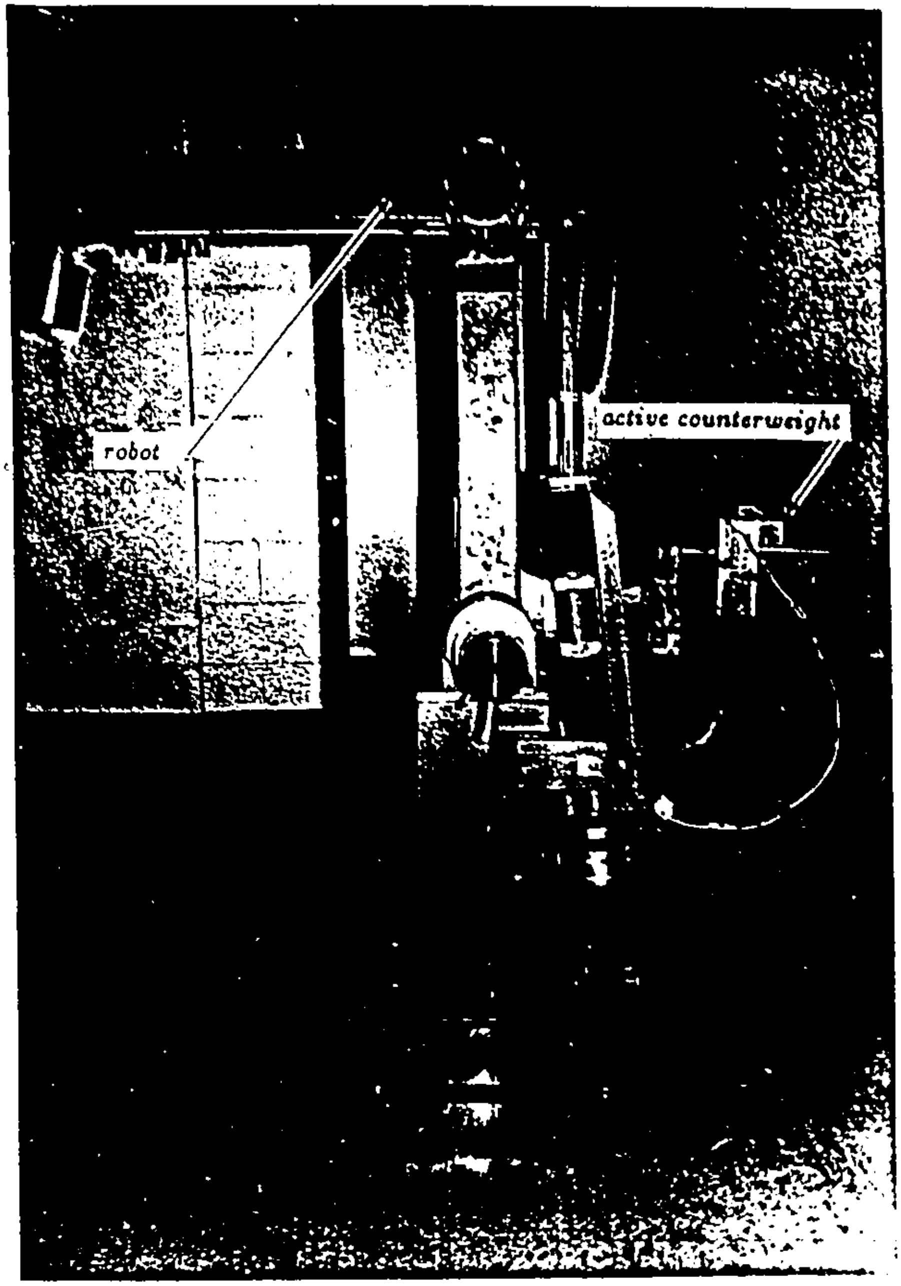

Figure B.16. Photograph of the active counterweight system prototype fixed on the ASEA Irb-6 robot arm

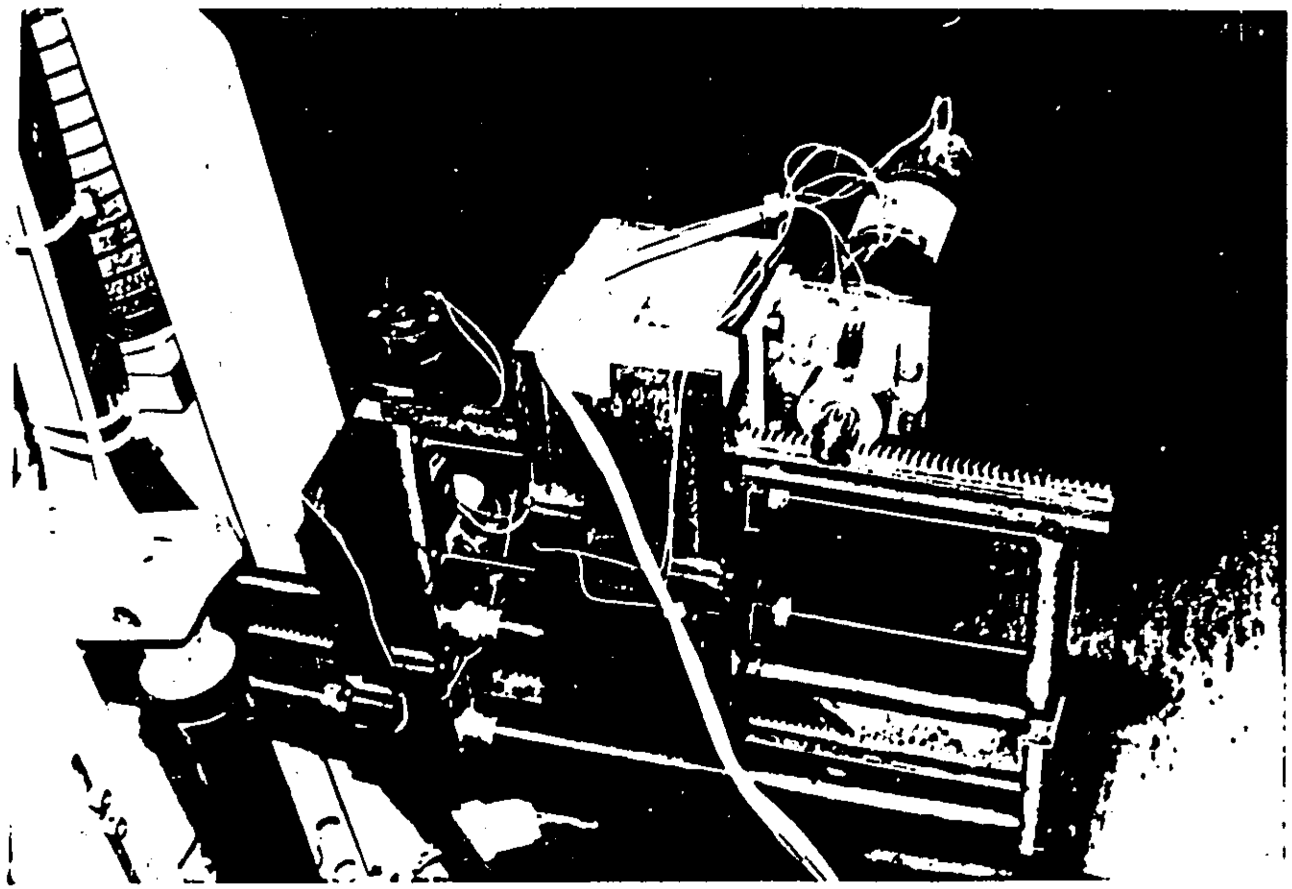

Figure B.17. Photograph of the active counterweight system prototype

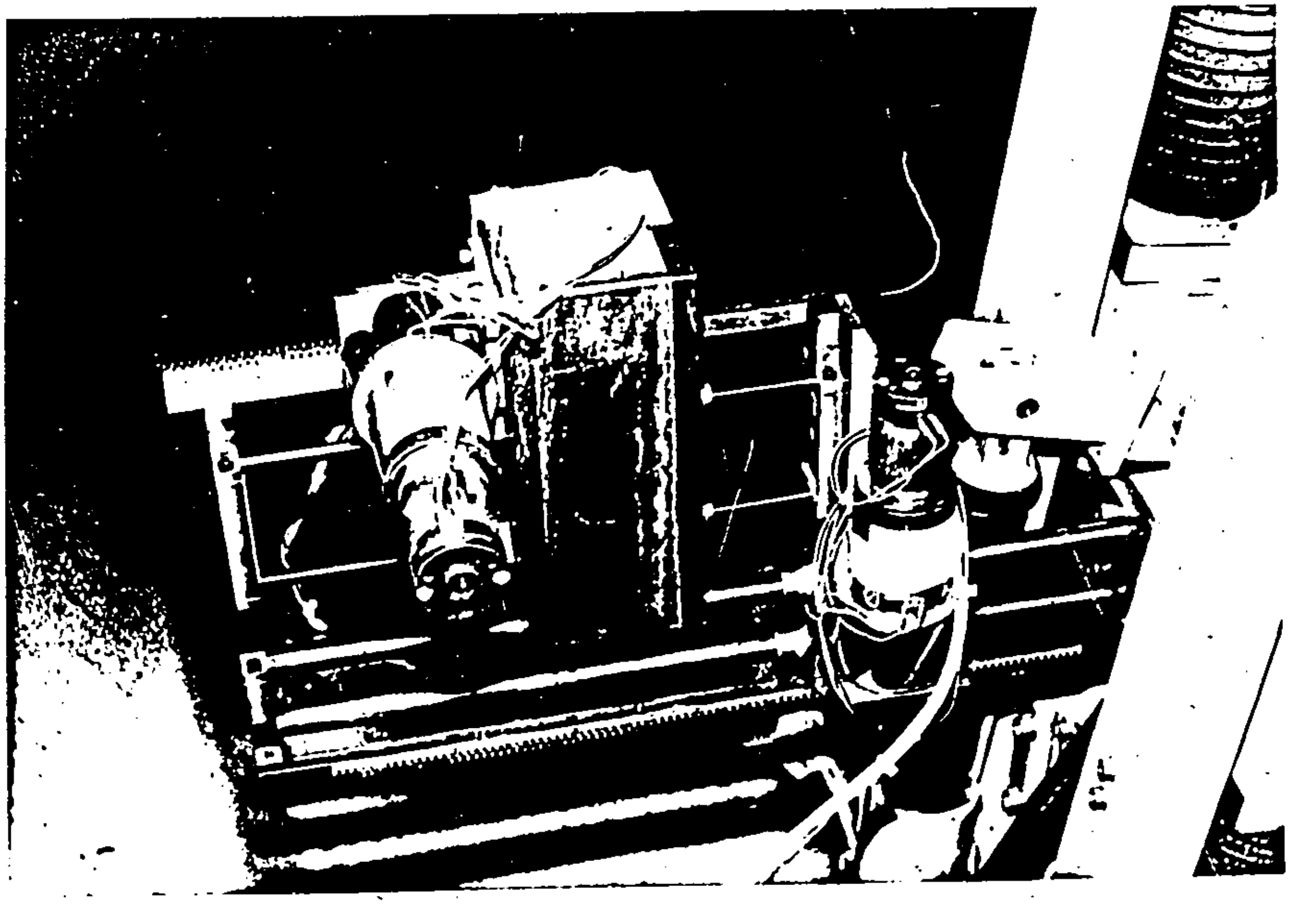

Figure B.18. Photograph of the active counterweight system prototype

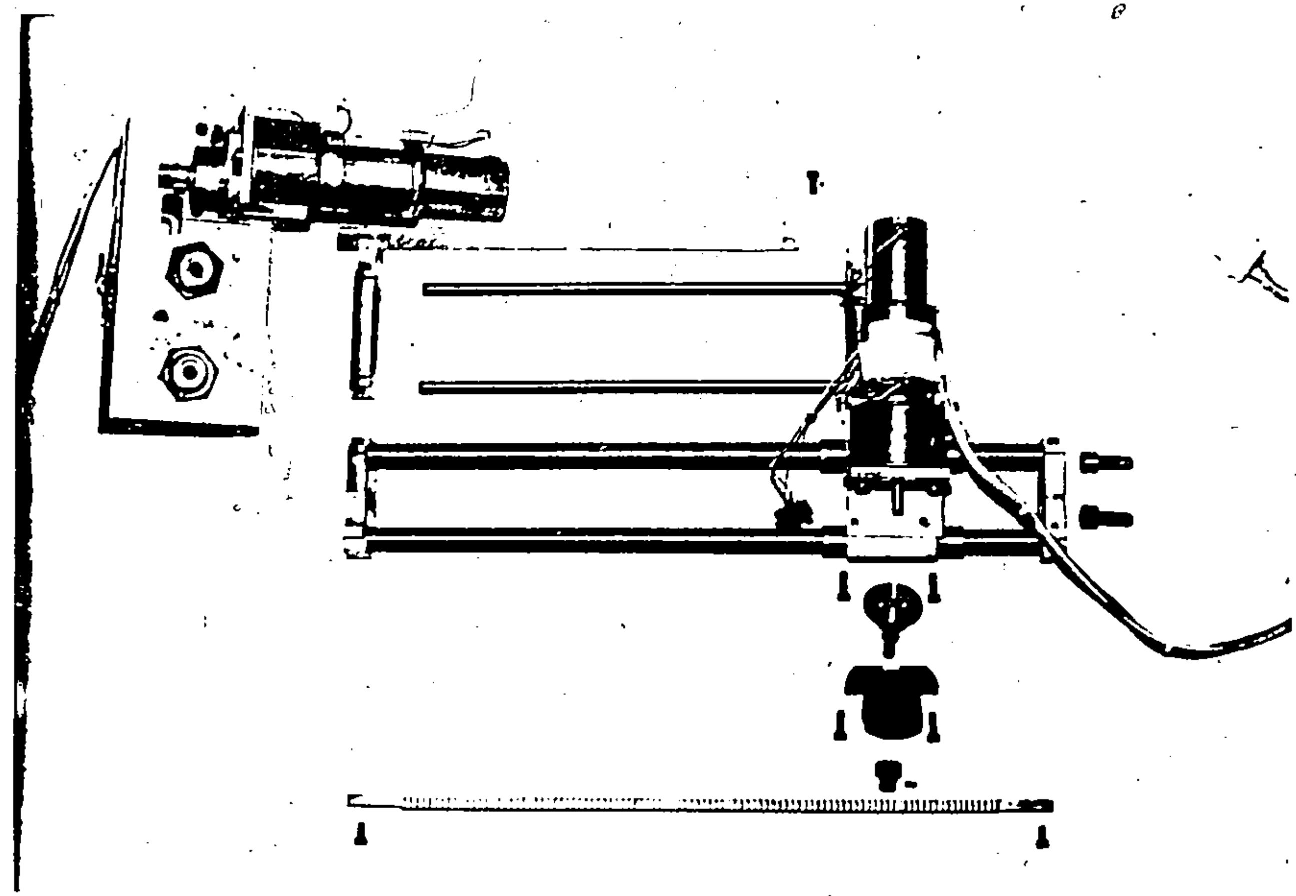

Figure B.19. Photograph of the prototype partly assembled

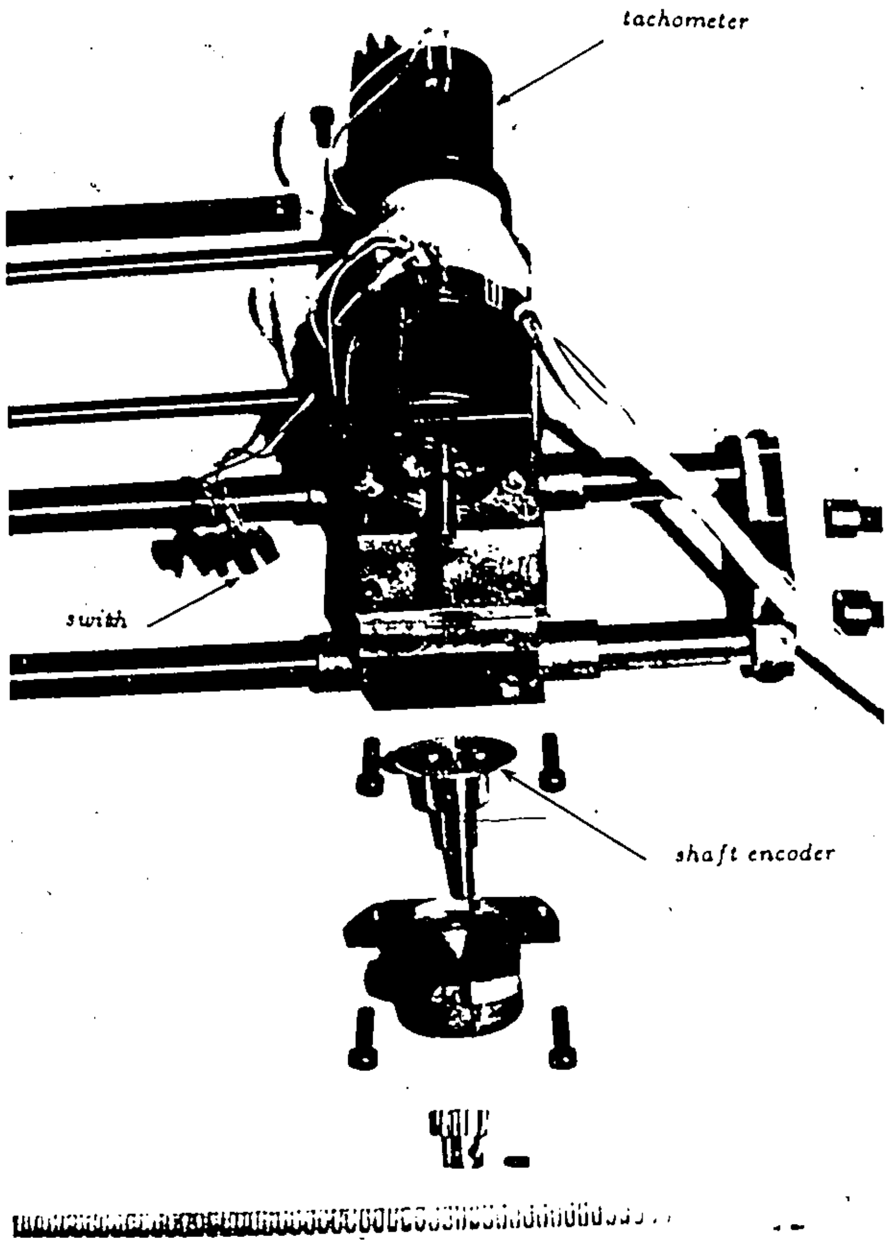

Figure B.20. Photograph of the feedback elements

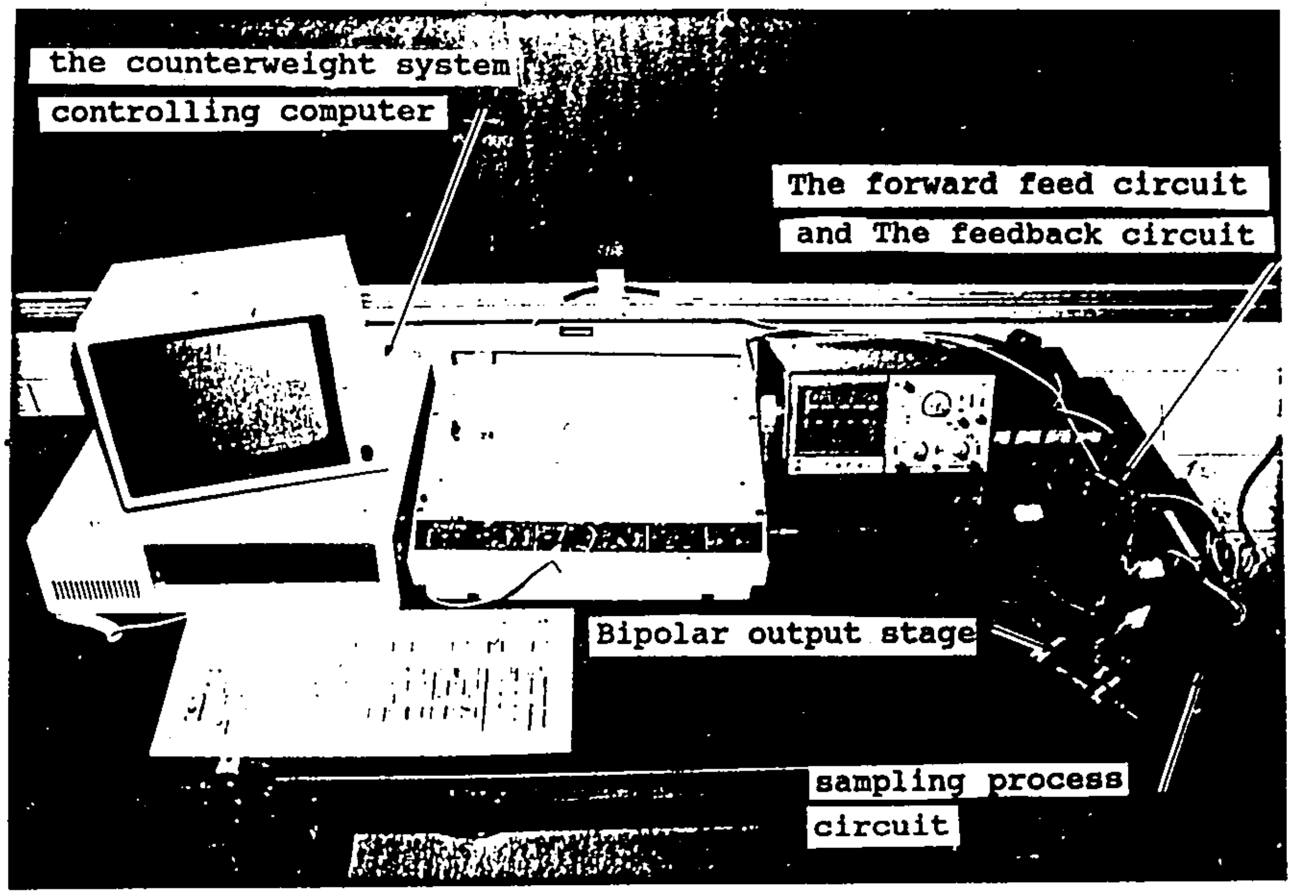

Figure B.21. Photograph of the control system for the prototype

APPENDIX C

Data acquisition and processing:

Assembler program for the Z8 microcomputer

FLOW CHARTS

-MAIN PROGRAM-

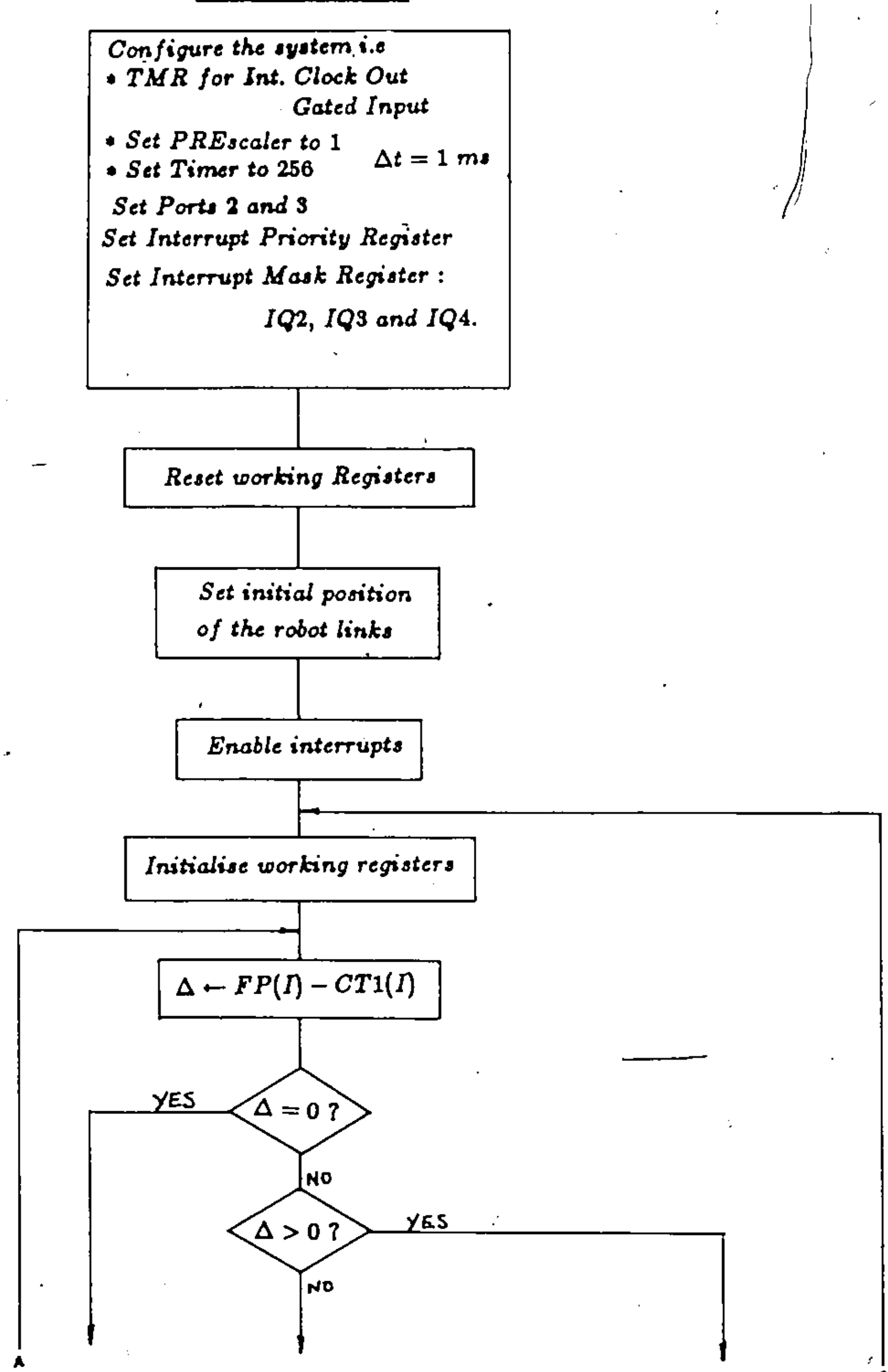

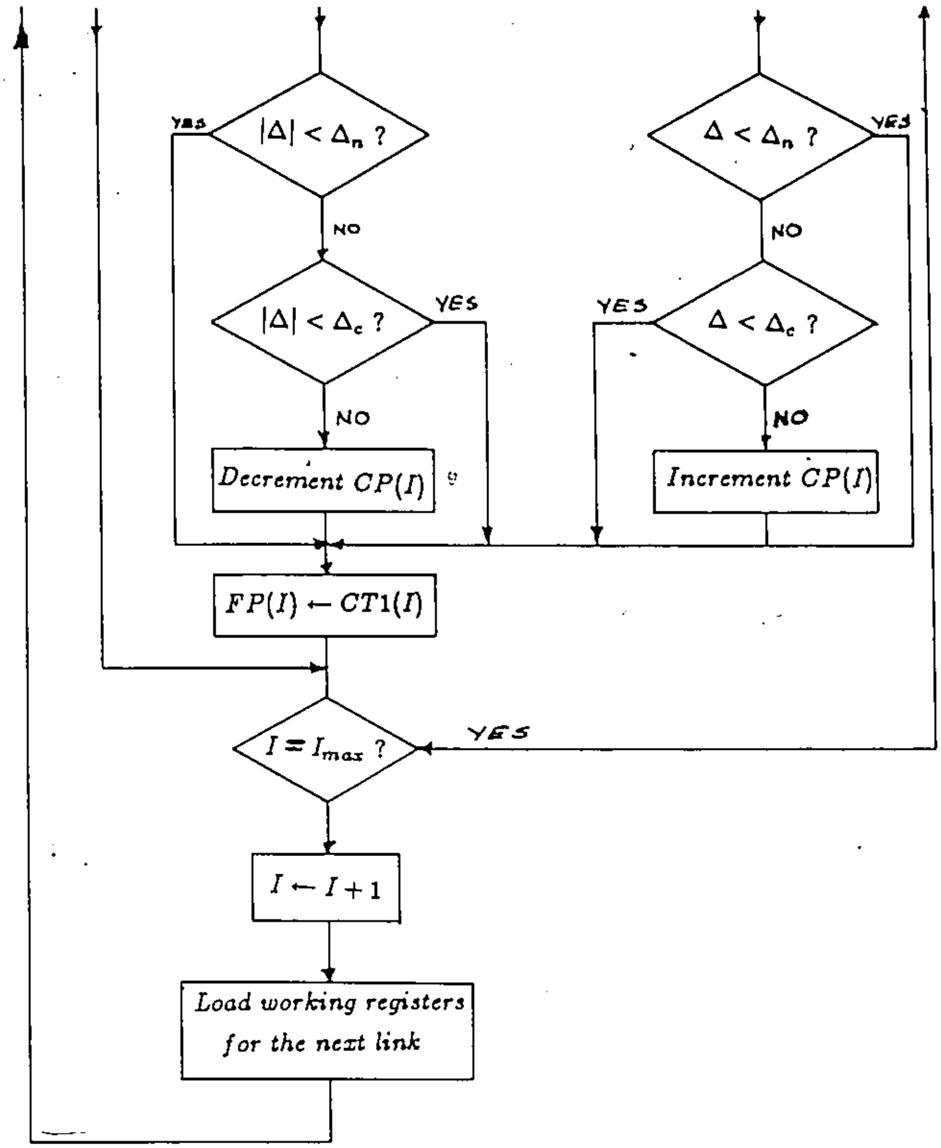

$|\Delta| < \Delta_n$?
YES
NO
$|\Delta| < \Delta_c$?
YES
NO
Decrement $CP(I)$
$\Delta < \Delta_n$?
YES
NO
$\Delta < \Delta_c$?
YES
NO
Increment $CP(I)$
$FP(I) \leftarrow CT1(I)$
$I = I_{max}$?
YES
$I \leftarrow I + 1$
Load working registers for the next link

-COUNTING SUBROUTINE-

Interrupt Request 2

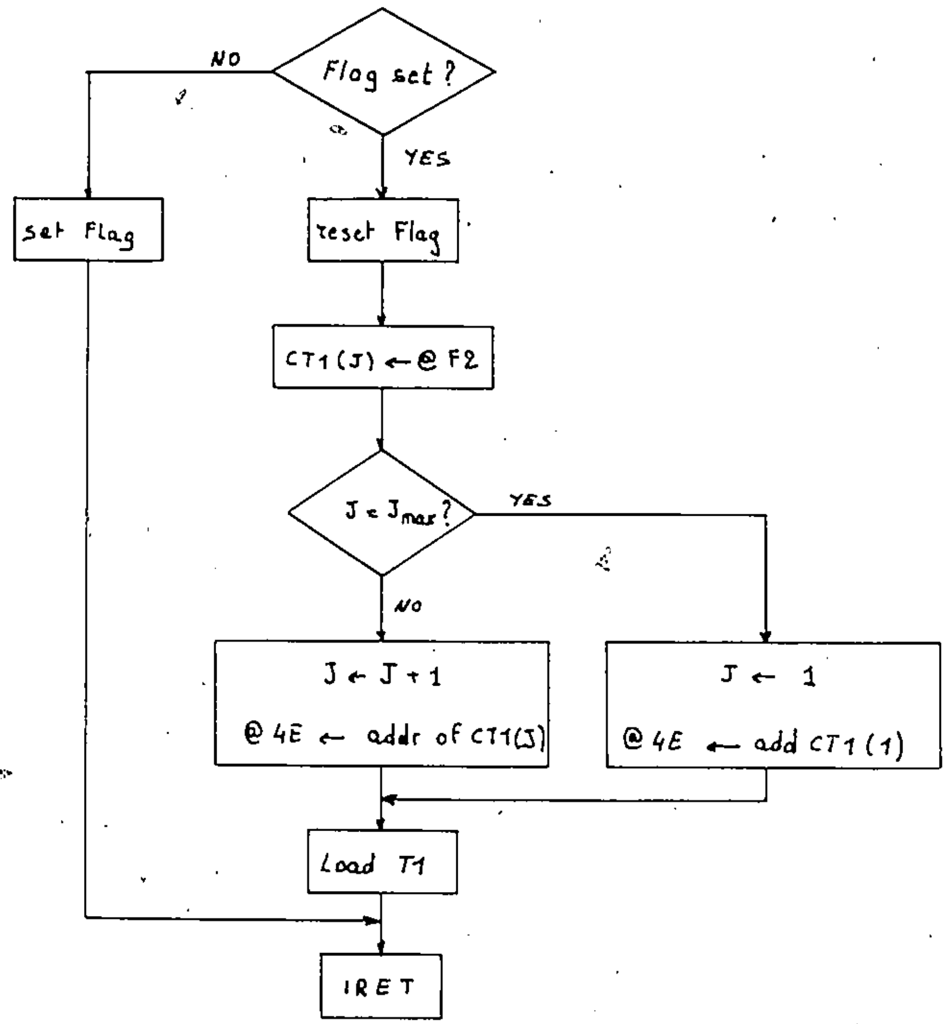

-COMMUNICATION SUBROUTINES-

. Interrupt request 3

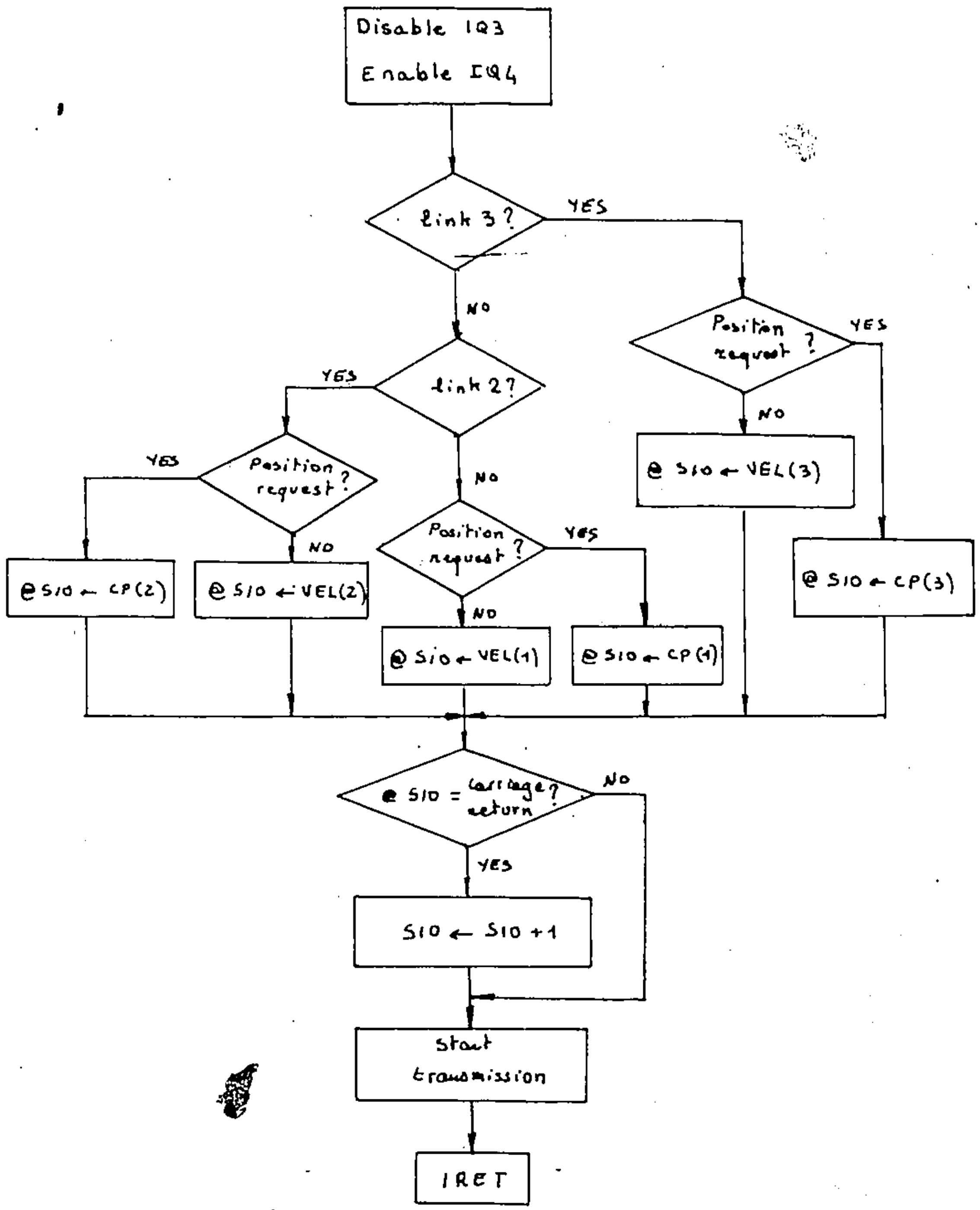

Interrupt request 4

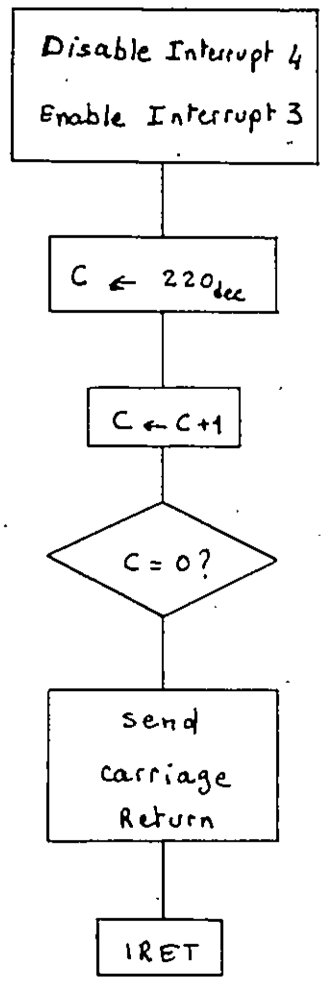

MEMORY MAPPING

ADDRESS (HEX)	VARIABLE
External memory (DAC)	
*********************	
8004	VEL(5) : Velocity of link 5
8003	VEL(4) : Velocity of link 4
8002	VEL(3) : Velocity of link 3
8001	VEL(2) : Velocity of link 2
8000	VEL(1) : Velocity of link 1
Working registers	
*****************	
4F	$\Delta \leftarrow FP(I) - CT1(I)$
4E	addr of CT1(J)
4D	J : counter selector
4C	addr of CT1(I)
4B	addr of FP(I)
4A	addr of CP(I)
48	IQ2 flag
47	used for serial communication
46	Initialisation register
45	$I_{max} = J_{max}$
44	I : link selector for processing
Data storage	
************	
43, 42	CP(5) : Full revolution counter for link 5
41	CT1(5) : timer value when sampling link 5
40	FP(5) : fine position of link 5.
3F, 3E	CP(4) : Full revolution counter for link 4
3D	CT1(4) : timer value when sampling link 4
3C	FP(4) : fine position of link 4
3B, 3A	CP(3) : Full revolution counter for link 3
39	CT1(3) : timer value when sampling link 3
38	FP(3) : fine position of link 3

ADDRESS (HEX)	VARIABLE
37	CP(2) : Full revolution counter for link 2
36	
35	CT1(2) : timer value when sampling link 2
34	FP(2) : fine position of link 2
33	CP(1) : Full revolution counter for link 1
32	
31	CT1(1) : timer value when sampling link 1
30	FP(1) : fine position of link 1

Communication registers
****

2F	addr of VEL(I)
2E	
2D	VEL(I)
21	counters
20	

ASSEMBLER PROGRAM

LBL	ADDR	OPCODE	ID	COMMENTS
	1006	8D 10 C0	JP IRQ2	
	1009	8D 10 E0	JP IRQ3	Interrupt
	100C	8D 11 5F	JP IRQ4	vectors

****

Initialisation

****

LBL	ADDR	OPCODE	ID	COMMENTS
	1020	E6 F1 D0	LD F1 ← D0	TMR set up: 11010000
	1023	E6 F7 41	LD F7 ← 41	P3M set up: 01000001
	1026	E6 F6 C0	LD F6 ← C0	P2M set up: 11000000
	1029	E6 F3 10	LD F3 ← 10	PRE1 set up: 00010000
	102C	E6 F2 00	LD F2 ← 00	T1=256 (T=1 ms)
	102F	E6 F9 3A	LD F9 ← 3A	IPR set up: 00111010
	1032	E6 FB 1C	LD FB ← 1C	IMR set up: 00001100
	1035	E6 2C 30	LD 2C ← 30	
A	1038	E7 2C 00	LD (2C)← 00	Reset
	103B	20 2C	INC 2C	working
	103D	A6 2C 50	CP 2C &'50'	registers
	1040	ED 10 38	JNZ A	
	1043	E6 45 03	LD 45 ← 03	Number of links: 3
	1046	31 40	SRP 40	
	1048	E6 46 30	LD 46 ← 30	
B	104B	E7 46 80	LD (46)← 80	
	104E	06 46 04	ADD 46 ,'04'	Initialisation of registers
	1051	A6 46 40	CP 46 &'40'	
	1054	ED 10 4B	JNZ B	
	1057	E6 46 33	LD 46 ← 33	
C	105A	E7 46 80	LD (46)← 80	Initial position of
	105D	06 46 04	ADD 46 ,'04'	the links: allows ±127
	1060	A6 46 43	CP 46 &'43'	revolutions for each link
	1063	ED 10 5A	JNZ C	
	1066	E6 4D 02	LD 4D ←'02'	$J_0 = 2$
	1069	E4 4D 02	LD 4D → 02	J_0 written at Port 2
	106C	E6 4E 35	LD 4E ←'35'	@4E= addr of CT1(2)
	106F	46 F1 0C	OR F1 ,'0C'	Load and enable T1
	1072	9F	EI	

Sampling loop

LBL	ADDR	OPCODE	ID	COMMENTS
D	1073	E6 44 02	LD 44 ←'02'	$I_0 = 2$
	1076	E6 4A 36	LD 4A ← 36	@4A= addr of CP(2)
	1079	E6 4B 34	LD 4B ← 34	@4B= addr of FP(2)
	107C	E6 4C 35	LD 4C ← 35	@4C= addr of CT1(2)
E	107F	E3 FB	LD 4F ←(4B)	Load FP(I)
	1081	23 FC	SUB 4F , 4C	$\Delta \leftarrow$ FP(I)-CT1(I)
	1083	6D 10 AC	JZ H	$\Delta = 0$?
	1086	FD 10 9A	JNC F	$\Delta > 0$?
	1089	A6 4F C4	CP 4F &'C4'	$\Delta_n - \lvert\Delta\rvert > 0$?
	108C	FD 10 A8	JNC G	
	108F	A6 4F 3F	CP 4F &'3F'	$\Delta_c - \lvert\Delta\rvert > 0$?
	1092	FD 10 A8	JNC G	
	1095	81 4A	DECW (4A)	
	1097	8D 10 A8	JP G	
F	109A	A6 4F 36	CP 4F ,'36'	$\Delta - \Delta_n < 0$?
	109D	7D 10 A8	JC G	
	10A0	A6 4F C1	CP 4F ,'C1'	$\Delta - \Delta_c < 0$?
	10A3	7D 10 A8	JC G	
	10A6	A1 4A	INCW (4A)	
G	10A8	E3 6C	LD 46 ←(4C)	FP(I) ← CT1(I)
	10AA	F3 B6	LD (4B)← 46	
H	10AC	A2 45	CP 44 , 45	$I = I_{max}$?
	10AE	6D 10 73	JZ D	
	10B1	4E	INC (44)	
	10B2	06 4A 04	ADD 4A ,'4'	
	10B5	06 4B 04	ADD 4B ,'4'	
	10B8	06 4C 04	ADD 4C ,'4'	
	10BB	8D 10 7F	JP E	

Interrupt routine IQ2: for each link selected, reads and stores the phase shift counter

LBL	ADDR	OPCODE	ID	COMMENTS
IQ2	10C0	A6 48 00	CP 48 &'0'	Flag = 0 ? (makes sure that
	10C3	6D 10 DB	JZ I1	the proper link is selected)
	10C6	F5 F2 4E	LD F2 →(4E)	Read and store CT1(I)
	10C9	A2 D5	CP 40 & 45	
	10CB	6D 11 80	JZ I2	
	10CE	DE	INC (4D)	J ← J + 1
	10CF	E4 4D 02	LD 4D → 02	Select link on multiplexer
	10D2	06 4E 04	ADD 4E ,'4'	
	10D5	B0 48	CLR 48	
	10D7	46 F1 0C	OR F1 ,'0C'	Load and enable T1
	10DA	BF	IRET	

LBL	ADDR	OPCODE	ID	COMMENTS
I1	10DB	8E	INC (48)	
	10DC	46 F1 0C	OR F1 ,'0C'	Load and enable T1
	10DF	BF	IRET	
I2	118D	E6 4D 02	LD 4D ←'2'	J = 2
	1183	E4 4D 02	LD 4D → 02	Select link 2
	1186	E6 4E 35	LD 4E ←'35'	@4E= addr of CT1(2)
	1189	B0 48	CLR 48	
	118B	46 F1 0C	OR F1 ,'0C'	Load and enable T1
	118E	BF	IRET	

****

Interrupt routine IQ3: serial communication

Sends the information (position or velocity) on request

****

LBL	ADDR	OPCODE	ID	COMMENTS
IQ3	10E0	E6 FB 14	LD FB ←'14'	Modify IMR : IQ2 & IQ4 only
	10E3	31 20	SRP 20	
	10E5	66 F0 03	TCM F0 ,'03'	Link 3 ?
	10E8	6D 11 25	JZ M	
	10EB	66 F0 02	TCM F0 ,'02'	Link 2 ?
	10EE	6D 11 0B	JZ K	
	10F1	66 F0 08	TCM F0 ,'08'	Position of link 1 ?
	10F4	6D 11 05	JZ J	
	10F7	E6 2E 80	LD 2E ←'80'	@(2E-2F) = addr of VEL(1)
	10FA	E6 2F 00	LD 2F ←'00'	
	10FD	82 DE	LDE 2D ←(2E-2F)	Get VEL(1)
	10FF	E4 2D 47	LD 2D → 47	Load VEL(1)
	1102	8D 11 3C	JP O	
J	1105	E4 33 47	LD 33 → 47	Load CP(1)
	1108	8D 11 3C	JP O	
K	110B	66 F0 08	TCM F0 ,'08	Position of link 2 ?
	110E	6D 11 1F	JZ L	
	1111	E6 2E 80	LD 2E ←'80'	@(2E-2F) = addr of VEL(2)
	1114	E6 2F 01	LD 2F ←'01'	
	1117	82 DE	LDE 2D ←(2E-2F)	Get VEL(2)
	1119	E4 2D 47	LD 2D → 47	Load VEL(2)
	111C	8D 11 3C	JP O	
L	111F	E4 37 47	LD 37 → 47	Load CP(2)
	1122	8D 11 3C	JP O	
M	1125	66 F0 08	TCM F0 ,'08'	Position of link 3 ?
	1128	6D 11 39	JZ N	
	112B	E6 2E 80	LD 2E ←'80'	@(2e-2F) = addr of VEL(3)
	112E	E6 2F 02	LD 2F ←'02'	
	1131	82 DE	LDE 2D ←(2E-2F)	Get VEL(3)
	1133	E4 2D 47	LD 2D → 47	Load VEL(3)
	1136	8D 11 3C	JP O	
N	1139	E4 3B 47	LD 3B → 47	
O	113C	A6 F0 0D	CP F0 ,'0D'	@SIO = carriage return ?
	113F	6D 11 51	JZ P	

LBL	ADDR	OPCODE	ID	COMMENTS
	1142	A6 F0 1A	CP F0 ,'1A'	
	1145	6D 11 51	JZ P	
	1148	E4 47 F0	LD 47 → F0	Final loading
	114B	46 F1 03	OR F1 ,'03'	Load and start T2 (transmit)
	114E	31 40	SRP 40	
	1150	BF	IRET	
P	1151	20 47	INC 47	
	1153	E4 47 F0	LD 47 → F0	Final loading
	1156	46 F1 03	OR F1 ,'03'	Start transmission
	1159	31 40	SRP 40	
	115B	BF	IRET	

****

Interrupt routine IQ4: serial communication
Sends the carriage return with the proper delay

****

IQ4	115F	E6 FB 0C	LD FB ←'0C'	
	1162	9F	EI	
	1163	E6 20 02	LD 20 ←'2'	Load
Q	1166	E6 21 DC	LD 21 ←'220'dec	counters
R	1169	00 21	DEC 21	
	116B	ED 11 69	JNZ R	Delay
	116E	00 20	DEC 20	process
	1170	ED 11 66	JNZ Q	
	1173	E6 F0 0D	LD F0 ←'0D'	Load carriage return
	1176	46 F1 03	OR F1 ,'03'	Start transmission
	1179	BF	IRET	

APPENDIX D

The balancing coordinator program

```
*****************************************************************
                  Balancing coordinator program
*****************************************************************

      CHARACTER*1 N2,N23,ND1,ND2,ND23
      INTEGER K2,K23,K3,I,K,N,X,J
      INTEGER*2 Z
      REAL SC(91,2),C2,S23,C23,S3,C3,TD1,TD2,TD23,TDD2,TDD23,A,B,C,D,
     1  R3,IX,IY,IZ,IPX,IPY,IPZ,M,M3,MP3,E3,B3,B2,ANGL,T1,T2,T3,T4,T5,
     2  T6,T7,T8,T,TD2P,TD23P,RF,MM,DELTA,RMIN,RMX,RP,R
      OPEN(1,FILE='COM1',ACCESS='DIRECT',FORM='UNFORMATTED',RECL=1)
      OPEN(2,FILE='COM2',ACCESS='DIRECT',FORM='UNFORMATTED',RECL=1)

*****************************************************************
                Interaction with the opperator
*****************************************************************

      WRITE (*,*) 'Number of iterations ?'
      READ (*,*) J
    1 WRITE(*,*) 'Enter the mass of the payload (10 kg maxi): '
      READ(*,*) M
      IF((M.GE.0.).AND.(M.LE.10.)) GOTO 2
      GOTO 1
    2 WRITE(*,*) ' Enter desired quasistatic location.'
      WRITE(*,*) ' Should be in the [.078 , .255 ] interval :'
    3 READ(*,*) DELTA
      IF((DELTA.GE.(.078)).AND.(DELTA.LE.(.255))) GOTO 4
      WRITE(*,*) ' Quasistatic location is out of range [.078 ,.255 ]'
      WRITE(*,*) ' Re-enter this position :'
      GOTO 3

*****************************************************************
     Location of the quasistatic counterweight  depending on
    the payload; Initial position of the dynamic counterweight
*****************************************************************

    4 N=INT(1328*(DELTA-0.078))+10
      WRITE(2) CHAR(1)
      WRITE(2) CHAR(N)
      WRITE(2) CHAR(0)
      WRITE(2) CHAR(10)
      RMIN=.077
      RMX=0.111
      RP=0.
      K=157
      T=.010
      G=9.81
      IX=.06
      IY=1.0
      IZ=1.0
      IPX=.05
      IPY=.09
```

```
      IPZ=.10
      M3=16.
      MP3=14.5
      MM=10.
      RF=.24+DELTA
      E3=.28
      B3=.77
      B2=.69
      T1=.013635385
      T2=-G*MP3
      T3=B2*(M3*E3+M*B3)
      T4=IY+IPY-IX-IPX+M3*E3*E3+M*B3*B3
      T5=G*(M3*E3+M*B3)
      T6=IZ+IPZ+M3*E3*E3+M*B3*B3
      T7=MP3/MM
      T8=REAL(K-10)/RMX
      TD2P=0.
      TD23P=0.

***************************************************************
         Calculation of the transendental look-up table
***************************************************************

      DO 10 I=1,91
        ANGL=2.2*REAL(I-46)
        SC(I,1)=SIN(ANGL)
        SC(I,2)=COS(ANGL)
   10 CONTINUE
      WRITE(*,*) 'Ready ?'
      READ(*,*) Z

***************************************************************
                          Main loop
***************************************************************

      DO 11 I=1,J
------------------------------------
Read the positions of the robot links
------------------------------------

      WRITE(1) 'J'
      READ(1) N2
      K2=174-ICHAR(N2)
      C2=-SC(K2,1)
      WRITE(1) 'K'
      READ(1) N23
      K23=174-ICHAR(N23)
      C23=SC(K23,2)
      S23=SC(K23,1)
      K3=ICHAR(N23)-ICHAR(N2)+46
      C3=-SC(K3,1)
      S3=-SC(K3,2)
```

```
--------------------------------------
Read the velocities of the robot links
--------------------------------------

      WRITE(1) 'E'
      READ(1) ND1
      TD1=T1*REAL(ICHAR(ND1)-122)
      WRITE(1) 'F'
      READ(1) ND2
      TD2=T1*REAL(122-ICHAR(ND2))
      TDD2=(TD2-TD2P)/T
      WRITE(1) 'G'
      READ(1) ND23
      TD23=T1*REAL(122-ICHAR(ND23))
      TDD23=(TD23-TD23P)/T

----------------------------
Solve the quadratic equation
----------------------------

      A=MP3*(TDD23+TD1*TD1*C23*S23)
      B=T2*C23
      C=T3*(TD1*TD1*S23*C2+TD2*TD2*S3+TDD2*C3)+T4*S23*C23*TD1*TD1
      C=C+T5*C23+T6*TDD23
      IF(A.EQ.0.) GOTO 50
        D=B*B-A*C*4.
        IF(D.LT.0.) GOTO 20
          R3=-(B-SQRT(D))/(A*2.)
          R=-RMIN+(R3-RF)*T7
        IF(R.LT.0.) GOTO 30
        IF(R.GT.RMX) GOTO 40
          GOTO 60
   20     R=RP
          GOTO 60
   30     R=0.
          GOTO 60
   40     R=RMX
          GOTO 60
   50   R3=-C/B
        R=-RMIN+(R3-RF)*T7
        IF(R.LT.0.) GOTO 30
        IF(R.GT.RMX) GOTO 40
   60 X=INT(R*T8)+10

-------------------------------------------------------
Send the optimum position of the dynamic counterweight
to its closed loop digital controller
-------------------------------------------------------

      WRITE(2) CHAR(0)
      WRITE(2) CHAR(X)
      RP=R
```

```
      TD2P=TD2
      TD23P=TD23
   11 CONTINUE
      STOP
      END
```

APPENDIX E

Digital controller of the counterweights drives

and feedback processing

FLOW CHARTS

-MAIN PROGRAM-

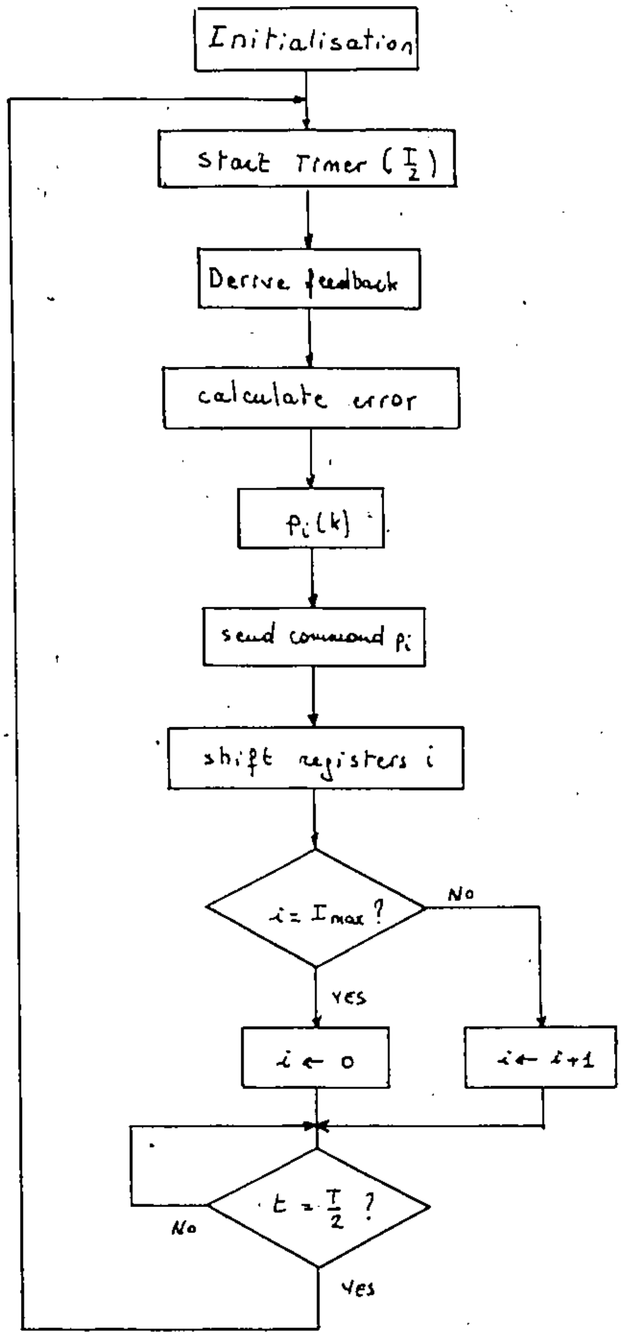

-COMMUNICATION ROUTINE-

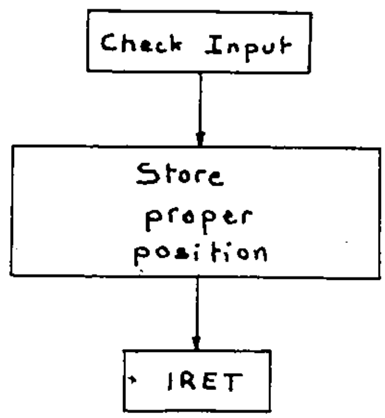

-POSITION FEEDBACK ROUTINE-

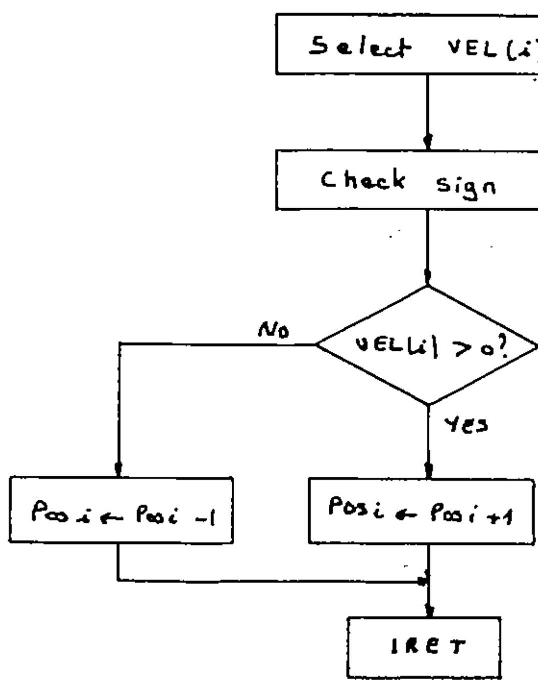

MEMORY MAPPING

ADDRESS (HEX)	VARIABLE

External memory (DAC)
****

ADDRESS (HEX)	VARIABLE
8001	VEL2 (k)
8000	VEL1 (k)

quasistatic counterweight data
****

ADDRESS (HEX)	VARIABLE
5F	$\}$ $p_2(k)$
5E	
5D	$\}$ $p_2(k-1)$
5C	
5B	$\}$ $e_2(k)$
5A	
59	$\}$ $e_2(k-1)$
58	
57	
56	
55	$(input)_2$
54	$(output)_2$
53	
52	$vel_2(k-1)$
51	$\}$ $pos_2(k)$
50	

Working registers
****

ADDRESS (HEX)	VARIABLE
4F	$\}$ used by IQ1 and IQ2
4E	
4D	$\}$ used by MUD1 Subroutine
4C	
4B	1
4A	T/2 counter
49	
48	
47	
46	i
45	$\}$ Σ
44	
43	x
42	$\div$
41	$\}$ #
40	

ADDRESS (HEX) VARIABLE

Active counterweight data
****

ADDRESS (HEX)	VARIABLE
3F	} $p_1(k)$
3E	
3D	} $p_1(k-1)$
3C	
3B	} $e_1(k)$
3A	
39	} $e_1(k-1)$
38	
37	
36	
35	$(input)_1$
34	$(output)_1$
33	
32	$vel_1(k-1)$
31	} $pos_1(k)$
30	

ASSEMBLER PROGRAM

LBL	ADDR	OPCODE	ID	COMMENTS
	1003	8D 12 40	JP IQ1	
	1006	8D 12 5A	JP IQ2	INTERRUPT
	1009	8D 12 74	JP IQ3	VECTORS
	100F	8D 12 9C	JP IQ5	

****

Initialisation

****

LBL	ADDR	OPCODE	ID	COMMENTS
	1020	E6 F6 00	LD F6 ← '0'	Port 2: outputs
	1023	E6 F7 41	LD F7 ← '41'	Config. Port 3
	1026	E6 02 80	LD 02 ← '80'	@ Port 2='80'
	1029	56 03 9F	AND 03 , '9F'	Sample #1 & #2 (Init.)
	102C	E6 F9 08	LD F9 ← '08'	IPR set up: 10011111
	102F	E6 FB 2E	LD FB ← '2E'	IMR set up: 00001000
	1032	E6 2F 30	LD 2F ← '30'	
A	1035	B1 2F	CLR (2F)	Clear working registers
	1037	20 2F	INC 2F	30 to 5F
	1039	A6 2F 60	CP 2F , '60'	
	103C	ED 10 35	JNZ A	
	103F	E6 4E 80	LD 4E ← '80'	@4E='80' (4E-4F = 80xx)
	1042	E6 31 0A	LD 31 ← '0A'	Initial position for both
	1045	E6 51 0A	LD 51 ← '0A'	motors: 10 increments
	1048	E6 35 0A	LD 35 ← '0A'	Initial inputs:
	104B	E6 55 0A	LD 55 ← '0A'	10 increments
	104E	E6 34 80	LD 34 ← '80'	Initial outputs:
	1051	E6 54 80	LD 54 ← '80'	no motion
	1054	E6 32 80	LD 32 ← '80'	Initial previous velocities:
	1057	E6 52 80	LD 52 ← '80'	nil (128 dec. for the ADC)
	105A	56 F1 33	AND F1 , '33'	TMR set up: 00110011
	105D	E6 F3 07	LD F3 ← '07'	PRE1 set up: 00000111
	1060	E6 F2 8A	LD F2 ← '8A'	v=138 (t=149.74 us)
	1063	56 36 FC	AND 36 , 'FC'	Clear flag register
	1066	E6 48 80	LD 48 ← '80'	@48='80' (48-49 = 80xx)
	1069	E6 4A 64	LD 4A ← '64'	Counter = 100 (T/2=14.97 ms)
	106C	31 40	SRP 40	
	106E	9F	EI	
	106F	46 F1 0C	OR F1 , '0C'	Load & start T1

****

First part of the loop: controller of the dynamic counterweight

****

LBL	ADDR	OPCODE	ID	COMMENTS
B	1072	18 31	LD 31 → '41'	Load
	1074	08 30	LD 30 → '40'	Pos 1
	1076	2C 00	LD 42 ← '0'	Div. by $2^0 = 1$ coeff. = 1
	1078	3C 01	LD 43 ← '1'	Mult. by 1

LBL	ADDR	OPCODE	ID	COMMENTS
	107A	D6 12 18	CALL MDI	
	107D	58 41	LD 41 → 45	Move result
	107F	48 40	LD 40 → 44	in (44-45)
	1081	26 32 80	SUB 32 , '80'	Sign VEL1(k-1)
	1084	DD 10 8C	JPL C	
	1087	0C FF	LD 40 ← 'FF'	Expend to a -ve 16 bit word
	1089	8D 10 8E	JP D	
C	108C	B0 40	CLR 40	
D	108E	18 32	LD 32 → 41	
	1090	2C 01	LD 42 ← '1'	$coeff = \frac{1}{2}$
	1092	3C 01	LD 43 ← '1'	
	1094	D6 12 18	CALL MDI	
	1097	22 51	SUB 45 , 41	45←45-41
	1099	32 40	SBC 44 , 40	44←44-40-C $\Big\}$ $\mathbf{Q}(44-45) = pos_1(k) - \frac{1}{2}vel_1(k)$
	109B	B0 49	CLR 49	
	109D	82 18	LDE 41 ←(48.49)	Load VEL1
	109F	19 32	LD 41 → 32	Store for next loop
	10A1	26 41 80	SUB 41 , '80'	Sign VEL1(k)
	10A4	DD 10 AC	JPL E	
	10A7	0C FF	LD 40 ← 'FF'	
	10A9	8D 10 AE	JP F	
E	10AC	B0 40	CLR 40	
F	10AE	2C 00	LD 42 ← '0'	
	10B0	3C 01	LD 43 ← '1'	
	10B2	D6 12 18	CALL MDI	
	10B5	02 51	ADD 45 , 41	45←45+41 $\quad \mathbf{Q}(44-45) =$
	10B7	12 40	ADC 44 , 40	44←44+40+C $\Big\}$ $pos_1(k) - \frac{1}{2}vel_1(k-1) + vel_1(k)$
	10B9	18 35	LD 35 → 41	Load input
	10BB	B0 40	CLR 40	
	10BD	2C 00	LD 42 ← '0'	$coeff. = 1$
	10BF	3C 01	LD 43 ← '1'	
	10C1	D6 12 18	CALL MDI	
	10C4	22 15	SUB 41 , 45	$\mathbf{Q}(40-41) = e_1(k)$
	10C6	32 04	SBC 40 , 44	
	10C8	19 3B	LD 41 → 3B	Store
	10CA	09 3A	LD 40 → 3A	error
	10CC	2C 02	LD 42 ← '2'	$coeff. = \frac{9}{4}$
	10CE	3C 09	LD 43 ← '9'	
	10D0	D6 12 18	CALL MDI	
	10D3	58 41	LD 41 → 45	
	10D5	48 40	LD 40 → 44	
	10D7	04 3D 45	ADD 45 , 3D	
	10DA	14 3C 44	ADC 44 , 3C	

LBL	ADDR	OPCODE	ID	COMMENTS
	10DD	18 39	LD 39 → 41	Load previous
	10DF	08 38	LD 38 → 40	error
	10E1	2C 05	LD 42 ← '5'	
	10E3	3C 41	LD 43 ← '41'	*coeff.* = $\frac{85}{32}$
	10E5	D6 12 18	CALL MDI	
	10E8	22 51	SUB 45 , 41	
	10EA	32 40	SBC 44 , 40	
	10EC	59 3F	LD 45 → 3F	Store command
	10EE	49 3E	LD 44 → 3E	signal
	10F0	18 45	LD 45 → 41	
	10F2	08 44	LD 44 → 40	
	10F4	2C 00	LD 42 ← '0'	
	10F6	3C 01	LD 43 ← '1'	
	10F8	D6 12 18	CALL MDI	
	10FB	A6 40 00	CP 40 '0'	0<command<255 ?
	10FE	6D 11 27	JZ J	If Yes, jump
	1101	A6 40 FF	CP 40 'FF'	-255<command<0 ?
	1104	6D 11 19	JZ I	If Yes, jump
	1107	76 40 80	TM 40 '80'	Command<0 ?
	110A	6D 11 13	JZ H	If No, jump
G	110D	E6 34 00	LD 34 ← '00'	Full reverse motion
	1110	8D 11 32	JP K	
H	1113	E6 34 FF	LD 34 ← 'FF'	Full forward motion
	1116	8D 11 32	JP K	
I	1119	76 41 80	TM 41 , '80'	-127<command<0 ?
	111C	6D 11 0D	JZ G	If No, jump
	111F	06 41 80	ADD 41 , '80'	Translate scale for the DAC
	1122	19 34	LD 41 → 34	
	1124	8D 11 32	JP K	
J	1127	76 41 80	TM 41 , '80'	127<command<0 ?
	112A	ED 11 13	JNZ H	If No, jump
	112D	06 41 80	ADD 41 , '80'	Tanslate scale for the DAC
	1130	19 34	LD 41 → 34	
K	1132	E4 3F 3D	LD 3F → 3D	
	1135	E4 3E 3C	LD 3E → 3C	Shift
	1138	E4 3B 39	LD 3B → 39	registers
	113B	E4 3A 38	LD 3A → 38	
L	113E	A6 4B 01	CP 4B , '01'	Wait for the
	1141	ED 11 3E	JNZ L	T/2 period

LBL	ADDR	OPCODE	ID	COMMENTS

****

Second part of the loop:
controller of the quasistatic counterweight
(Same form as for the first part)

****

	1144	18 51	LD 51 → 41	
	1146	08 50	LD 50 → 40	
	1148	2C 00	LD 42 ← '0'	coeff. = 1
	114A	3C 01	LD 43 ← '1'	
	114C	D6 12 18	CALL MDI	
	114F	58 41	LD 41 → 45	
	1151	48 40	LD 40 → 44	
	1153	26 52 80	SUB 52 , '80'	
	1156	DD 11 5E	JPL M	
	1159	0C FF	LD 40 ← 'FF'	
	115B	8D 11 60	JP N	
M	115E	B0 40	CLR 40	
N	1160	18 52	LD 52 → 41	
	1162	2C 01	LD 42 ← '1'	$coeff. = \frac{1}{2}$
	1164	3C 01	LD 43 ← '1'	
	1166	D6 12 18	CALL MDI	
	1169	22 51	SUB 45 , 41	
	116B	32 40	SBC 44 , 40	
	116D	9E	INC 49	
	116E	82 18	LDE 41 ←(48-49)	
	1170	19 52	LD 41 → 52	
	1172	26 41 80	SUB 41 , '80'	
	1175	DD 11 7D	JPL O	
	1178	0C FF	LD 40 ← 'FF'	
	117A	8D 11 7F	JP P	
O	117D	B0 40	CLR 40	
P	117F	2C 03	LD 42 ← '3'	$coeff. = \frac{7}{8}$
	1181	3C 07	LD 43 ← '7'	
	1183	D6 12 18	CALL MDI	
	1186	02 51	ADD 45 , 41	
	1188	12 40	ADC 44 , 40	
	118A	18 55	LD 55 → 41	
	118C	B0 40	CLR 40	
	118E	2C 00	LD 42 ← '0'	
	1190	3C 01	LD 43 ← '1'	
	1192	D6 12 18	CALL MDI	
	1195	22 15	SUB 41 , 45	
	1197	32 04	SBC 40 , 44	

LBL	ADDR	OPCODE	ID	COMMENTS
	1199	19 5B	LD 41 → 5B	
	119B	09 5A	LD 40 → 5A	
	119D	2C 03	LD 42 ← '3'	$coeff. = \frac{17}{8}$
	119F	3C 11	LD 43 ← '11'	
	11A1	D6 12 18	CALL MDI	
	11A4	58 41	LD 41 → 45	
	11A6	48 40	LD 40 → 44	
	11A8	04 5D 45	ADD 45 , 5D	
	11AB	14 5C 44	ADC 44 , 5C	
	11AE	18 59	LD 59 → 41	
	11B0	08 58	LD 58 → 40	
	11B2	2C 04	LD 42 ← '4'	$coeff. = \frac{31}{16}$
	11B4	3C 1F	LD 43 ← '1F'	
	11B6	D6 12 18	CALL MDI	
	11B9	22 51	SUB 45 , 41	
	11BB	32 40	SBC 44 , 40	
	11BD	59 5F	LD 45 → 5F	
	11BF	49 5E	LD 44 → 5E	
	11C1	18 45	LD 45 → 41	
	11C3	08 44	LD 44 → 40	
	11C5	2C 00	LD 42 ← '0'	
	11C7	3C 01	LD 43 ← '1'	
	11C9	D6 12 18	CALL MDI	
	11CC	A6 40 00	CP 40 , '0'	
	11CF	6D 11 F8	JZ T	
	11D2	A6 40 FF	CP 40 , 'FF'	
	11D5	6D 11 EA	JZ S	
	11D8	76 40 80	TM 40 , '80'	
	11DB	6D 11 E4	JZ R	
Q	11DE	E6 54 00	LD 54 ← '0'	
	11E1	8D 12 03	JP U	
R	11E4	E6 54 FF	LD 54 ← 'FF'	
	11E7	8D 12 03	JP U	
S	11EA	76 41 80	TM 41 , '80'	
	11ED	6D 11 DE	JZ Q	
	11F0	06 41 80	ADD 41 , '80'	
	11F3	19 54	LD 41 → 54	
	11F5	8D 12 03	JP U	
T	11F8	76 41 80	TM 41 , '80'	
	11FB	ED 11 E4	JNZ R	
	11FE	06 41 80	ADD 41 , '80'	
	1201	19 54	LD 41 → 54	
U	1203	E4 5F 5D	LD 5F → 5D	
	1206	E4 5E 5C	LD 5E → 5C	
	1209	E4 5B 59	LD 5B → 59	
	120C	E4 5A 58	LD 5A → 58	

LBL	ADDR	OPCODE	ID		COMMENTS
V	120F	A6 4B 00	CP	4B '0'	
	1212	ED 12 0F	JNZ	V	
	1215	8D 10 72	JP	B	

****

Subroutine MDI: multiplies a 16-bit number stored in the (40-41) pair of registers by a coeficient of the form $n/2^d$ where both n and d are integers: 0<n<255 and 0<d<9.
n is stored in register 42 and p in register 43.
The result is writen in the (40-41) pair of registers

****

LBL	ADDR	OPCODE	ID		COMMENTS
MDI	1218	B0 4C	CLR	4C	
	121A	B0 4D	CLR	4D	
	121C	A6 43 00	CP	43 , '0'	Multiply by zero ?
	121F	ED 12 23	JNZ	AM	
	1222	AF	RET		
AM	1223	02 D1	ADD	4D , 41	Multiplication loop
	1225	12 C0	ADC	4C , 40	
	1227	00 43	DEC	43	
	1229	ED 12 23	JNZ	AM	
	122C	A6 42 00	CP	42 '0'	No division ?
	122F	6D 12 3B	JZ	CM	
BM	1232	D0 4C	SRA	4C	Division loop
	1234	C0 4D	RRC	4D	
	1236	00 42	DEC	42	
	1238	ED 12 32	JNZ	BM	
CM	123B	18 4D	LD	4D → 41	Result stored in the (40-41) pair of registers
	123D	08 4C	LD	4C → 40	
	123F	AF	RET		

****

Interrupt routine IQ1: Updates the position feedback of the quasistatic counterweight

****

LBL	ADDR	OPCODE	ID		COMMENTS
IQ1	1240	46 03 10	OR	03 10	Check the direction of motion
	1243	FF	NOP		
	1244	76 03 04	TM	03 04	
	1247	6D 12 4D	JZ	A1	
	124A	A0 50	INCW	50	Increment position
	124C	BF	IRET		
A1	124D	FC 01	LD	4F ← '01'	Debouncing process: ignore interrupt signals when there is no motion
	124F	82 7E	LDE	47 ←(4E-4F)	
	1251	A6 47 7E	CP	47 , '7E'	
	1254	6D 12 59	JZ	B1	
	1257	80 50	DECW	50	Decrement position
B1	1259	BF	IRET		

LBL	ADDR	OPCODE	ID	COMMENTS

****

Interrupt routine IQ2: Updates the position feedback of the active counterweight

****

LBL	ADDR	OPCODE	ID	COMMENTS
IQ2	125A	56 03 EF	AND 03 EF	Check the
	125D	FF	NOP	direction
	125E	76 03 04	TM 03 04	of motion
	1261	6D 12 67	JZ A2	
	1264	A0 30	INCW 30	Increment position
	1266	BF	IRET	
A2	1267	FC 00	LD 4F ← '0'	Debouncing process: ignore
	1269	82 7E	LD 47 ←(4E-4F)	interrupt signals when there
	126B	A6 47 7E	CP 47 '7E'	is no motion
	126E	6D 12 73	JZ B2	
	1271	80 30	DECW 30	Decrement position
B2	1273	BF	IRET	

****

Interrupt routine IQ3: serial communication.
Receives the desired positions for both counterweights

****

LBL	ADDR	OPCODE	ID	COMMENTS
IQ3	1274	76 36 01	TM 36 '01'	Motor selection ?
	1277	ED 12 8B	JNZ B3	Jump if Not
	127A	46 36 01	OR 36 '01'	
	127D	A6 F0 00	CP F0 '0'	Active (0) or quasistatic
	1280	ED 12 87	JNZ A3	(1) selection
	1283	56 36 FD	AND 36 'FD'	Motor (0)
	1286	BF	IRET	
A3	1287	46 36 02	OR 36 '02'	Motor (1)
	128A	BF	IRET	
B3	128B	56 36 FE	AND 36 'FE'	Data input:
	128E	76 36 02	TM 36 02	
	1291	ED 12 98	JNZ C3	
	1294	E4 F0 35	LD F0 → 35	Store command for motor (0)
	1297	BF	IRET	
C3	1298	E4 F0 55	LD F0 → 55	Store command for mator (1)
	129B	BF	IRET	

LBL	ADDR	OPCODE	ID			COMMENTS

****

Interrupt routine IQ5: 1)Monitors the sample and hold process of both counterweights motors every 149.74 us
2) controls the sampling period

****

LBL	ADDR	OPCODE	ID			COMMENTS
IQ5	129C	A6 46 00	CP	46	'00'	If i=0:
	129F	ED 12 AF	JNZ	A5		
	12A2	46 03 20	OR	03	'20'	Hold SH quasistatic
	12A5	6E	INC	46		
	12A6	E4 34 02	LD	34 →	02	Load command for active
	12A9	56 03 BF	AND	03 ,	'BF'	Sample SH active
	12AC	8D 12 BA	JP	B5		
A5	12AF	46 03 40	OR	03	'40'	If i=1: hold SH active
	12B2	B0 46	CLR	46		
	12B4	E4 54 02	LD	54 →	02	Load command for quasistatic
	12B7	56 03 DF	AND	03	DF	Sample SH quasistatic
B5	12BA	00 4A	DEC	4A		Decrement sampling counter
	12BC	6D 12 C0	JZ	C5		Time = half-sampling period
	12BF	BF	IRET			
C5	12C0	A6 4B 00	CP	4B	00	
	12C3	ED 12 CA	JNZ	D5		
	12C6	BE	INC	4B		j←1 if j=0
	12C7	AC 64	LD	4A ←	'64'	Reload sampling counter
	12C9	BF	IRET			
D5	12CA	B0 4B	CLR	4B		j←0 if j=1
	12CC	AC 64	LD	4A ←	'64'	Reload sampling counter
	12CE	BF	IRET			